PLUTONIUM FUTURES
THE SCIENCE
26-29 September 2022
AVIGNON (France)

Book of Abstracts

Posters

Plutonium Futures – The Science 2022

POSTER SESSION

Surface Science and Corrosion 3
T. Barral 4
A. J. Nelson 6
Compounds, Complexes And Coordination Chemistry 9
Jacob Branson 10
T. Dalger 12
T. Duckworth 13
D. Fellhauer 15
Nicholas Katzer 17
O. Lemoine 18
Marisa Monreal 19
A. Peterson 21
J.C. Shafer 22
M. Virot 23
Condensed Matter Physics 25
F. Gendron 26
Environmental Behavior And Chemistry 29
M. Altmaier 30
C. Méhault 33
T.Montaigne 34
D. T. Reed 36
Metallurgy And Materials Science 41
N. Anwar 42
L. B. F. dos Santos 44
B. C. Childs 46
A. Friskney 49
L. Gardner 50
Michael Z. Ling 53
E.E. Moore 54
M. K. O'Brien 56
S. Reinhard 58
Cheng K. Saw 60
S. Simpson 64
A. Swift 65
Dr V. H. Varsani 66
O. Walter 67
Clarissa A. Yablinsky 68
S. Parker 71
Nuclear Fuel Cycle 73
S. Benarib 74
Lewis R. Blackburn 76
R.A. Carvajal-Ortiz 77
Hammer, Phillip 79
A. Hautecouverture 81
K. S. Holliday 83
J. Margate 84
T. D. Tran 85
K. Van Hecke 86
A. Perrot 103
Detection And Analysis 89
G. Bailly 90
S Crooks 92
S. Cross 93
Aurélie DIACRE 95
A. Alexa Hanson 96
R. Sanderson 97
Brian L. Scott 98
Dung M. Vu 100
S.M. Webb 101

Surface Science and Corrosion

P1	**Thomas Barral (CEA)** *"Understanding the evolution of an interface during the dissolution of Nd-doped UO_2 by macro-/microscopic dual approach."*
P2	**Art Nelson (LLNL)** *"Electrochemical surface modification and oxidation of Pu characterized by X-ray photoelectron spectroscopy"*

P1. Understanding the evolution of an interface during the dissolution of Nd-doped UO_2 by macro-/microscopic dual approach

T. Barral, L. Claparede, R. Podor, N. Dacheux

ICSM, Univ Montpellier, CEA, CNRS, ENSCM, Site de Marcoule 30207, Bagnols-sur-Cèze, France

thomas.barral@cea.fr

Actinide reprocessing is a key issue in considering the preservation of natural fissile resources and the reduction of long-term radiotoxicity of high-level waste under underground repository. Due to the high radioactivity of spent nuclear fuels, the use of model compounds is necessary to study the influence of experimental parameters affecting the dissolution kinetics during their reprocessing.

This work aims at monitoring the evolution of the solid/liquid interface during the dissolution of sintered Nd-doped UO_2 pellets using a dual macro-/microscopic approach. First, precursors of $(U,Nd)O_2$ samples were prepared by co-precipitation of U^{4+} and Nd^{3+} as hydroxide using a large excess of ammonia [1]. Nano-sized powders with high specific surface area were obtained. These powders were then shaped by uniaxial pressing at 500 MPa and sintered at 1600°C under inert (Ar) or reducing (Ar-4%H_2) atmosphere. At the macroscopic scale, multiparametric dissolution tests of the sintered model compounds were performed in nitric medium under static conditions with various concentrations, temperatures and compositions (Figure 1).

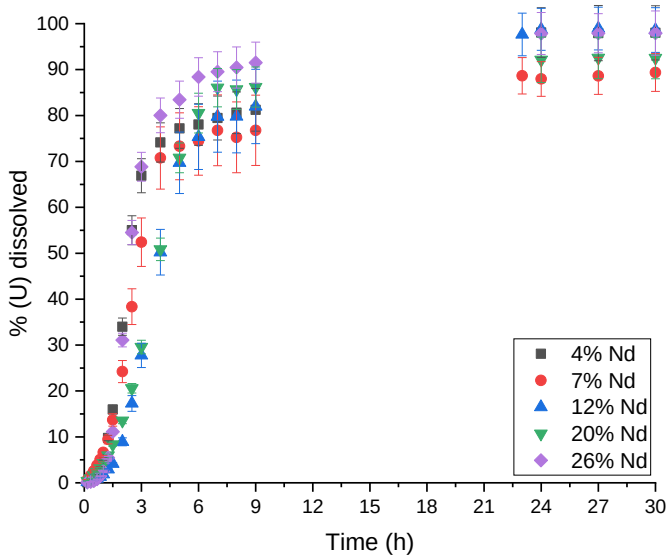

Figure 1: Evolution of the uranium dissolved mass during dissolution tests in 2M HNO_3 at 60°C of $U_{1-x}Nd_xO_2$ samples presenting various compositions and sintered at 1600°C under reducing atmosphere.

At the microscopic scale, *operando* monitoring of the solid/liquid interface was implemented by ESEM to follow the consequences of the dissolution on the pellet microstructure (Figure 2). By operating in 2M HNO_3 at 60°C, it was shown that the use of an inert or reducing sintering atmosphere induced different dissolution mechanisms even if the complete dissolution was reached in almost 24 hours in

both cases. Indeed, a grain size of a few micrometers and a low open porosity were obtained under reducing conditions. A preferential dissolution localized at the grain boundaries was observed as well as the formation of grain surface features characteristic to the crystallographic orientation [2]. Conversely, the materials obtained during sintering under inert atmosphere showed grains of several tens of micrometers and a significant open porosity. A more homogeneous dissolution of the pellet was then highlighted, along with the formation of grain surface features and triangular corrosion pits.

The use of this dual approach allowed to show that even if the change of sintering atmosphere did not seem to influence the chemical durability of the Nd-doped UO_2 sample at the macroscopic scale, the study of the evolution of the solid/liquid interface during its dissolution highlighted noticeable differences at the microscopic scale.

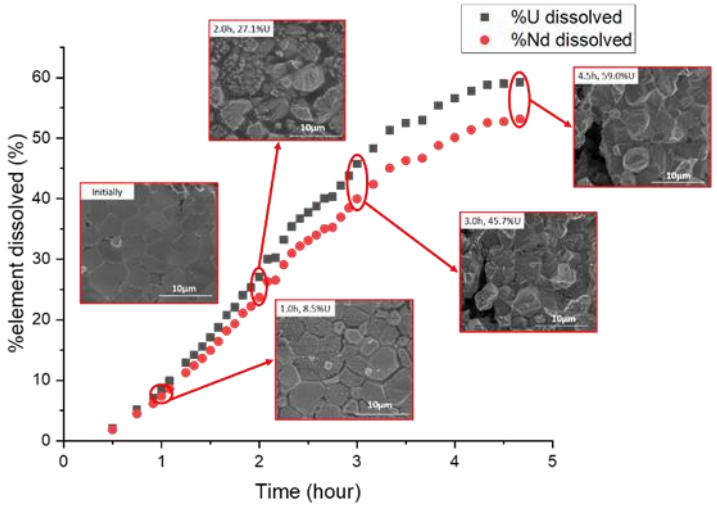

Figure 2: Operando monitoring of the solid/liquid interface during the dissolution in 2M HNO_3 at 60°C of a Nd-doped UO_2 sample sintered at 1600°C under reducing atmosphere.

[1] J. Martinez *et al.*, "An original precipitation route toward the preparation and the sintering of highly reactive uranium cerium dioxide powders," *J. Nucl. Mater.*, vol. 462, pp. 173–181, 2015, doi: 10.1016/j.jnucmat.2015.03.053.

[2] S. Bertolotto *et al.*, "Effect of surface orientation on dissolution rate and surface dynamics of UO2 single crystals in nitric acid," *Corros. Sci.*, vol. 176, p. 109020, 2020, doi: 10.1016/j.corsci.2020.109020.

P2. Electrochemical surface modification and oxidation of Pu characterized by X-ray photoelectron spectroscopy

A. J. Nelson, W. A. Talbot, and D. J. Roberts

Lawrence Livermore National Laboratory, Livermore, CA 94550, nelson63@llnl.gov

---

INTRODUCTION

The study of oxidation/reduction reactions on plutonium metal usually requires a clean surface dependent on sample preparation prior to analyses. Electrolytic polishing, an anodic dissolution technique, is typically used to remove surface contamination fixed in the Pu surface layer or to preferential remove Pu and expose inclusions and grain boundary species. [1] The quantity of Pu dissolved is dependent on process time and on the pH of the electrolyte solution that includes the solvent. These process factors affect surface composition, oxidation state and surface morphology. [2] Qualification and quantification of these process factors for Pu have not been thoroughly investigated.

Quantitative analysis of plutonium surface chemistry during electrolytic polishing can elucidate the effects of electron transfer kinetics due to solution chemistry variations. Plutonium metal can react with the organic solvent of the electrolyte. The solvency power and polarity index are two factors that can affect the rates of chemical reactions including oxidation. [3]

X-ray photoelectron spectroscopy (XPS) has been used to analyze the composition of the passive layer on the electropolished metal surfaces. X-ray photoelectron spectroscopy core-level chemical shifts have established that the stable oxides of Pu are plutonium sesquioxide (Pu_2O_3, O/Pu = 1.5, Pu^{3+}) and plutonium dioxide (PuO_2, O/Pu = 2.0, Pu^{4+}) that typically form a layered structure on the surface of Pu metal. [4-6] Auger electron spectroscopy (AES) has also shown the layered oxide structure on the surface of Pu metal. [7, 8]

This investigation utilizes XPS Pu 4f, Ga 2p, O 1s and C 1s core-level spectra to provide definitive information on the effects of electrochemical solutions on surface chemistry.

DESCRIPTION OF THE ACTUAL WORK

The samples studied were cast gallium stabilized δ-Pu alloy (≈ 0.6 $^{w}/_{o}$) that were mechanically polished with alumina and finished to 0.25 μm. The δ-Pu alloy was then electro-polished at 18 V using either ethylene glycol/HNO_3 or dimethylformamide (DMF)/HNO_3 to remove any α phase from mechanical polishing before mounting. Note that ethylene glycol has a higher relative polarity than dimethylformamide (DMF), 0.790 versus 0.386. [3] This process was repeated for different durations to investigate the electrochemical surface modification and oxidation. The electropolished surfaces were examined with optical microscopy to determine differences in the surface morphology and noting that the DMF/HNO_3 processed surface had a rougher appearance. XPS experiments were performed with a PHI Quantera II scanning X-ray microprobe using a focused, monochromatic Al Kα X-ray (1486.6 eV) source for excitation. Sputter etching of the Pu surfaces was performed with 4 kV Ar^+ ions rastered over an area of 1 x 1 mm. Following sample loading into the XPS analytical chamber, the

base pressure was ~2 x 10^{-9} torr before proceeding with analysis. Residual gaseous species present were primarily H_2, H_2O and CO.

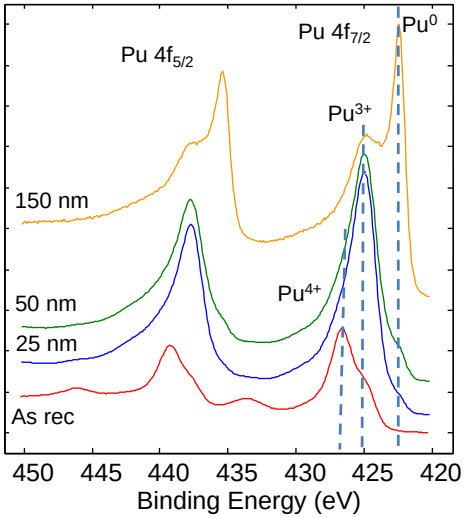

Fig 1. Evolution of the Pu $4f_{7/2,5/2}$ spin-orbit pair versus oxide depth to identify Pu oxidation states on ethylene glycol/HNO_3 electropolished surface for 10 cycles.

RESULTS

The influence of solution chemistry on the electrochemical oxidation of the cast δ-Pu surface is illustrated by the Pu 4f data in Figures 1 and 2. Note that initially there is a Pu_2O_3 layer on the mechanically polished δ-Pu prior to electropolishing.

The initial Pu 4f line-shape for ethylene glycol/HNO_3 processed surface shown in Fig. 1 represents a mixture of Pu_2O_3 and PuO_2 while the initial Pu 4f line-shape for DMF/HNO_3 processed surface shown in Fig. 2 reveals predominantly PuO_2. Sputter depth profiling through these electrochemically oxidized surfaces using identical ion beam parameters indicates that the DMF/HNO_3 solution results in a thicker oxide.

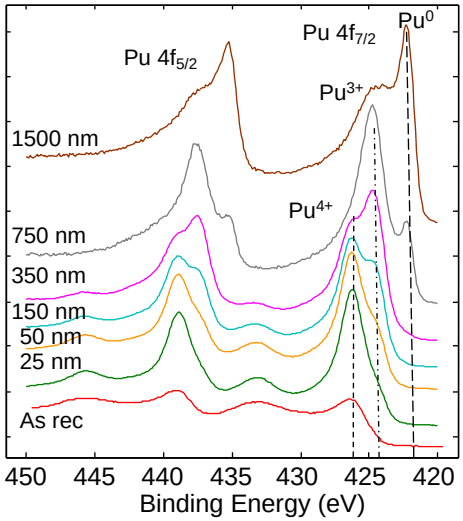

Fig. 2. Evolution of the Pu $4f_{7/2,5/2}$ spin-orbit pair versus oxide depth to identify Pu oxidation states on DMF/HNO_3 electropolished surface after 10 cycles.

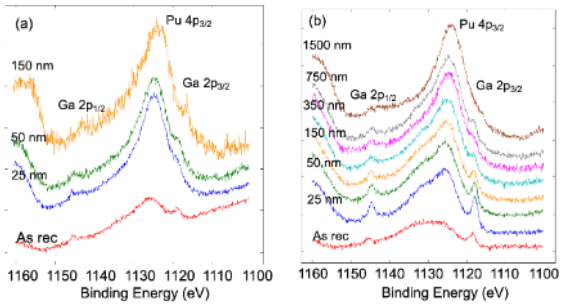

Fig. 3. Comparison of Ga $2p_{3/2,1/2}$ spectra for the (a) ethylene glycol/HNO_3 and (b) DMF/HNO_3 processed surfaces.

In addition, electropolishing δ-Pu with DMF/HNO_3 results in a higher concentration of Ga at the surface by qualitatively comparing the intensity of the Ga $2p_{3/2,1/2}$ peaks. [Fig. 3] Quantification is difficult due to the overlap with Pu $4p_{3/2}$ peak. [9]

In summary, XPS results qualify the influence of solution chemistry (pH, relative polarity) on the electrochemical oxidation of the cast δ-Pu surface.

This work performed under the auspices of the U.S. Department of Energy by Lawrence Livermore National Laboratory under Contract DE-AC52-07NA27344.

REFERENCES

[1] K. S. BERGSTRESSER, “Plutonium electropolishing cell” Los Alamos Technical Report LA-1106 (1950).
[2] T. C. KASPER, C. L. ARENDT, D. L. NEAL, S. L. RIECHERS, C. RUTHERFORD, A. SCHEMER-KOHRN, S. R. SPURGEON, L. E. SWEET, V. V. JOSHI, C. A. LAVENDER, R. W. SHIMSKEY, “Characterization of surface layers formed on DU10Mo ingots after processing steps and high humidity exposure” *J. Nucl. Materials.* **514,** 28 (2019).
[3] CHRISTIAN REICHARDT, THOMAS WELTON, *Solvents and Solvent Effects in Organic Chemistry, Fourth Edition 2011*, WILEY-VCH Verlag GmbH.
[4] M. T. BUTTERFIELD, T. DURAKIEWICZ, E. GUZIEWICZ, J. J. JOYCE, A. J. ARKO, K. S. GRAHAM, D. P. MOORE and L. A. MORALES, “Photoemission of Surface Oxides and Hydrides of Delta Plutonium,” *Surf. Sci.* **571**, 74 (2004).
[5] H. G. GARCIA FLORES and D. L. PUGMIRE, “The growth and evolution of thin oxide films on δ-plutonium surfaces,” *IOP Conf. Series: Mater. Sci. Eng.* **9**, 012038 (2010).
[6] A. J. NELSON and P. ROUSSEL, “Low Temperature Oxidation of Plutonium,” *J. Vac. Sci. Technol.* A **31(3)**, 031406 (2013).
[7] S. B. DONALD, J. A. STANFORD, W. McLEAN and A. J. NELSON, “Application of Linear Least Squares to the Analysis of AES Depth Profiles of Plutonium Oxides,” *J. Vac. Sci. Technol.* **A 36(3),** 03E104 (2018).
[8] S. B. DONALD, J. A. STANFORD, J. M. HASCHKE, D. D. ASHLEY, W. A. TALBOT. D. J. ROBERTS, A. J. NELSON, B. W. CHUNG and W. McLEAN, **“**Parabolic Oxidation Kinetics of a Plutonium Alloy at Room Temperature,” *Corrosion Sci.***187**, 109527 (2021).
[9] P. ROUSSEL and A. J. NELSON, “Quantitative XPS of plutonium: Evaluation of the Pu4f peak shape, relative sensitivity factors and estimated detection limits,” *Surf. Interface Anal.* **54** (2022)

Compounds, Complexes And Coordination Chemistry

P3	**Jacob Branson (LBNL)** *"Evaluating the Electronic Structure of Actinide(IV) Hexafluorides Using Fluorine K-edge X-ray Absorption Spectroscopy and Time-Dependent Density Functional Theory"*
P4	**Thomas Dalger (CEA)** *"Stabilization of spent salts by an oxidation and distillation process: focus on sodium carbonates stability in molten salts"*
P5	**Tamara Duckworth (HZDR)** *"Coordination chemistry of N-Donor Ligands with early Actinides"*
P6	**David Fellhauer (KIT)** *"Crystal structure and stability of pentavalent $Ca_1/3Na_1/3PuO_2(OH)_2$ and $Ca_{0.5}NpO_2(OH)_2$"*
P7	**Nicholas Katzer (LBNL)** *"Synthesis of a Transplutonium Organometallic"*
P8	**Olivier Lemoine (CEA)** *"Electrochemical behavior of plutonium in molten calcium chloride and fluoride medium"*
P9	**Marisa Monreal (LANL)** *"Investigating the Local Structure of Actinide-Molten Salts Using Neutron Pair-Distribution Function Analysis"*
P10	**Appie Peterson (LBNL)** *"Amidate Supported Single-Molecule Precursors for Actinide Oxide Materials"*
P11	**Jenifer Shafer (Colorado School of Mines)** *"Soft Donor vs Soft Matter: Controlling Transplutonium Chemistry"*
P12	**Matthieu Virot (CEA)** *"Multi-Scale Characterization of Pu Nanostructures using Synchrotron-based SAXS and XAS Techniques"*

P3. Evaluating the Electronic Structure of Actinide(IV) Hexafluorides Using Fluorine K-edge X-ray Absorption Spectroscopy and Time-Dependent Density Functional Theory

Jacob Branson [1,2], Jochen Autschbach [4], Enrique Batista [3], Alex Ditter [2], S. Olivia Gunter [2], Joe Kasper [3], Stosh Kozimor [3], Stefan Minasian [2], Dumitru-Claudiu Sergentu [4], David Shuh [2], Ping Yang [3]

[1] Department of Chemistry, University of California, Berkeley, Berkeley, California 94720, United States.
[2] Chemical Sciences Division, Lawrence Berkeley National Laboratory, Berkeley, California 94720, United States.
[3] Los Alamos National Laboratory, Los Alamos, New Mexico 87545, United States.
[4] Department of Chemistry, University at Buffalo, State University of New York, Buffalo, New York 14260, USA.

The actinide—fluorine bond is of particular interest due to the role of actinide fluorides in the nuclear fuel cycle. Moreover, the covalent character of these bonds is of fundamental interest to actinide bonding. Ligand K-edge X-ray Absorption Spectroscopy (XAS) probes the transitions of ligand 1*s* orbitals into metal-based molecular orbitals and has been established as direct probe of metal—ligand covalency.[1] In this work, Fluorine K-edge X-ray XAS is used to evaluate bond covalency in MF_6^{2-} (M = Ti, Zr, Hf, Ce, U, Np, Pu). Chloride K-edge XAS was previously used to determine relative *d*- and *f*-orbital contributions to covalency in the analogous metal chloride species.[2–4] These data are compared to elucidate differences in bonding between actinide fluorides and chlorides. Spectral assignments are guided by TD-DFT spectral simulations and ground state electronic structure calculations. For all complexes, transitions into *d*-based orbitals of t_{2g} symmetry are observed. Examining CeF_6^{2-}, a large pre-edge feature is observed corresponding with transitions into 4*f* orbitals. Finally, pre-edge features associated with transitions into 5*f* orbitals are observed in all AnF_6^{2-} (An = U, Np, Pu). In UF_6^{2-}, a single pre-edge feature is observed as a shoulder on the rising edge. For NpF_6^{2-} and PuF_6^{2-}, multiple pre-edge features associated with transitions into the t_{1u} and t_{2u} *f*-orbital sets are observed. The intensities of these features are used to analyze the bonding in these molecules within a perturbational molecular orbital framework.

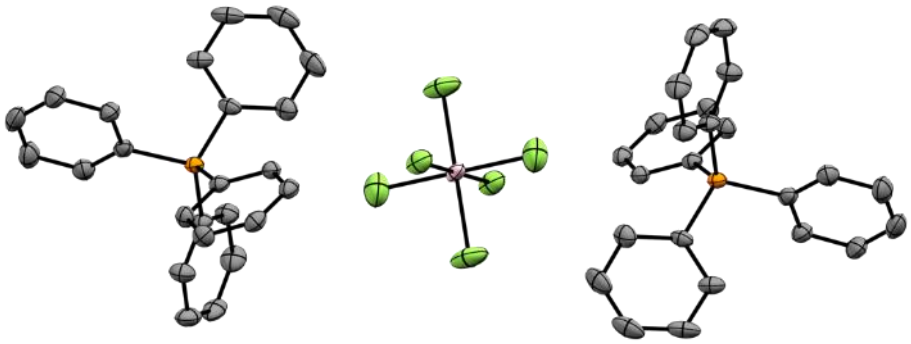

Figure 1. Thermal ellipsoid (50%) plot of $(Ph_4P)_2PuF_6$.

References:

(1) Glaser, T.; Hedman, B.; Hodgson, K. O.; Solomon, E. I. *Acc. Chem. Res.* **2000**, *33* (12), 859–868. https://doi.org/10.1021/ar990125c.
(2) Minasian, S. G.; Keith, J. M.; Enrique R. Batista; Boland, K. S.; Clark, D. L.; Conradson, S. D.; Kozimor, S. A.; Martin, R. L.; Schwarz, D. E.; Shuh, D. K.; Wagner, G. L.; Wilkerson, M. P.; Wolfsberg, L. E.; Yang, P. *J. Am. Chem. Soc.* **2012**, *134* (12), 5586–5597. https://doi.org/10.1021/ja2105015.
(3) Su, J.; Batista, E. R.; Boland, K. S.; Bone, S. E.; Bradley, J. A.; Cary, S. K.; Clark, D. L.; Conradson, S. D.; Ditter, A. S.; Kaltsoyannis, N.; Keith, J. M.; Kerridge, A.; Kozimor, S. A.; Löble, M. W.; Martin, R. L.; Minasian, S. G.; Mocko, V.; La Pierre, H. S.; Seidler, G. T.; Shuh, D. K.; Wilkerson, M. P.; Wolfsberg, L. E.; Yang, P. *J. Am. Chem. Soc.* **2018**, *140* (51), 17977–17984. https://doi.org/10.1021/jacs.8b09436.
(4) Löble, M. W.; Keith, J. M.; Altman, A. B.; Stieber, S. C. E.; Batista, E. R.; Boland, K. S.; Conradson, S. D.; Clark, D. L.; Lezama Pacheco, J.; Kozimor, S. A.; Martin, R. L.; Minasian, S. G.; Olson, A. C.; Scott, B. L.; Shuh, D. K.; Tyliszczak, T.; Wilkerson, M. P.; Zehnder, R. A. *J. Am. Chem. Soc.* **2015**, *137* (7), 2506–2523. https://doi.org/10.1021/ja510067v.

P4. Stabilization of spent salts by an oxidation and distillation process: focus on sodium carbonates stability in molten salts

T. Dalger, B. Claux, O. Lemoine, S. Faure, G. Bourges [1],

CEA, DAM, VALDUC, F-21120 Is sur Tille, France [1]

thomas.dalger2@cea.fr

Spent salts from plutonium pyrochemical processing are composed of mixtures of NaCl, KCl, and $CaCl_2$ with various dissolved/precipitated actinide-based species depending on the process used and storage conditions.

In order to stabilize these materials, a two-step pyrochemical treatment has been developed by CEA Valduc. It consists in a pyro-oxidation treatment [1] and a distillation process [2]. The waste salt after distillation meets the radiologic requirement to be discarded as low-level waste. The pyro-oxidation, also known as oxidation-chlorination, converts actinides into stable oxides by carbonates ions: AnO_2. Cl_2 gas is used to remove excess carbonate through the exhaust of CO_2 and O_2 gases and to provide the best thermochemical conditions to produce actinide dioxides.

Work is still underway to gain a deeper understanding of the stability of carbonate in the salt mixtures. Preliminary results suggest that carbonate ions can be completely decomposed into carbon dioxide and oxide anions by changing the composition of the molten salts bath. Indeed, salts containing $CaCl_2$ showed quick and total decomposition of carbonates. Upcoming work needs to be done to assess the feasibility of substituting the hazardous chlorination step by using a solvent oxo-acidity adjustment.

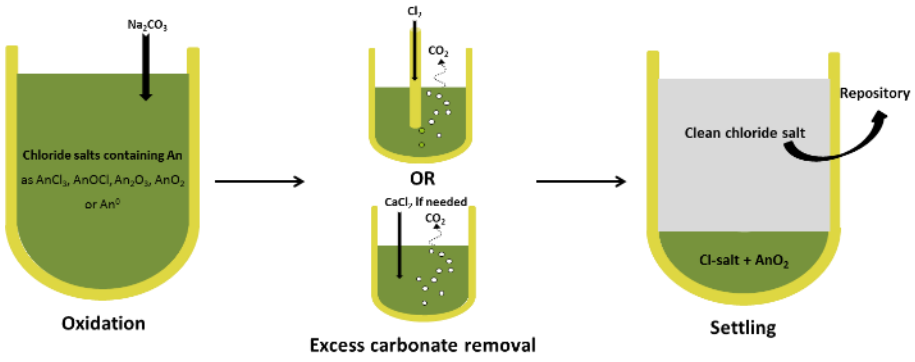

Figure 1: Stabilization of actinides-bearing spent salts by carbonate oxidation and removal of excess carbonates

[1] O. Lemoine, J. Serp, G. Bourgès, S. Faure, Atalante 2012, 2012

[2] G. Bourgès, S. Faure, B. Fiers, S. Saintignon, O. Lemoine, D. Cardona-Barrau, D. Devillard, Atalante 2012, 2012

P5. Coordination chemistry of N-Donor Ligands with early Actinides

T. Duckworth [1], J. März [1], P. Kaden [1], N. Schwarz [2], G. Greif [2], M. Schmidt [1], T. Stumpf [1]

[1] Helmholtz-Zentrum Dresden-Rossendorf, Institute of Resource Ecology, Bautzner Landstraße 400, 01328 Dresden, Germany

[2] Karlsruhe Institute of Technology (KIT), Institute for Inorganic Chemistry, 76131 Karlsruhe, Germany

t.duckworth@hzdr.de

The development and investigation of N-donor ligands e.g. for actinide/lanthanide separation is an ongoing field of study, in particular with respect to understanding the structure-property-relationship.

In this context we have been exploring the coordination chemistry of the early actinides (Th – Am) with tridentate chelating ligands containing pyridine and bipyridine moieties.

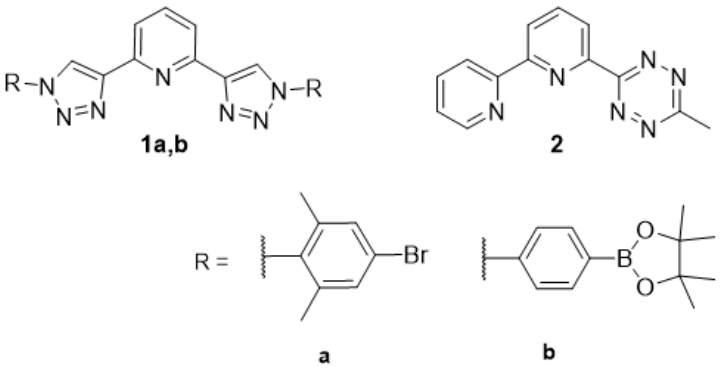

Figure 1: N-Donor ligands of interest for our studies.

Ligands **1** and **2** were successfully used for complexation with trivalent lanthanides.

Encouraged by these results, we have been focusing on their coordination chemistry with tri- and tetravalent early actinides. We aim to understand the reactivity of these ligands that exploit the unique electronic structure of the early 5f-elements.

The synthesis of such complexes was carried out in acetonitrile with recrystallization from methanol.

For instance, the synthesized U(IV) complex of **1a** which was characterized by single crystal XRD revealed a nine-fold coordinated uranium center. In contrast to the nine-fold Ln(III) complex which exhibits a ligand to metal ratio of 3:1 the U(IV) complex shows a 2:1 ratio with additional methanolato and iodo ligands for charge compensation.

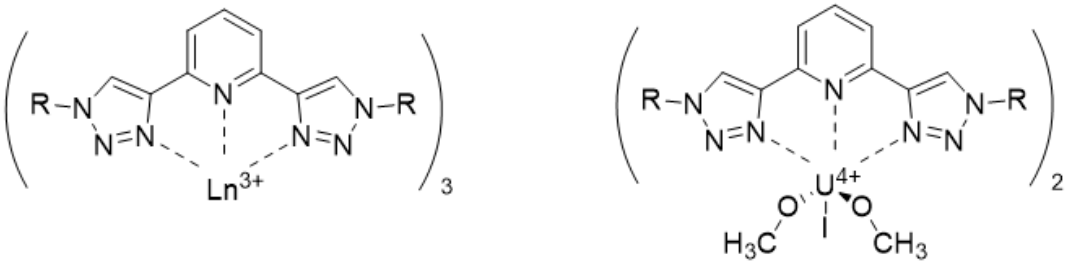

*Figure 2: Complexation reaction of ligand **1a** with Ln(III) and U(IV) salts*

Expanding the series to the tri- and tetravalent transuranic metals and characterizing the obtained complexes both structurally and spectroscopically will help to elucidate the differences between the coordination behavior of the lanthanides compared to the actinides

Acknowledgement

This work was supported by the German Federal Ministry of Education and Research (BMBF) under project number 02NUK059 (f-char).

P6. Crystal structure and stability of pentavalent $Ca_{1/3}Na_{1/3}PuO_2(OH)_2$ and $Ca_{0.5}NpO_2(OH)_2$

D. Fellhauer [1], O. Walter [2], N. A. DiBlasi [1], D. Schild [1], J. Rothe [1], X. Gaona [1], M. Altmaier [1]

[1] Karlsruhe Institute of Technology - Institute for Nuclear Waste Disposal (INE), Germany

[2] European Commission, Joint Research Centre Karlsruhe (JRC-KRU), Germany

david.fellhauer@kit.edu

Among the thermodynamically stable oxidation states of actinide elements in aqueous solutions, An(III)-An(VI), the highest mobility is ascribed to An(V) due to its weak sorption properties and high solubility. The latter is particularly evident if binary $AnO_2OH(am)$ is considered as solubility limiting solid phase [1]. In the case of Np, which exists as Np(V) over a wide range of (pH+pe) conditions, recent studies demonstrated that $NpO_2OH(am)$ is metastable in alkaline NaCl and $CaCl_2$ solutions with respect to transformation into ternary hydroxide phases, M-Np(V)-OH(s) with M = Na and Ca [2-5]. Based on the results of systematic solubility studies and the evaluated thermodynamic constants, these M-Np(V)-OH phases lead to a pronounced stabilization of the Np(V) redox state in alkaline electrolyte solutions. Pu(V) is known to be significantly less stable compared to Np(V), and very little is reported for Pu(V) hydroxide compounds. For example, the current NEA-TDB volume selects thermodynamic constants for only two Pu(V) hydroxide compounds, namely $PuO_2OH(am)$ and $PuO_2OH(aq)$ [1]. Similarly, systematic solubility studies are practically not available for Pu(V). As actinides of the same oxidation state typically show an analogous behaviour, and considering the comprehensive results available for Np(V), it is likely that the stability of Pu(V) in aqueous solutions may be also enhanced by the formation of potential ternary M-Pu(V)-OH solid phases. In the present work, we report on the successful synthesis of two novel isostructural Ca(Na)-An(V)-OH solid phases with An = Pu(V) and Np(V) from aqueous solution, the analysis of their crystal structure and the investigation of their thermodynamic stability in aqueous solution.

Experiments were performed under anoxic Ar atmosphere with ^{237}Np and ^{242}Pu. $Ca_{0.5}Np(V)O_2(OH)_2(cr)$ was prepared by hydrothermal treatment of the hydrated precursor $Ca_{0.5}Np(V)O_2(OH)_2{\cdot}1.3H_2O(cr)$ reported in [2] in dilute $Ca(OH)_2$ solution. $Ca_{1/3}Na_{1/3}Pu(V)O_2(OH)_2(cr)$ was obtained by long-term equilibration (several months to years at room temperature) of initial hexavalent Pu(VI) in a NaOH dominated solution containing traces of calcium. This procedure was successfully reproduced twice. Solids were characterized by powder and single crystal XRD, SEM-EDX, chemical analysis by combined LSC+OES, solid state Vis/NIR and Raman spectroscopy. The Np(V) solid was also studied by Np L_{III}-edge XANES and EXAFS at the *INE Beamline for Radionuclide Research at the KIT Light Source*. To obtain information about their thermodynamic stability, solubility studies in dilute Ca(Na)-Cl-OH solutions are currently ongoing.

The synthesis of $Ca_{0.5}NpO_2(OH)_2(cr)$ follows a straight forward path starting from the well-defined compound $Ca_{0.5}NpO_2(OH)_2{\cdot}1.3H_2O(cr)$. During hydrothermal treatment of the latter, structural water is released and $Ca_{0.5}NpO_2(OH)_2(cr)$ is obtained as homogeneous monocrystalline material. The preparation of a Pu(V) phase by a similar synthesis route starting from initial Pu(V) failed, however, due to rapid disproportionation of Pu(V) in alkaline solutions. A successful and reproducible synthetic

path to prepare a Pu(V)-OH solid phase was found by long-term equilibration of hexavalent Pu(VI) in hyperalkaline Na-Ca-OH solutions where the initial Pu(VI) slowly reduces to Pu(V) (≈20% after 3 months, ≈70% after 24 months) resulting in the formation of single crystals of $Ca_{1/3}Na_{1/3}PuO_2(OH)_2$(cr). Due to its high crystallinity / density, an enrichment of $Ca_{1/3}Na_{1/3}PuO_2(OH)_2$(cr) by fractional sedimentation steps was possible leading to a purity of about 90±5%. The results from the solid phase characterization confirm that $Ca_{0.5}NpO_2(OH)_2$(cr) and $Ca_{1/3}Na_{1/3}PuO_2(OH)_2$(cr) are An(V) compounds (analysis of acid digested solid phase fractions by either liquid extraction or Vis/NIR, solid state Vis/NIR, Raman, XANES for Np). Powder XRD and SEM analysis reveal that both are isostructural and crystallize as hexagonal needles. EDX and OES further underpin the slightly different chemical compositions in both solids. A structural model was evaluated for both An(V) compounds based on the successful single crystal XRD analysis of the Pu(V) solid phase.

In the presentation, the results of the solid phase characterization and an assessment of the thermodynamic stability of the Ca(Na)-An(V)-OH phases will be discussed.

[1] Grenthe, I., Gaona, X., Plyasunov, A.V., Rao, L., Runde, W.H., Grambow, B., Konings, R. J. M., Smith, A.L., Moore, E.E. (2020). Second Update on the Chemical Thermodynamics of Uranium, Neptunium, Plutonium, Americium and Technetium, Chemical Thermodynamics. OECD Nuclear Energy Agency, Boulogne-Billancourt, France.

[2] Fellhauer, D., Rothe, J., Altmaier, M., Neck, V., Runke, J., Wiss, T., Fanghänel, Th. (2016). "Np(V) solubility, speciation and solid phase formation in alkaline $CaCl_2$ solutions. Part I: Experimental results". Radiochim. Acta 104: 355-379.

[3] Fellhauer, D., Altmaier, M., Gaona, X., Lützenkirchen, J., Fanghänel, Th. (2016). "Np(V) solubility, speciation and solid phase formation in alkaline $CaCl_2$ solutions. Part II: Thermodynamics". Radiochim. Acta 104: 381-397.

[4] Petrov, V., Fellhauer, D., Gaona, X., Dardenne, K., Rothe, J., Kalmykov, S. N., Altmaier, M. (2017). "Solubility and hydrolysis of Np(V) in dilute to concentrated alkaline NaCl solutions: formation of Na–Np(V)–OH solid phases at 22 °C". Radiochim. Acta 105: 1-20.

[5] Fellhauer, D., Lee, J.-Y., DiBlasi, N. A., Walter, O., Gaona, X., Schild, D., Altmaier, M. (2022). "Crystal-structure and stability in aqueous solution of $Na_{0.5}[NpO_2(OH)_{1.5}]\cdot 0.5H_2O$ and $Na[NpO_2(OH)_2]$", submitted.

P7. Synthesis of a Transplutonium Organometallic

Nicholas Katzer [1,2], Dominic Russo [1,2], Alyssa Gaiser [1], Amy Price [1,2], Jennifer Wacker [1], Jacob Branson [1,2], Patrick W. Smith [1] Appie Peterson [1], S. Olivia Gunther [1], Rebecca Abergel [1,3], Stefan Minasian [1], Polly Arnold [1,2]

[1] Chemical Sciences Division, Lawrence Berkeley National Laboratory, Berkeley, California 94720, United States [2] Department of Chemistry, University of California, Berkeley, California 94720, United States [3] Department of Nuclear Engineering, University of California, Berkeley, California 94720, United States

pla@berkeley.edu

The transplutonium members of the actinides are significantly less studied than their earlier counterparts. Their availability is limited to milligram quantities and the radiological hazards of these short-lived isotopes necessitate rigorous *optimization of synthetic conditions* with non-radioactive analogs and an abundance of engineered safety controls. The organometallic chemistry of these rare elements under air- and water-free conditions is particularly lacking with only recent reports expanding the field to include crystallographically characterized Am–C[1,2] and Cf–C bonds[3]. Organometallic chemistry has been foundational in developing our understanding of fundamental electronic structure and bonding across the periodic table. High-symmetry, cyclic, aromatic ligands such as arenes[4–6] and cyclooctatetraenides[7,8] foster complexes with unique electronic structures that improve our understanding of bonding in the actinides by allowing for greater *f*-orbital covalency[9,10]. Here we expand the synthetic field of organometallic transplutonium chemistry to include new bonding motifs.

[1] Goodwin, C. A. P.; Su, J.; Albrecht-Schmitt, T. E.; Blake, A. V.; Batista, E. R.; Daly, S. R.; Dehnen, S.; Evans, W. J.; Gaunt, A. J.; Kozimor, S. A.; Lichtenberger, N.; Scott, B. L.; Yang, P. *Angew. Chem. Int. Ed.* **2019**, *58* (34), 11695–11699.

[2] Long, B. N.; Beltrán-Leiva, M. J.; Celis-Barros, C.; Sperling, J. M.; Poe, T. N.; Baumbach, R. E.; Windorff, C. J.; Albrecht-Schönzart, T. E. *Nat. Commun.* **2022**, *13* (1), 201.

[3] Goodwin, C. A. P.; Su, J.; Stevens, L. M.; White, F. D.; Anderson, N. H.; Auxier, J. D.; Albrecht-Schönzart, T. E.; Batista, E. R.; Briscoe, S. F.; Cross, J. N.; Evans, W. J.; Gaiser, A. N.; Gaunt, A. J.; James, M. R.; Janicke, M. T.; Jenkins, T. F.; Jones, Z. R.; Kozimor, S. A.; Scott, B. L.; Sperling, J. M.; Wedal, J. C.; Windorff, C. J.; Yang, P.; Ziller, J. W. *Nature* **2021**, 1–4.

[4] Baudry, D.; Bulot, E.; Charpin, P.; Ephritikhine, M.; Lance, M.; Nierlich, M.; Vigner, J. *J. Organomet. Chem.* **1989**, *371* (2), 155–162.

[5] Dutkiewicz, M. S.; Farnaby, J. H.; Apostolidis, C.; Colineau, E.; Walter, O.; Magnani, N.; Gardiner, M. G.; Love, J. B.; Kaltsoyannis, N.; Caciuffo, R.; Arnold, P. L. *Nat. Chem.* **2016**, *8* (8), 797–802.

[6] Arnold, P. L.; Halliday, C. J. V.; Puig-Urrea, L.; Nichol, G. S. *Inorg. Chem.* **2021**, *60* (6), 4162–4170.

[7] Streitwieser, A.; Mueller-Westerhoff, U. *J. Am. Chem. Soc.* **1968**, *90* (26), 7364–7364.

[8] Karraker, D. G.; Stone, J. A.; Jones, E. R.; Edelstein, N. *J. Am. Chem. Soc.* **1970**, *92* (16), 4841–4845.

[9] Minasian, S. G.; Keith, J. M.; Batista, E. R.; Boland, K. S.; Clark, D. L.; Kozimor, S. A.; Martin, R. L.; Shuh, D. K.; Tyliszczak, T. *Chem. Sci.* **2013**, *5* (1), 351–359.

[10] Kerridge, A. *RSC Adv.* **2014**, *4* (24), 12078–12086.

P8. Electrochemical behavior of plutonium in molten calcium chloride and fluoride medium

O. Lemoine[a], J. Claquesin[a,b], L. Massot[b], M. Gibilaro[b], P. Chamelot[b], G. Bourgès[a]

[a] *CEA, DAM, Valduc, F-21120, Is-sur-Tille, France*

[b] *LGC UMR 5503 UPS-CNRS-INP, Université de Toulouse, F-31062, Toulouse, France*

olivier.lemoine@cea.fr

Plutonium metal preparation by calciothermic reduction generates a salt residue called slag. A slag is mainly composed of fluorite (CaF_2) and contains until 5 wt.% of various plutonium species with an oxidation state varying from 0 to IV (metal, fluorides and oxides), resulting from process operating conditions and from interim storage environment. The development of a pyrochemical process is in progress to remove plutonium from this slag in order to meet radiological requirements of middle activity – long life waste repositories.

The process baseline is a metallothermic extraction, with calcium used as a reducing agent.

To obtain a liquid form of the slag an additional amount of $CaCl_2$ is added in order to decrease the operating temperature below 1000°C, in agreement with the available setup in our facilities. The molten slag is assumed as a CaF_2-$CaCl_2$-CaO mixture.

In fact, the extraction process is operated in a molten chloro-fluoride salt that is complex and quite unknown. Pu investigation in simplified mediums, chloride and fluoride, must lead to understand the mechanism of Pu reduction in chloro-fluoride media.

In this work, a detailed electrochemical study was carried out on plutonium in calcium chloride ($CaCl_2$) and calcium fluoride (CaF_2) salts. For the fluoride system, the selected solvent is a mixture of two well-known salts: LiF-CaF_2. Cyclic voltammetry, square wave voltammetry and chronopotentiometry were coupled with thermodynamic calculations (potential-oxoacidity diagram) to investigate the electrochemical system and assess feasibility of Pu extraction from the chloro-fluoride melt.

P9. Investigating the Local Structure of Actinide-Molten Salts Using Neutron Pair-Distribution Function Analysis

Marisa Monreal[1], J. Matt Jackson[1], Boris Khaykovich [2], David Andersson [1], Sven Vogel [1]

[1] Los Alamos National Lab, Los Alamos, New Mexico, USA

[2] Massachusetts Institute of Technology, Boston, Massachusetts, USA

mmonreal@lanl.gov

Investigating the chemical and thermophysical properties of actinide-molten salts is currently an active area of research. Despite actinide-molten salts being the central system for pyroprocessing of plutonium and high enriched uranium—processes that have been carried out for decades—there do exist gaps in knowledge and recent, accurate data, in particular for chloride salt systems, and even more so for systems including plutonium. Since actinide molten salts are also the central system in certain designs of the molten salt reactor (MSR), an advanced nuclear reactor concept receiving high interest and investments of late, there is a dual need to fill the knowledge gaps, and perform the needed research on actinide-molten salt systems: to underpin the development and deployment of the MSR, and to optimize pyroprocesses for plutonium and uranium purification and recovery, including improving efficiency, reducing waste, and increasing safety.

One of the main objectives of the research program at the Molten Salt Chemistry Lab (MSCL) at LANL is to gain a better understanding of *how* and *why* actinides affect the macroscale properties of molten salts. In molten salt systems, the atomic-scale interactions between ions govern the local and intermediate-range order of the system, which in turn affect macroscale properties (e.g., density, viscosity, corrosivity) of the molten solution. Our research effort comprises a combination of novel methods to make, measure, and model actinide-molten salt systems, and we apply these methods to examine local structure towards an understanding of these macroscale effects.

To this end, one of the methods we are developing at LANL to examine actinide-molten salt local structure is neutron pair distribution function (nPDF) analysis; the pair distribution function (PDF) gives the probability of finding an atom at a distance *r* from an atom at the origin, and thus provides information on the local order of a material. For example, scattering characterizations of molten UCl_3 (that is, not dissolved in salt) using PDF analysis have reported that the U^{3+} ion in molten UCl_3 is coordinated on average by six-eight Cl atoms.[3-5] In the melt, U–Cl distances of 2.82 Å and 2.85 Å[4,5] have been observed. While such studies on the pure UCl_3 end-member are of importance for fundamental understanding of the system, for the applications mentioned above, the same properties need to be known in molten mixtures of actinide halide and alkali and alkaline earth metal halides.[6] For this reason, simulations based on density functional theory (DFT) have been developed, but require experimental data to benchmark the predictions or develop the required pair potentials.

We have had recent success utilizing the unique LANL capability that is the Los Alamos Neutron Science Center (LANSCE) to obtain accurate measurements of the liquid density of actinide-molten salts.[1, 2] In

that work, we developed the experimental apparatus and sample containment required to study actinide-molten salts and are now leveraging that knowledge towards nPDF studies. Importantly, LANSCE has the capability to study plutonium materials as well, which supports these research efforts to ultimately study plutonium-bearing molten salts using neutrons. We have recently reported our observations on the evolution of the crystal structure of uranium trichloride (UCl_3) from room temperature to melting point, made during our early work towards nPDF of actinide molten salts[7]; this work will be described, as will our progress and results from our empirical and modelling research efforts using nPDF analysis to gain insight into actinide-molten salt local structure.

[1] Parker, S., Long, A., Lhermitte, C., Vogel, S., Monreal, M., Jackson, J. M., *J. Mol. Liq.,* 2022, *346,* 118147.

[2] Long, A., Parker, S., Carver, T. Jackson, J. M., Monreal, M., Newmark, D., Vogel, S. "*J. Imaging*, 2021, *7*, 88.

[3] Y. Okamoto, F. Kobayashi, and T. Ogawa, *J. Alloys Compd.* 1998, 271, 355.

[4] A.K. Adya, H. Matsuura, R. Takagi, L. Rycerz, and M. Gaune-Escard, *Proc. Electrochem. Soc.* 1999(1), 341.

[5] Y. Okamoto, P.A. Madden, and K. Minato, *J. Nucl. Mater.* 2005, 344, 109.

[6] A. Nakayoshi, S. Kitawaki, M. Fukushima, T. Murakami, and M. Kurata, *J. Nucl. Mater.* 2013, 441, 468.

[7] Vogel, S., Andersson, D., Monreal, M., Jackson, J. M., Parker, S., Wang, G., Yang, P., Zhang, J. *JOM,* 2021**,** *73,* 3555–3563.

P10. Amidate Supported Single-Molecule Precursors for Actinide Oxide Materials

A. Peterson [1], M. Straub [1,2], S. Kelly [1,2], J. Branson [1,2], D. Russo [1,2], S. G. Minasian* [1]

[1] Chemical Sciences Division, Lawrence Berkeley National Laboratory, Berkeley, California 94720, United States

[2] Department of Chemistry, University of California, Berkeley, California 94720, United States

sgminasian@lbl.gov

Information about the behavior of nuclear fuel materials can be gleaned from studying the properties of bulk AnO_2 materials (An = actinide),[1] particularly with regard to controlling grain size to mitigate the hazards of self-heating nuclear fuel.[2] While the relationship between synthetic perturbations (i.e., size, morphology) and electronic behavior for many transition-metal nanoparticles is well-understood, the field of actinide-containing nanomaterials is comparatively young with great opportunities for synthetic and spectroscopic advancement. Previous success utilizing single-molecule uranium and thorium amidate complexes as precursors to size-controlled uranium dioxide (UO_2) and thorium dioxide (ThO_2) thin-film nanomaterials inspired the extension of analogous techniques to transuranic actinides.[3-5] In this work, we explore the synthesis, spectroscopic characteristics, and decomposition to AnO_2 materials of homoleptic amidate complexes of trivalent cerium and americium, and tetravalent neptunium and plutonium. The volatile amidate ligands allow for direct decomposition from the homoleptic complex to actinide oxides without contamination from organic byproducts, ultimately revealing electronic structure and reactivity of AnO_2 materials through rigorous spectroscopic characterization.

1. Amaya, M., J. Nakamura, and T. Fuketa, *Measurements of Crystal Lattice Strain and Crystallite Size in Irradiated UO2Pellet by X-ray Diffractometry.* Journal of Nuclear Science and Technology, 2008. **45**(3): p. 244-250.
2. Yin, Q., et al., *Electronic correlation and transport properties of nuclear fuel materials.* Physical Review B, 2011. **84**(19).
3. Moreau, L.M., et al., *Structural properties of ultra-small thorium and uranium dioxide nanoparticles embedded in a covalent organic framework.* Chemical Science, 2020. **11**(18): p. 4648-4668.
4. Straub, M.D., et al., *Chemical Vapor Deposition of Phase‐Pure Uranium Dioxide Thin Films from Uranium(IV) Amidate Precursors.* Angewandte Chemie International Edition, 2019. **58**(17): p. 5749-5753.
5. Straub, M.D., et al., *Thorium amidates function as single-source molecular precursors for thorium dioxide.* Chemical Communications, 2021. **57**(40): p. 4954-4957.

P11. Soft Donor vs Soft Matter: Controlling Transplutonium Chemistry

J.C. Shafer[1]

1500 Illinois Street, Golden, CO, 80401

jshafer@mines.edu

The elements at the basement (er…foundation) of the periodic table represent where chemistry is both the least understood and most desperately needs to be controlled to address 21st century energy and security needs. Recent discoveries in the chemistry of the actinides heavier than plutonium have suggested our current understanding of chemical bonding is insufficient to fully predict actinide chemistry across the series. This has ramifications for our ability to develop more efficient and proliferation resistant advanced nuclear fuel cycles, secure the actinides for long-term geological disposal and advance nuclear forensics technologies. This presentation will focus on highlighting the unique, fun chemistry of the heaviest actinides. Heavy actinide chemistry discussions will consider how covalency manifests for the heavier actinides and provide some preliminary thoughts regarding what questions still exist in controlling actinide-ligand interactions relevant to practical systems. The material presented will both highlight how experimental chemical information can be discerned from nanogram amounts of a given element and interpreted in more detail using computational methodologies. We will seriously consider the chemistry of dipicolinic acid, and derivatives thereof, as well as thio-based extractants in this discussion.

P12. Multi-Scale Characterization of Pu Nanostructures using Synchrotron-based SAXS and XAS Techniques

M. Virot [1], T. Dumas [2], M. Cot-Auriol [1], C. Tamain [2], S. Dourdain [1], C. Micheau [1], D. Menut [3], P. L. Solari [3], L. Venault [2], O. Diat [1], P. Moisy [2], S. I. Nikitenko [1]

[1] ICSM, CEA, Univ Montpellier, CNRS, ENSCM, Bagnols sur Cèze, France

[2] CEA, DES, ISEC, DMRC, Univ Montpellier, Marcoule, France

[3] Synchrotron SOLEIL, L'Orme des Merisiers Saint Aubin, Gif-sur-Yvette, France

matthieu.virot@cea.fr

The thorough characterization of actinide nanostructures play an important role in modern actinide science because of environmental and technological issues.[1,2] Predicting the formation and behaviour of such species requires the thorough characterization of their size, morphology (i.e. shape), coordination environment and oxidation states. Nevertheless, advanced structural characterizations of actinide samples are often hindered by the chemical toxicity and strong radioactivity of the considered elements.

Recently, researchers from ICSM Marcoule, CEA Marcoule and SOLEIL/MARS beamline have combined synchrotron SAXS (Small-Angle X-ray Scattering) and XAS (X-ray Absorption Spectroscopy) techniques to probe quasi-simultaneously the multi-scale structural properties of Pu nanostructures.[3] Stable suspensions of intrinsic Pu colloids were prepared by hydrolysis and sonolysis before being characterized using this approach. SAXS investigations revealed contrasted scattering patterns evidencing significant differences in the size and morphology of the nanoparticles composing the suspensions. XAS measurements carried out at the Pu L_3 edge indicated the (+IV) oxidation state for Pu atoms that further organize in a PuO_2 like structure.

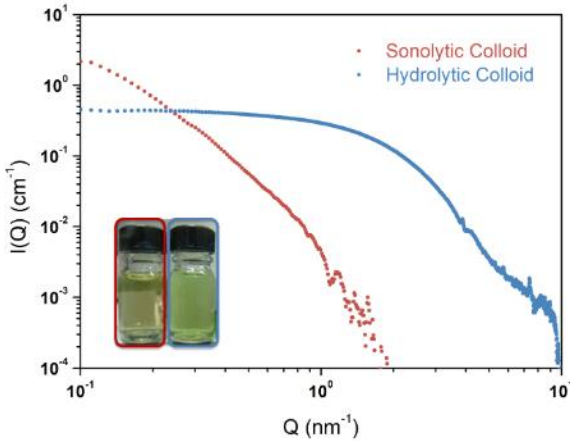

Figure 1: SAXS scattering diagrams acquired on intrinsic Pu colloids prepared by "conventional" hydrolysis and sonolysis (20 kHz, Ar/(10%)CO, H_2O, 20°C).

Meeting the results from both techniques allowed describing intrinsic colloids as PuO_2 nanoparticles covered by a disordered Pu(IV) shell whose properties are highly influenced by the preparation method.[3] More recently, a similar approach was used to probe a water-soluble hexanuclear Pu cluster whose deciphered properties were found to be in excellent agreement with its resolved crystal structure offering interesting perspectives for the characterization of very small polynuclear species.[4,5]

More generally, these results demonstrate the possible description of actinide coordination modes and structures in dilute solutions. Combining synchrotron SAXS and XAS approaches provides in-situ information, averaged over a large sample volume also measured directly in the native environment. This overcome analytical challenge appears particularly useful for the description of radioactive actinide nanostructures.

[1] Walther et al. *Chem. Rev.* 113, 995 (2013).
[2] Khanal et al. *Energy Technol.* 8, 1901070 (2020).

[3] Micheau et al. *Environ. Sci.: Nano* 2, 214 (2020).

[4] Dumas et al. *Journal of Synchrotron Radiation* 29, 30 (2022).

[5] Tamain et al. *Eur. J. Inorg. Chem.* 22, 3536 (2016).

Condensed Matter Physics

P13 **Frédéric Gendron (CEA)**
"Electronic Structure and Magnetic Properties of PuO_2"

P14 **Christine Wu (LLNL)**
"Thermodynamics for plutonium monocarbides and mononitrides from first principles"

P13. Electronic Structure and Magnetic Properties of PuO_2

F. Gendron [1][2], B. Amadon [1][2]

[1] CEA DAM DIF, F-91297 Arpajon France

[2] Laboratoire Matière en Conditions Extrêmes, Université Paris-Saclay, CEA, F-91680 Bruyères-le-châtel, France

frederic.gendron@cea.fr

The PuO_2 solid has been well characterized experimentally over the last century. It crystallizes in cubic CaF_2 structure with eight-coordinate octahedral plutonium sites and four-coordinate oxygen sites. The Pu4+ ion has four valence electrons with the ability to generate a large panel of magnetic and non-magnetic states. Experimentally, it has been shown that PuO_2 exhibits a non-magnetic ground state and a temperature-independent paramagnetism (TIP) up to 1000 K. Interestingly, this relatively simple system has proven to be extremely challenging to be described theoretically. Neither crystal-field theory nor Density Functional Theory (DFT) have led to satisfactory pictures that allow to reproduce properly both the electronic structure, i.e. the band insulating character, and the magnetic properties, i.e. the quenching of the ground state magnetic moment.[1] Here we will present the results of molecular electronic structure calculations that use relativistic wave-function theory method such as the complete-active space (CAS) approach that includes spin-orbit coupling. These calculations allowed to us to show that the TIP behavior of PuO_2 is only valid up to 300 K. At higher temperature, we found an almost perfect cancellation of temperature-dependent contributions to the magnetic susceptibility that depends delicately on the mixing of ion levels in the electronic states, their relative energies, and the magnetic coupling between them. This molecular picture will be then discussed with regard to preliminary results obtained using Dynamical Mean-Field Theory (DMFT) calculations.[3]

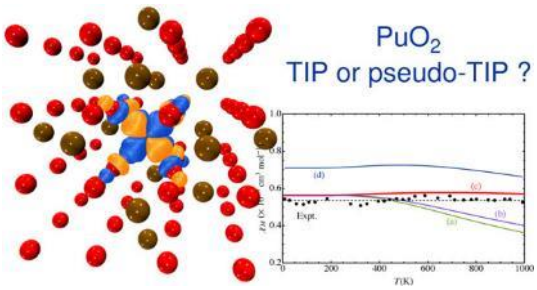

Figure 1: Calculated and experimental magnetic susceptibility of solid PuO2 from Ref. [2].

[1] X.-D. Wen, R. L. Martin, T. M. Henderson, G. E. Scuseria *Chem. Rev.* **2013**, *113*, 1063-1096.

[2] F. Gendron, J. Atuschbach *J. Phys. Chem. Lett.* **2017**, *8*, 673-678

[3] J.-B. Morée, R. Outerovitch, B. Amadon *Phys. Rev. B.* **2021**, *103*, 045113

P14. Thermodynamics for plutonium monocarbides and mononitrides from first principles

Per Söderlind[1], Emily Moore[1] and Christine Wu[1]

[1] Lawrence Livermore National Laboratory, Livermore, CA, United States

soderlind1@llnl.gov & wu5@llnl.gov

Thermodynamics of plutonium monocarbides and mononitrides is studied from first-principles theory that includes relativistic electronic structure and anharmonic lattice vibrations. Density-functional theory (DFT) is expanded, when necessary, to include orbital-orbital coupling in addition to the relativistic spin-orbit interaction for the electronic structure and it is combined with anharmonic, temperature dependent, lattice dynamics derived from the self-consistent ab initio lattice dynamics (SCAILD) method. For some systems, formation enthalpy, specific heat, and Gibbs energy calculated from the anharmonic model are compared to a calculation of phase diagram (CALPHAD) assessments. Overall, the theory reproduces CALPHAD results rather well, but the comparison is hampered by the sub-stoichiometric nature of the real systems.

Environmental Behavior And Chemistry

P15	**Marcus Altmaier (KIT)**	*"Cement-organics-radionuclide-interactions studied within the collaborative EC funded project EURAD-CORI"*
P16	**Annie Kersting (LLNL)**	*"Plutonium transport under acidic solution conditions in vadose zone sediments at the Hanford Site, USA"*
P17	**Camille Mehault (CEA)**	*"Modelling the gas generation of actinide bearing materials in storage containers"*
P18	**Théo Montaigne (CEA)**	*"MOX fuel alteration mechanisms under deep geological repository conditions"*
P19	**Donald Reed (LANL)**	*"Waste Isolation Pilot Plant (WIPP) TRU Repository Actinide Research"*
P20	**Pascal Reiller (CEA)**	*"Formation of alkaline earth(II) triscarbonatouranyl(VI) complexes: thermodynamic study and ionic strength influence by time-resolved laser-induced fluorescence spectroscopy"*

P15. Cement-organics-radionuclide-interactions studied within the collaborative EC funded project EURAD-CORI

M. Altmaier [1], D. García [2], P. Henocq [3], N. Mace [4], T. Missana [5], D. Ricard [3], J. Vandenborre [6]

[1] KIT-INE, Karlsruhe, Germany;
[2] Amphos 21, Barcelona, Spain;
[3] Andra, Châtenay-Malabry, France;
[4] CEA, Gif-sur-Yvette, France;
[5] CIEMAT, Madrid, Spain;
[6] SUBATECH, Nantes, France;
Karlsruher Institut für Technologie (KIT), Institut für Nukleare Entsorgung (INE)

Hermann-von-Helmholtz-Platz 1, 76344 Eggenstein-Leopoldshafen, Germany

marcus.altmaier@kit.edu

The CORI (Cement-Organics-Radionuclides-Interactions) Workpackage integrated into EURAD [1] performs research studies to improve the knowledge on the organic release issues which can enhance the radionuclide migration in the context of the post closure phase of geological repositories for ILW and LLW/VLLW including surface/shallow disposal. Plutonium and its oxidation state chemical analogs is one of the main elements studied in this particular project context. The R&D in CORI extends the current state-of-the-art and will contribute to optimize disposal solutions and considers questions of regulatory concern. CORI results will help member states to further develop their national R&D programs and support programs at an early implementation stage.

CORI research is addressing topics in the context of cement-organics-radionuclides-interactions. Organic materials are present in some nuclear waste and as admixtures in cement-based materials and can potentially influence the performance of a geological disposal system, especially in the context of low and intermediate level waste disposal. The potential effect of organic molecules is related to the formation of complexes in solution with some radionuclides of interest (actinides and lanthanides) which can (i) increase radionuclide solubility and (ii) decrease radionuclide sorption. Organic substances require special attention since a significant quantity exists in the waste and in the cementitious materials, with a large degree of chemical diversity. Cement-based materials will be degraded with time, leading to specific alkaline pH conditions under which the organics can degrade, thus increasing their impact on repository performance. CORI has prepared a State-of-the-Art document [2] which gives an introduction to the main research topics targeted in CORI.

The three R&D Tasks in CORI are:

Organic Degradation. Focus is on the characterization of soluble organic species generated by radiolytic and hydrolytic degradation of selected organics (PVC, cellulose, resins, superplasticizers). Studies also include the analysis of degradation and stability of small organic molecules such as carboxylic acids and the determination of degradation rates.

Organic-Cement-Interactions. Studies focus on investigating the mobility of selected organic molecules in cement-based materials. Mobility of organic molecules includes sorption and transport properties. Organics will also include small ^{14}C bearing molecules as identified in the EC EURATOM project CAST. Both retention on individual cement phases and cementitious systems are investigated.

Radionuclide-Organic-Cement-Interactions. Consistent with the set of organics, individual cement phases and materials identified in the above two Tasks, radionuclide migration processes are studied in the ternary system. The role of organic molecules on the transfer properties of radionuclides are investigated through sorption and transport experiments. Selected radionuclides cover a range of chemical characteristics and redox states relevant for conditions in L/ILW disposal.

Within this contribution, the scope and status of the work performed in EURAD-CORI will be presented, and further activities, points of contacts and potential modes of interaction and exchange with this large collaborative activity highlighted.

References

[1] EURAD – European Joint Programme on Radioactive Waste Management. https://www.ejp-eurad.eu/

[2] The CORI State-of-the-Art report is available at the EURAD Website at:

https://www.ejp-eurad.eu/publications/eurad-deliverable-31-cori-sota-cement-organic-radionuclide-interactions-content-lilw

Acknowledgements:

The project leading to this application has received funding from the European Union's Horizon 2020 research and innovation programme under grant agreement No 847593.

P16. Plutonium transport under acidic solution conditions in vadose zone sediments at the Hanford Site, USA

Teresa Baumer[1], Annie B. Kersting*[1],Carolyn Pearce[2], Hilary P. Emerson[2], Mavrik Zavarin[1]

[1] Glenn T. Seaborg Institute, Physical & Life Sciences Directorate, Lawrence Livermore National Laboratory, Livermore, CA 94550, USA

[2] Energy and Environment Directorate, Pacific Northwest National Laboratory, Richland, WA 99352, USA

Plutonium has migrated in the subsurface under a variety of different geochemical and hydrogeologic environments; yet, the specific biogeochemical mechanisms by which this transport occurs are not fully understood. At the Hanford Site, WA, over 200 kg of Pu were released into the subsurface between 1943 and 1994, and an estimated 50-140 kg of this Pu was released directly into the Z-9 trench in 4 million liters of acidic processing waste. The majority of the Pu precipitated in the first several centimeters beneath the unlined trench, but a small fraction was detected in the vadose zone at depths up to 37 m[1]. The exact mechanisms controlling Pu mobility beneath the trench are still not well understood. In an effort to better understand the Pu migration process below the Z-9 trench, we undertook a series of column experiments using Hanford sediments and Pu in a range of high nitrate, acidic solution compositions with and without TBP in dodecane. The effluent was analyzed for Pu, changes in pH and solution chemistry and the data compared and modeled. Pu migration is likely driven by weak sorption of aqueous Pu under low pH conditions as well as the formation of Pu-TBP-nitrate complexes in the organic phase.

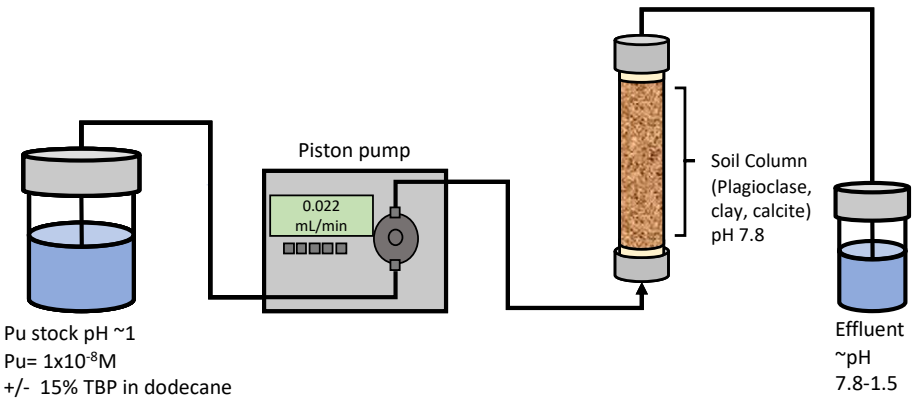

Figure 1: Simplified schematic of column experiment set-up

[1]Cantrell, K. J.; Riley, R. G. A review of subsurface behavior of plutonium and americium at the 200-PW-1/3/6 operable units; PNNL-SA-58953, 2008.

This work performed under the auspices of the U.S. Department of Energy by Lawrence Livermore National Laboratory under Contract DE-AC52-07NA27344.

P17. Modelling the gas generation of actinide bearing materials in storage containers

C. Méhault [1], S. Saintignon [1], C. Le Pennec [1], S. Faure [1]

[1] CEA, DAM, VALDUC, F-21120 Is sur Tille, France

camille.mehault@cea.fr

Actinides processing generates by-products with low contents of radioactive elements. These products are placed in dedicated packaging arrangements with several containers for medium to long interim storage. However, during storage, the products evolve by generating gases as a result of radiochemical reactions. Indeed, molecules of the plastic parts of the packaging (containers, plastic envelopes), adsorbed water and matrix material of the product (salts) can be decomposed under ionizing radiation leading to the generation of primary radicals that react with others by homogeneous reactions to form stable gases [1-5].

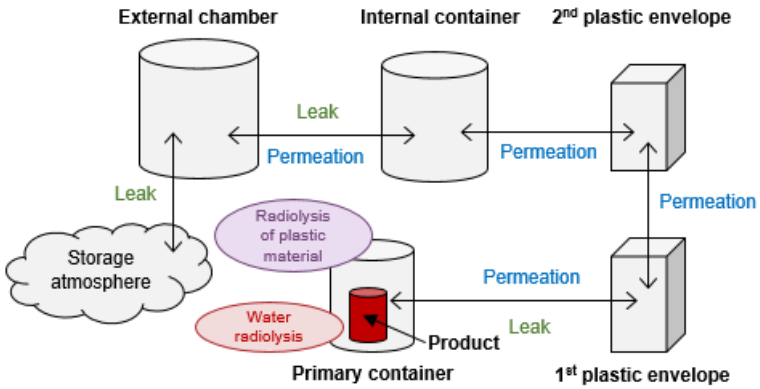

Figure 1: Scheme of each phenomenon taken into account in the model

To improve our knowledge of the evolution of these items containing alpha emitters, a model was developed using a macroscopic approach. This phenomenological model can be divided in two parts. First, plastic and water radiolysis models were used to evaluate gas generation closed to the nuclear materials. Secondly, the transportation of gases between the different containers were evaluated. The model takes into account two transfer phenomena: leakage as a result of a total pressure difference between two compartments and permeation as a result of a partial pressure gradient from each side of a plastic wall. The model was computed in Matlab using ODE solvers and was confronted to experimental measurements. Chosen key parameters were adjusted to fit the experimental data. The model allows us to highlight the parameters influencing the gas generation.

[1] Berg, J.M., et al., Moisture and Gas Production in Storage Containers of Plutonium Oxide, in Plutonium Futures - The Sciences. 2010
[2] Veirs, D.K., et al., Evidence of Corrosive Gas formed by Radiolysis of Chloride Salts in Plutonium-bearing Materials. Journal of Nuclear Materials Management, 2010. 38(3), p. 25-31.
[3] Vladimirova, M.V. and I.A. Kulikov, Formation of H_2 and O_2 in Radiolysis of water sorbed on PuO_2. Radiochemistry, 2002. 44(1), p. 86-90.
[4] Almond, P.M., et al., Gas Analysis from Headspace of Plutonium-Bearing Materials Containers. 2010, Savannah River National Laboratory: Aiken, SC 29808.
[5] Tandon, L., Radiolysis of Salts and Long-Term Storage Issues for Both Pure and Impure PuO_2 Materials in Plutonium Storage Containers, in LA-13725-MS. 2000, Los Alamos National Laboratory: New Mexico.

P18. MOX fuel alteration mechanisms under deep geological repository conditions

T.Montaigne [1], S. Szenknect [1], V. Broudic [2], C. Martin [3], F. Tocino [4], C. Jégou [2], N. Dacheux [1]

[1] ICSM, Univ Montpellier, CNRS, CEA, ENSCM, Site de Marcoule, Bagnols/Cèze, France
[2] CEA, DES, ISEC, DE2D, Univ Montpellier, Marcoule, France
[3] ANDRA, R & D Division, 1/7 rue Jean Monnet 92298, Châtenay-Malabry, France
[4] EDF R & D, les Renardières, 77818 Moret-sur-Loing, France

theo.montaigne@cea.fr

Although the reprocessing of spent fuel remains the reference way in France, direct disposal in a deep geological repository is also studied as an option within the framework of the French national plan for the management of radioactive waste. This is especially the case for MOX spent fuel for which the option of multi-recycling in Light Water Reactor is under investigation, as is the possibility of direct disposal. Even though UO_2 spent fuel alteration mechanisms has an extensive literature, it is not the case when considering $U_{1-x}Pu_xO_2$ MOX fuels and especially, Mimas® MOX fuels. This work is focused on the alteration of both fresh heterogeneous Mimas® MOX fuel and surrogate materials $U_{1-x}Ce_xO_2$ with various Ce contents and microstructures in oxidizing and anoxic conditions. The objective of this work is to better understand the mechanisms associated to MOX fuel alteration under oxidizing and anoxic conditions while integrating the effects of environmental chemistry. This chemistry is linked to the presence of argillite (Callovo-Oxfordian clay rock) and environmental materials such as cement (filling material) and iron (container). The influence of oxidizing species produced by water radiolysis such as H_2O_2 and of groundwater cations is especially studied.

Firstly, homogeneous and heterogeneous $U_{1-x}Ce_xO_2$ dense pellets, as surrogates of the MOX fuel with x ranging from 0 to 0.25 were prepared via wet and dry chemistry routes, respectively. Surrogate materials were submitted to dynamic leaching experiments for approximately two weeks at room temperature and pH = 7.2 in order to investigate the influence of the oxidizing conditions induced by radiolytically produced H_2O_2. The feeding solution contained 2×10^{-4} mol.L^{-1} H_2O_2, was kept under air ($[HCO_3^-]$ = 0.16 mmol.L^{-1}; $[O_2]$ = 0.26 mmol.L^{-1}) and renewed every 48 to 72h to guarantee the stability of H_2O_2 during all the experiment. Normalized alteration rates were determined from the U concentration measured in the leachates by using ICP-MS after reaching the steady state, as cerium concentration was below the quantification limit for all the systems studied. When considering homogeneous $(U,Ce)O_2$ materials, the dissolution rate was divided by a factor 3 when increasing the Ce molar content from 0.08 to 0.25. However, studtite precipitation was observed all over UO_2 surface, retroactively decreasing uranium concentration in solution. The same results were obtained with heterogeneous $U_{0.92}Ce_{0.08}O_2$. However, for the latter, studtite was found to precipitate on UO_2 grains only. This result is in very good agreement with that observed for heterogeneous $(U,Pu)O_2$ in the same conditions [1], which ascertains the reliability of cerium as a valuable plutonium analogue **(Figure1)**.

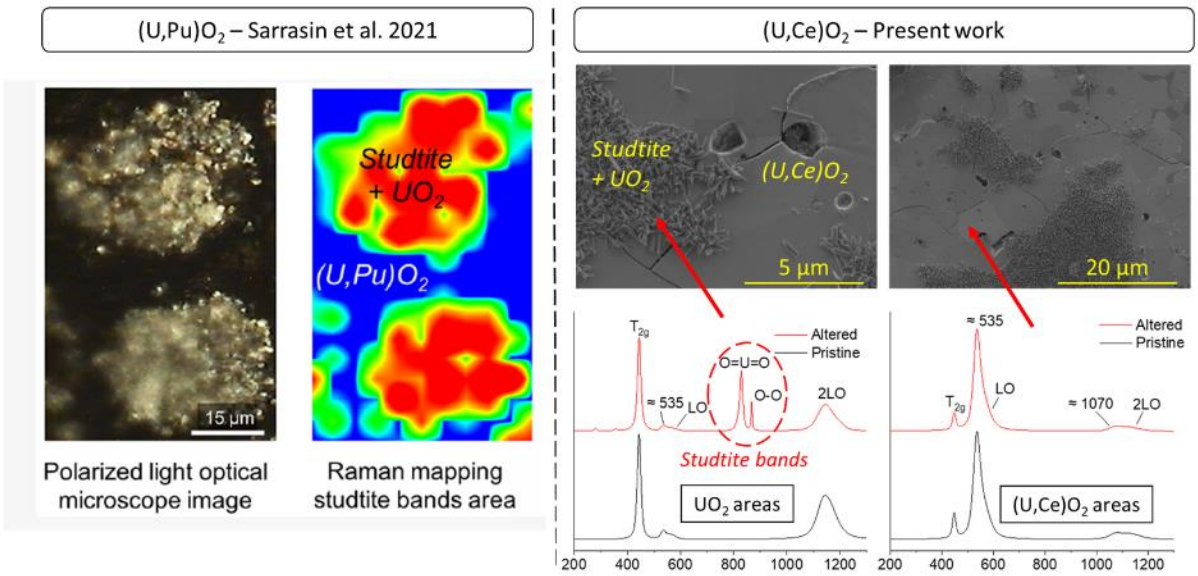

Figure 1: Comparison between the results obtained from reference [1] with Mimas® MOX fuel and the present work with heterogeneous (U,Ce)O₂

Secondly, heterogeneous Mimas® MOX fuel and surrogate materials $U_{1-x}Ce_xO_2$ were altered over several months under static conditions in simplified solutions containing $[Ca^{2+}]$ = 8.5 mmol.L^{-1}, [Si] = 0.18 mmol.L^{-1} or $[Ca^{2+}]$ = 8.5 mmol.L^{-1} + [Si] = 0.18 mmol.L^{-1}, at pH 7.2 and room temperature. These concentration values were chosen according to the measured value in groundwater at the equilibrium with the Callovo-Oxfordian clay rock. Along with these experiments, a set of leaching tests was also performed in silicate containing solution at pH = 12 to estimate the influence of alkaline conditions. All these currently ongoing experiments provide further information on the alteration mechanisms between the considered elements in solution and the fuel surface.

[1] Sarrasin, L.; Miro, S.; Jégou, C.; Tribet, M.; Broudic, V.; Marques, C.; Peuget, S. Studtite Formation Assessed by Raman Spectroscopy and ^{18}O Isotopic Labeling during the Oxidative Dissolution of a MOX Fuel. *J. Phys. Chem. C* **2021**, *125* (35), 19209–19218. https://doi.org/10.1021/acs.jpcc.1c04392.

P19. Waste Isolation Pilot Plant (WIPP) TRU Repository Actinide Research

D. T. Reed, J. Beam, J. Swanson, A. Navarrette, C. Aslani, U. Kaplan, J. Knox

1400 University Drive, Carlsbad NM, USA

Actinide Chemistry and Repository Science Project team,

Los Alamos National Laboratory

dreed@lanl.gov

The Waste Isolation Pilot Plant (WIPP) was first certified in 1998 and began operation in March of 1999 as the nuclear waste repository for transuranic defense waste in the USA. As of March 2022, over 13000 waste shipments have been made and over 185,000 TRU waste containers were emplaced. Since the start of operations, the WIPP has been recertified by the EPA four times but its actinide Pitzer model has remained more or less unchanged for the past 20 years. A summary of recent progress [1-7] and ongoing efforts to develop the needed experimental data to update this model, along with the corresponding modeling strategy, will be provided.

The WIPP project has always had an approach to actinide solubility that is based on the Pitzer approach (I>5 m) that views the solubility of each actinide as the sum of its likely oxidation-state-specific contributions. The An(III) actinides (Pu and Am) are modeled using a combination of Am^{3+} and Nd^{3+} data; the An(IV) actinides (U, Np and Pu) are modeled by analogy with Th(IV) data; the An(V) actinide (Np) is modeled using Np(V) data; and the only An(VI) actinide (U) is not modeled but assumed to be 1 mM under WIPP-relevant conditions. Key complexants that impact solubility are hydrolysis, carbonate and borate complexation, and organic chelators (EDTA, Citrate, Oxalate and Acetate). Additionally, estimates of four colloidal contributors (intrinsic, mineral, humic/fulvic and microbial) are determined and added to the solubilities to form the mobile actinide source term that is used in PA to estimate potential release from the WIPP under low-probability direct brine release (DBR) scenarios that are driven by human intrusion assumptions that saturate and subsequently pressurize the repository with brine.

Plutonium, primarily as Pu-239, continues to be the actinide of most concern with respect to release in the WIPP concept. There is currently 12.5 metric tons categorized as WIPP-bound waste and increasing this to a total of ~ 50 metric tons is under discussion [8]. Under WIPP-relevant conditions, only Pu(III) and Pu(IV) oxidation states are expected. The importance of these two oxidation states is under investigation to evaluate the relative effects of radiolysis, various iron minerals and organic complexants on the oxidation state distribution. Currently plutonium chemistry is modeled with Am/Nd data for Pu(III) and thorium data for Pu(IV) and these oxidation-state specific models are being strengthened to better account for the effects of organics [4-6] and high pH speciation [4, 6].

Americium, although present in much smaller quantities (~ 336 Kg is WIPP-bound) primarily as Am-241, has a significant impact on release due to its higher activity during the earlier times of repository performance. This only exists in the An(III) oxidation state, and model assessment investigations are

centered on EDTA and Citrate complexation and the identification/confirmation of the solubility controlling phase.

Thorium is a minor contributor to the overall potential release from WIPP but continues to be the An(IV) analog in the WIPP model. This remains unsatisfactory and plans to replace this with U(IV) and Np(IV) data are underway. Studies to assess the overall impacts of high pH organic species and borate on the An((IV) model are also in progress.

The only important An(V) oxidation state predicted in the WIPP is Np(V). This oxidation state was largely ignored due to inventory arguments in past recertification, but is now included. The current projected inventory is ~ 48.5 Kg but this grows in with time as this is the decay product of Am-241. Current WIPP modeling predicts that the dominant speciation in WIPP will be the acetate complex. This is being directly evaluated using site specific solubility data along with a review/experimental assessment of the organic complexation data for this actinide.

The only important An(VI) actinide is U(VI) which has a minor contribution to release in the WIPP. The WIPP has no An(VI) model but, based on concerns over carbonate speciation, the EPA has mandated a 1 mM concentration to be used in WIPP PA. The validity of this mandate is being challenged experimentally and it is expected that this will be reduced given that this is not consistent with the current understanding of carbonate effects. In the longer term, a WIPP model that accounts for hydrolysis, carbonate, borate and organic complexation is under consideration.

Lastly, the four colloid enhancement factors, which currently more than double the effective solubilities in the mobile actinide source term, have been reassessed to establish their time dependency and to reflect a broader spectrum of samples for different actinide and analog brine systems.

All of these model challenges, updates and assessments will in time lead to model updates that will provide a stronger basis for WIPP PA over the next decades of operations.

References:

[1] U.S. Department of Energy (DOE). 2019. *Title 40 CFR Part 191 Subparts B and C. Compliance Recertification Application for the Waste Isolation Pilot Plant (March)*. Appendix SOTERM. Carlsbad Field Office, Carlsbad, NM.

[2] Reed, D.T., M. Borkowski, J. Swanson, M. Richmann, H. Khaing, J.f. Lucchini and D. Ams. 2011. Redox-controlling processes for multivalent metals and actinides in the WIPP. 3rd Annual Workshop Proceedings, 7th EC FP - ReCosy CP, pp. 1-12.

[3] D.T. Reed. 2018. *Plutonium Oxidation State Distribution in the WIPP: Conceptual Model, Project-Specific Data, and Current/Ongoing Issues*. LA-UR-18-25748. Los Alamos National Laboratory; Carlsbad, NM.

[4] Yalcintas E., Gaona, X., Richmann, M.K., Dardenne, K., Altmaier, M., Reed, D.T. 2019. "Spectroscopy and Solubility of U(IV) in Dilute to Concentrated NaCl Solutions in the Presence of EDTA at pH_m 1-11." Los Alamos Report LA-UR 19-28330. Los Alamos National Laboratory, Carlsbad NM, 88220.

[5] DiBlasi, N.A.; Yalçintaş, E.; Stanley, F.E.; Reed, D.T.; Hixon, A.E. Influence of ethylenediaminetetraacetic acid on the long-term oxidation state distribution of plutonium. *Chemosphere*, **2021**, *274*, 129741. DOI: 10.1016/j.chemosphere.2021.129741Appendix SOTERM

[6] DiBlasi, N.A.; Tasi, A.G.; Gaona, X.; Fellhauer, D.; Dardenne, K.; Rothe, J.; Reed, D.T.; Hixon, A.E.; Altmaier, M. Impact of Ca(II) on the Aqueous Speciation, Redox Behavior, and Environmental Mobility of Pu(IV) in the Presence of EDTA. *J. Sci. Tot. Environ.*, **2021**, *783*, 146993. DOI: 10.1016/j.scitotenv.2021.146993.

[7] Colas, E., D. Garcia and L. Duro. 2020. "Systematic Calculation of Pu Pourbaix Diagrams: Modelling Support for the LANL ACRSP Team." Los Alamos report LA-UR-20-26859.

[8] National Academy of Sciences. 2020. Review of the Department of Energy's Plans for Disposal of Surplus Plutonium in the WIPP. National Academies Press, Washington, DC, USA.

P20. Formation of alkaline earth(II) triscarbonatouranyl(VI) complexes: thermodynamic study and ionic strength influence by time-resolved laser-induced fluorescence spectroscopy

C. Shang, P.E. Reiller

Université Paris-Saclay, CEA, Service d'Études Analytiques et de Réactivité des Surfaces (SEARS), F-91191 Gif-sur-Yvette CEDEX

pascal.reiller@cea.fr

Since their first evidence in a seepage water from a uranium mine tailing pile in 1996 [1], the formation of alkaline earth(II) triscarbonatouranyl(VI) species have been the object of extensive studies. The available data — see Grenthe, et al. [2], and references therein —were allowing to expect a dominant role of these species in various geochemical contexts [3-4]. Their presence has also been evidence experimentally [5-6].

The thermodynamic constants and functions of $^{II}M_nUO_2(CO_3)_3^{(4-2n)-}$ complexes have only recently been selected in the widely recognized commissioned review of the OECD-NEA [2]. Nevertheless, the provided extrapolation of thermodynamic constants to infinite dilution was not possible in the framework of the specific ion interaction theory, as only few systematic studies at varying ionic strength were existing. Particularly, no specific ion interaction coefficients $\varepsilon(^{II}M_nUO_2(CO_3)_3^{(4-2n)-}, {}^{I}M^+X^-)$ were proposed for these species. To circumvent this lack, some authors proposed either a charge analogy between $^{II}MUO_2(CO_3)_3^{2-}$ and $UO_2(CO_3)_3^{2-}$, or the usual null value for $^{II}M_2UO_2(CO_3)_3(aq)$, when experimental evidences already suggested more complicated patterns.

A systematic study of the formation of the $^{II}M_nUO_2(CO_3)_3^{(4-2n)-}$ complexes has been undertaken for the two most important alkaline earth metals in natural environment, *i.e.* Mg and Ca, at varying ionic strength and at equilibrium with atmospheric $CO_2(g)$. The complexometric titrations were not built using the typical mono-parameter variation, to obtain the thermodynamic constants, but were adapted to a two varying parameter, *i.e.* [Ca] *vs.* pH, to avoid $CaCO_3$ precipitation at controlled ionic strength (Figure 1a). Taking advantages of the luminescence properties of uranium(VI) in general, and of the hypsochromic shift of the triscarbonatouranyl(VI) species in particular, the formation constants of $^{II}M_nUO_2(CO_3)_3^{(4-2n)-}$ (n = {1, 2}) were determined in time-resolved laser-induced fluorescence spectroscopy (TRLFS) (Figure 1b) at varying NaCl (0.1 to 1 M) and $NaClO_4$ (0.1 to 3 M) ionic strengths [7-9]. The luminescence increase was treated by slope analyses to evidence the change in stoichiometry and complexation constants.

There is a good agreement between the literature and the newly obtained data at comparable ionic strengths. The more extensive set of data allows extrapolating the constants to infinite dilution, proposing Gibbs energies of formation under standard conditions, and proposing the corresponding $\varepsilon(^{II}M_nUO_2(CO_3)_3^{(4-2n)-}, Na^+X^-)$ values. These data are providing a complete set of parameters that are necessary to predict more accurately the uranium speciation, in wide fields of geochemical contexts, including mining applications, environmental monitoring, seawater, or radioactive waste management [4,7,9]. Particularly, the predominance domains of the different $^{II}M_nUO_2(CO_3)_3^{(4-2n)-}$ complexes can be linked to combinations of H^+, Mg^{2+}, Ca^{2+}, HCO_3^-, and Na^+ activities in solution (Figure 2).

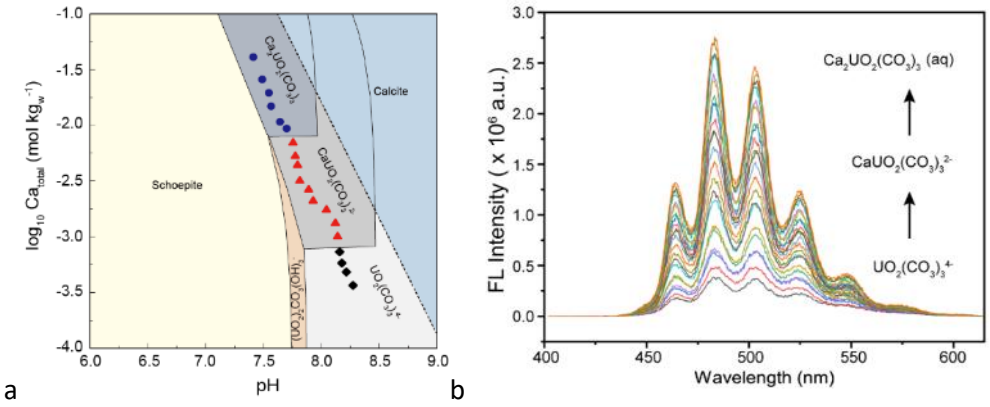

Figure 1: (a) predominance plots of Ca-UO_2-CO_3 system at [U(VI)] = 50 µmol kg_w^{-1}, $P(CO_2) = 10^{-3.5}$ atm and I_m = 0.2 mol kg_w^{-1} NaCl, experimental points giving slopes ca. 1 and 2 are highlighted with red triangles and blue filled circles, respectively. The black diamonds represent the beginning of titration where the $UO_2(CO_3)_3^{4-}$ complex dominates; (b) measured luminescence emission spectra of uranium(VI) at various calcium concentrations and pH values, $P(CO_2) = 10^{-3.5}$ atm, and I_m = 0.5 mol kg_w^{-1} NaCl; initial delay time of D = 25 ns and gate width W = 1 µs

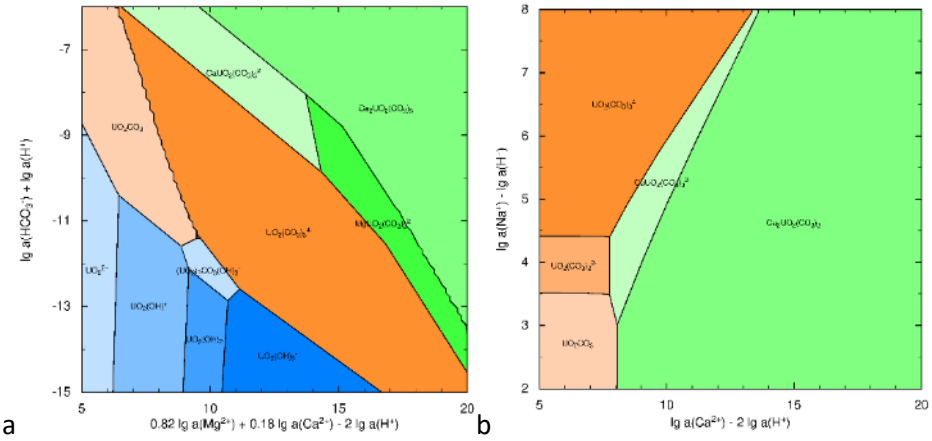

Figure 2: activity predominance plots of 10^{-6} mol kg_w^{-1} U at $P(O_2)$ = 0.21 atm: (a) at [NaCl] = 0.5 mol kg_w^{-1}; (b) lg a(HCO_3^-) + lg a(H^+) = -8.

References

[1] G. Bernhard, G. Geipel, V. Brendler, H. Nitsche, Radiochim. Acta 74 (1996) 87.
[2] I. Grenthe, X. Gaona, A.V. Plyasunov, L. Rao, W.H. Runde, B. Grambow, R.J.M. Koning, A.L. Smith, E.E. Moore, Chemical Thermodynamics 14. Second Update on the Chemical Thermodynamics of Uranium, Neptunium, Plutonium, Americium and Technetium, OECD Nuclear Energy Agency Data Bank, Eds., OECD Publications, Paris, France, 2020.
[3] M. Grivé, L. Duro, E. Colàs, E. Giffaut, Appl. Geochem. 55 (2015) 85.
[4] P.E. Reiller, M. Descostes, Chemosphere 251 (2020) 126301.
[5] O. Prat, T. Vercouter, E. Ansoborlo, P. Fichet, P. Perret, P. Kurttio, L. Salonen, Environ. Sci. Technol. 43 (2009) 3941.
[6] M. Maloubier, H. Michel, P.L. Solari, P. Moisy, M.-A. Tribalat, F.R. Oberhaensli, M.Y. Dechraoui Bottein, O.P. Thomas, M. Monfort, C. Moulin, C. Den Auwer, Dalton Trans. 44 (2015) 20584.
[7] C. Shang, P.E. Reiller, Dalton Trans. 49 (2020) 466.
[8] C. Shang, P.E. Reiller, T. Vercouter, Dalton Trans. 49 (2020) 15443.
[9] C. Shang, P.E. Reiller, Dalton Trans. 50 (2021) 4363.

Metallurgy And Materials Science

P12	**Nabeel Anwar (University of Southampton)** *"Large-Scale Quantum Mechanical Simulations for Actinide Oxides containing Defects"*
P22	**Luiza Braga Ferrreira dos Santos (HZDR)** *"Incorporation of lanthanides into zirconia: a study of solid phase transformations"*
P23	**Bradley Childs (LLNL)** *"Alternative Pathways to Produce Actinide Metals"*
P24	**Franz Freibert (LANL)** *"Glenn T. Seaborg Institute, LANL"*
P25	**Aidan Friskney (University of Sheffield)** *"Hot isostatic pressing: A thermal treatment process for Pu immobilization"*
P26	**Laura Gardner (University of Sheffield)** *"Dissolution of U-doped zirconolite: A ceramic candidate for the management of the civil UK Pu inventory"*
P27	**Zachary Levin (LANL)** *"Stress Relaxation Experiments in Plutonium"*
P28	**Michael Ling (AWE)** *"Observation on the thermal stability of a Pu-Ga alloy containing very low Ga"*
P29	**Emily Moore (LLNL)** *"Actinide Phase Diagrams: Thermodynamic Assessment of the Pu-U-Fe-Ga-Al-Ni system"*
P30	**Elanor Murray (University of Birmingham)** *"Molecular Dynamics Simulations of Helium Diffusion and Clustering in PuO_2"*
P31	**Mary O'Brien (LANL)** *"Investigating the Effect of Soluble Hydrogen on Plasticity in Uranium"*
P32	**Sandra Reinhard (Leibniz Universität Hannover, Institute of Radioecology and Radiation Protection)** *"Comparison of ^{239}Pu- and ^{242}Pu-Colloids: Influence of radiolysis on structure and stability"*
P33	**Cheng Saw (LLNL)** *"Linear Oxide Growth on a Uranium Surface at 50C"*
P34	**Scott Simpson (LLNL)** *"Small Scale Pyrochemistry with In-situ Material Doping"*
P35	**Andrew Swift (LLNL)** *"Chemical Compatibility and Characterization of Materials for Nuclear Applications"*
P36	**Vijay Varsani (AWE)** *"Plutonium Casting Modelling – Beyond the Present"*
P37	**Olaf Walter (European Commission - JRC)** *"Actinide oxalates for nano-oxides"*
P38	**Clarissa Yablinsky (LANL)** *"Comparison of Techniques for Collecting Young's Modulus Data in Alpha and Delta Plutonium"*
P39	**Stephen Parker (LANL)** *"Thermophysical Properties of Liquid Actinide Halides"*

P21. Large-Scale Quantum Mechanical Simulations for Actinide Oxides containing Defects

N. Anwar [1], R. Harker [2], M. T. Storr [2], M. Molinari [3], C.-K. Skylaris [1]

[1] University of Southampton, United Kingdom, SO17 1BJ [2] AWE, United Kingdom, RG7 4PR [3] University of Huddersfield, United Kingdom, HD1 3DH

na5g20@soton.ac.uk

Complex actinide materials play an important role within the nuclear fuel cycle, due to their thermal and chemical stability [1]. However, the high toxicity and radioactivity of actinide containing materials limits experimental investigations into their properties. Computational methods such as density functional theory (DFT), is an effective method for accurately determining their characteristics. Although conventional DFT methods are limited to calculations to just tens of atoms by unfavourable (cubic) scaling of computational effort with the number of atoms. However, the development of linear-scaling DFT methods within the ONETEP package [2], allows simulations with thousands of atoms (Figure 1).

To accurately simulate materials containing heavy, *f*-block elements, it is key to include complex electronic effects such as relativistic effects in the description of the electrons. Inclusion of relativistic effects is crucial, as this significantly influences the geometries and chemistry of these materials. In our calculations these effects are included by representing the core actinide electronic states with an effective core potential or pseudopotential. This eliminates the core states and describes the valence electrons with pseudo-wavefunctions with fewer nodes, reducing computational cost. The description of the electronic ground state of these systems, which may be strongly correlated, is further improved by a Hubbard, *U* correction. This correction reduces self-interaction errors of DFT which artificially delocalise the electrons [3], producing more accurate bandgap energies.

Actinide oxides are susceptible to radiation damage from ionising radiation, particularly from fission product nuclei and α-particles. A fission process in (U^{235}) can produce up to 60,000 defects over a 7 μm range for a heavy fission product such as Ba. An α-decay event in Am^{241} can produce ~200 defects over 15 μm for the α-particle and ~1500 defects over 20 nm from the recoil atom [4]. Other radiative processes (β, γ, neutrons) may also act to displace atoms in the structure. Defect formation influences the physical properties of actinide oxide materials, degrading their thermal and mechanical performance as a nuclear fuel [5].

Exploiting the linear-scaling performance of ONETEP, we present large scale simulations of defect containing actinide oxide materials. Of interest is the mechanical properties and performance of the material as it degrades, changing its composition over time. The aging processes and radiation damage introduce defects into the material, for which formation energies are predicted. Our investigation may then be extended, to explore transport mechanisms of intrinsic and extrinsic defects in the material.

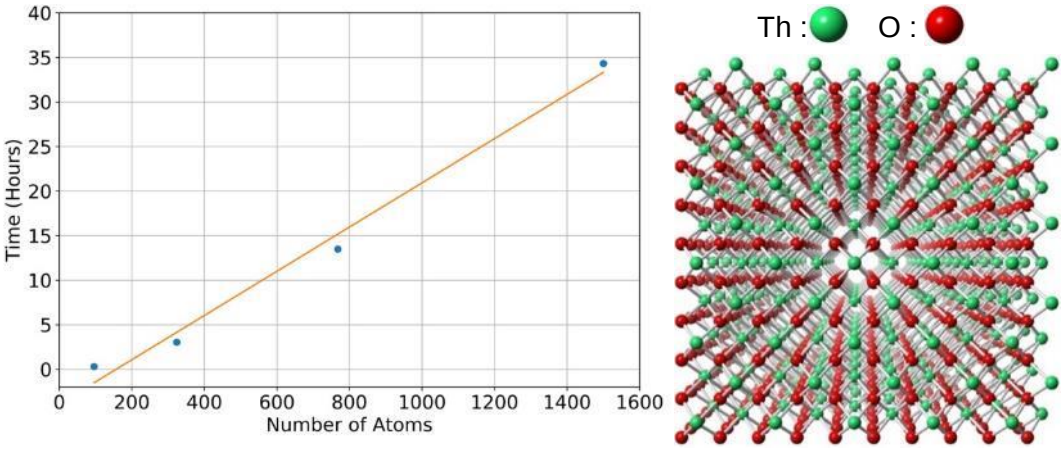

Figure 1: Scaling of computational time for ONETEP linear-scaling DFT calculations for increasing system size of ThO_2 from 96 to 1500 atoms.

[1] J. T. Pegg, X. Aparicio-Anglès, M. T. Storr and N. H. de Leeuw, *J. Nucl. Mater.*, 2017, **492**, 269-278.

[2] J. C. A. Prentice, J. Aarons, J. C. Womack, A. E. A. Allen, L. Andrinopoulos, L. Anton, R. A. Bell, A. Bhandari, G. A. Bramley, R. J. Charlton, R. J. Clements, D. J. Cole, G. Constantinescu, F. Corsetti, S. M.-M. Dubois, K. K. B. Duff, J. M. Escartín, A. Greco, Q. Hill, L. P. Lee, E. Linscott, D. D. O'Regan, M. J. S. Phipps, L. E. Ratcliff, Á. Ruiz Serrano, E. W. Tait, G. Teobaldi, V. Vitale, N. Yeung, T. J. Zuehlsdorff, J. Dziedzic, P. D. Haynes, N. D. M. Hine, A. A. Mostofi, M. C. Payne, C.-K. Skylaris, *J. Chem. Phys.*, 2020, **152**, 174111.
[3] L. Shi, E. Vathonne, V. Oison, M. Freyss and R. Hayn, *Phys. Rev. B*, 2016, **94**, 115132.
[4] H. Matzke, *Radiation Effects in Solids*, Springer, Dordrecht, 2007, ch.14, pp. 401-420.
[5] S. T. Murphy, M. W. D. Cooper and R. W. Grimes, *Solid State Ionics*, 2014, **267**, 80-87.

P22. Incorporation of lanthanides into zirconia: a study of solid phase transformations

L. B. F. dos Santos [1], J. Marquardt [2], J. Nießen [3], T. Tonnesen [3], V. Svitlyk [1, 4], C. Hennig [1, 4], T. Stumpf [1], N. Huittinen [1]

[1] Helmholtz-Zentrum Dresden-Rossendorf, Institute of Resource Ecology, Dresden, Germany. [2] Goethe-Universität Frankfurt am Main, Department of Geosciences, Frankfurt, Germany. [3] RWTH Aachen University, Institute of Mineral Engineering, Aachen, Germany [4] Rossendorf Beamline at European Synchrotron Radiation Facility, Grenoble, France.

l.braga@hzdr.de

Introduction: Zirconia (ZrO_2) is the primary corrosion product of the Zircaloy cladding material surrounding nuclear fuel rods [1]. It has also been envisioned as a ceramic host phase for specific high-level waste streams, immobilizing radionuclides and being able to become a protective barrier. In the case of doped ZrO_2 matrices, a very high radiation tolerance has been reported, however, discrepancies exist regarding the role of the different structural polymorphs in the high radiation resistance. Ce has been used as a surrogate for Pu due to comparable chemical properties in the oxidation states +III and +IV, similar ionic radius, and its easier handling [2]. In the current study, phase transformations occurring in the ZrO_2 material when doped with Ce(IV) and Gd(III), have been explored.

Methodology: Binary Ce-doped ZrO_2 ($Zr_{1-x}Ce_{1x}O_2$) and ternary Ce/Gd co-doped ZrO_2 ($Gd_yZr_{1-y}Ce_{0.18}O_2$) solid solutions have been synthesized by the co-precipitation route. In the synthesis, 0,4 g of $ZrOCl_2$ was dissolved in a 0.01 M HCl solution. An adequate amount of Ce and Gd stock solutions were added on the acidic Zr^{4+} solution. It was thereafter added to 12.5% NH_4OH, resulting in an instantaneous precipitate. The solid phases were separated via centrifugation and the precipitates were washed with MilliQ-grade water. The samples were dried and then sintered at 1,500°C for 48h to obtain a crystalline solid. The structural evolution as a function of Ce or Ce/Gd concentration was analyzed with Powder X-Ray Diffraction (PXRD). Measurements of Ce-doped samples were done on a Rigaku MiniFlex 300 diffractometer, while Ce/Gd co-doped samples were measured on PANalytical X'Pert Pro MPD. The Rietveld Refinement was done using the PDXL2 program.

Results: To know the composition of the synthesized solid phases, Rietveld refinement was performed on all samples. Table 1 summarizes the sample compositions and the results of the structural refinement. Analyzing the PXRD diffractograms presented in Figure 1, no single-phase compositions of samples doped with only cerium can be identified. The two smaller diffraction peaks seen in the sample with 18 mol% Ce, at 28.5° and 31.7°, are characteristic of the monoclinic phase. The most predominant phase, however, is the tetragonal one, with 96%, which is characterized by a diffraction peak at around 30°. In the purely Ce-doped samples, the diffraction peaks are shifted to lower 2θ with increasing Ce-concentration (from 18 to 30 mol%) due to the larger size of the Ce^{4+} cation (0.97 Å) in comparison to Zr^{4+} (0.84 Å) [3]. In addition, increasing the Ce^{4+} concentration, increases the intensity of the diffraction peak of the cubic phase around 29.3°, while the peaks of tetragonal phase decrease. The maximum cubic phase percentage obtained in the binary system was in the sample with 30 mol% of Ce. The situation changes when the cerium-doped zirconium samples are additionally co-doped with gadolinium, a larger (1.05 Å) trivalent cation, which is responsible for the creation of oxygen vacancies

in the crystal structure for charge compensation. Incorporating 5 mol% of Gd^{3+} in zirconia doped with 18 mol% Ce is enough to transform the crystal structure to a mainly cubic phase. A pure cubic phase is stabilized in the compounds with 15 mol% of Gd or more. At the same time, it is possible to see the peak of the cubic phase be shifted to lower 2θ because Gd^{3+} is a larger cation than Ce^{4+}

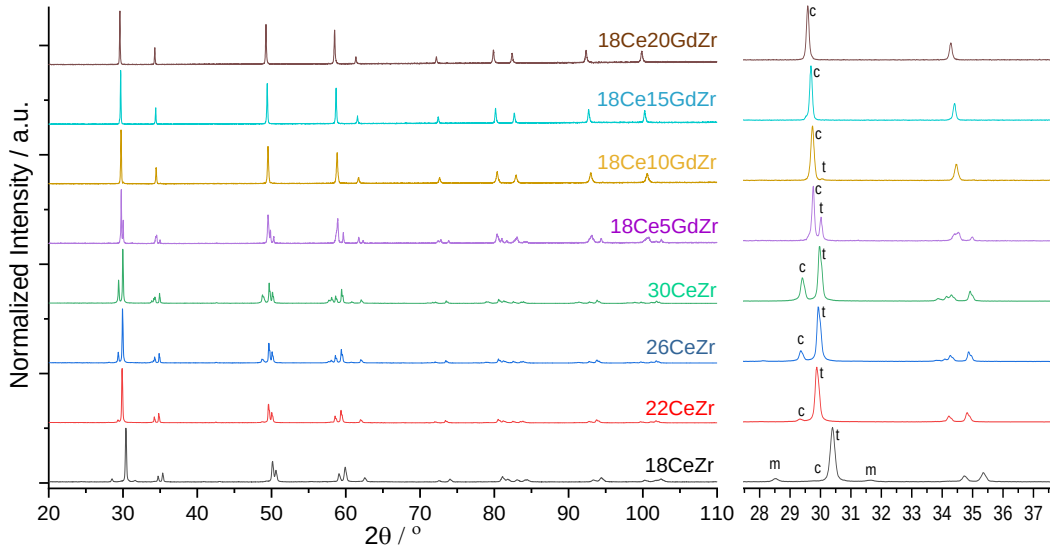

Figure 1: *X-Ray Diffraction pattern of zirconia doped with cerium and co-doped with gadolinium;*

Table 1: *Concentration of cerium and gadolinium incorporated into zirconia during the synthesis process, and the phase percentages obtained through Rietveld refinement;*

Sample name	Concentration (mol %)		Phase Percentage (%)			s
	Cerium	Gadolinium	m	t	c	
18CeZr	18	0	2	97	1	2.56
22CeZr	22	0	0	95	5	1.69
26CeZr	26	0	0	86	14	1.88
30CeZr	30	0	0	65	35	2.15
18Ce5GdZr	18	5	0	20	80	1.83
18Ce10GdZr	18	10	0	5	95	1.38
18Ce15GdZr	18	15	0	0	100	1.93
18Ce20GdZr	18	20	0	0	100	1.87

Legends: m = monoclinic ($P2_1/c$); t = tetragonal ($P4_2/nmc$); c = cubic ($Fm\bar{3}m$); s = goodness of fit

Outlook: Raman spectroscopic studies will be done to complement the structural characterizations. Thereafter, dense ceramics will be manufactured from the crystalline powders and the amorphous-precursor phases; these ceramics will be used as targets in planned irradiation studies to elucidate the radiation tolerance of the different zirconia structure types. Preliminary results from the Raman investigations and the ceramic manufacturing process will be presented at the conference.

[1] Celbová, L., Ashcheulov, et al.. Materials, 14(21), 6315, 2021.

[2] Gantenbein, M., Wang, L., et al.. Scientific reports, 7(1), 1-9, 2017.

[3] Arifin, D., et al.. International Journal of Hydrogen Energy, 45(1), 160-174, 2020.

P23. Alternative Pathways to Produce Actinide Metals

B. C. Childs [1], A. A. Martin[1], A. Perron[1], E. E. Moore[1], Y. Idell[1], T. Heo[1], D. L. Rosas[1], C. Schaeffer-Cuellar[1], R. L. Stillwell[1], P. Söderlind[1], A. Landa[1], K. S. Holliday[1], J. R. Jeffries[1]

[1] Physical and Life Sciences Directorate, Lawrence Livermore National Laboratory, Livermore, California 94550, USA

childs4@llnl.gov

The production of gram quantities of uranium metal with a controlled approach has been challenging when using traditional methods. The complexities of the chemistry involved as well as the extreme thermal conditions that precursors must endure beg the question as to whether a novel method can be used to produce this material.

Initially, uranium triiodide has been successfully used to produced uranium metal by usage of a hot filament along with an intermediate of uranium tetraiodide. In this study, a tetra-arc furnace was used to produce uranium metal from uranium triiodide. In a search for a more controlled environment that would allow for high temperature modification of material, a controlled laser heating apparatus was designed to observe the decomposition of uranium triiodide to metal.

This led to a subsequent study involving another binary uranium precursor, uranium mononitride. A computational thermodynamic approach was able to identify a pathway to decomposition by exceeding temperatures of 2500 K. Temperatures this extreme were achieved by the use of laser-induced heating. This method allowed for fine control of the heating process location and allowed for rapid cooling of the sample. Uranium mononitride was irradiated by a controlled laser under high-vacuum, argon, and nitrogen environments. Observations indicated that yields up to 96% uranium metal were produced.

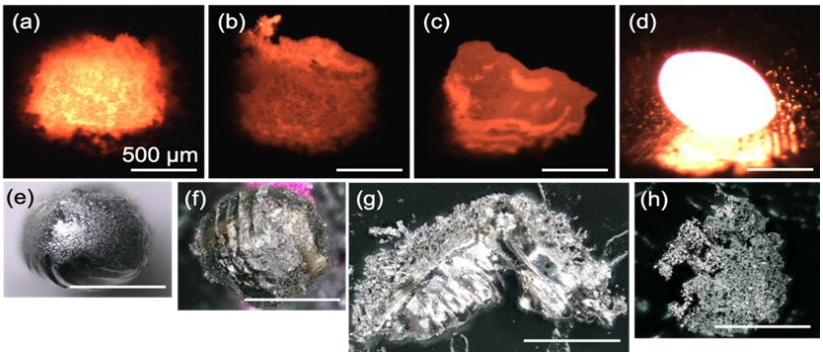

Figure 1: Laser heating of approximately 300 µm thick UN powder layer on W plate. (a-d) In situ optical images of a region of UN powder irradiated by the laser under high-vacuum. (a-c) The region was heated for (a) 30 s at 10 W laser power using a defocused beam, (b) 30 s at 20 W laser power using a defocused beam, and (c) 30 s at 50 W laser power using a defocused beam. (d) Heating at 50 W laser power with a focused beam condition. (e-h) Laser heating results of UN powder after 900 s in (e) high-vacuum, (f) argon, (g) 5% nitrogen in argon, and (h) nitrogen atmospheres. All scale bars are 500 µm

The products were confirmed based X-ray diffraction, energy-dispersive X-ray spectroscopy, and density. Residual gas analysis was also conducted in coordination with laser irradiation under high-

vacuum conditions to identify products lost during the melting process. Further results and characterization will be discussed.

This work was performed under the auspices of the U.S. Department of Energy by Lawrence Livermore National Laboratory under Contract DE-AC52-07NA27344.

[1] Childs et al. *Materials & Design*, 2020, 108706. https://doi.org/10.1016/j.matdes.2020.108706.

[2] Childs, B.C., Martin, A.A., Moore, E.E. *et al. J Radioanal Nucl Chem* **329,** 1427–1437 (2021). https://doi.org/10.1007/s10967-021-07888-5

P24. Glenn T. Seaborg Institute, Los Alamos National Laboratory

Jessica Ryan, Franz Freibert, Ping Yang, Owen Summerscales

Los Alamos National Laboratory
PO Box 1663, MS T001
Los Alamos, NM 87545

Email: seaborg@lanl.gov

The Glenn T. Seaborg Institute of Los Alamos National Laboratory (LANL) serves as an advocate for advancing actinide science, technology and engineering of the light actinide elements, with a special emphasis on plutonium. This is accomplished by integrating research programs on the chemical, physical, nuclear, and metallurgical properties, and their applications to support national, global, and energy security programs via successful collaboration of multidisciplinary fields.The Seaborg Institute strives to promote cutting edge ideas in actinide science, technology and engineering by encouraging international collaboration; by supporting and developing education and training for LANL staff, technicians, and students; and by engaging visiting scientists, researchers, and university faculty to implement its education and research mission.

The Seaborg Institute engages as a key partner at LANL, the U.S. national Plutonium Center of Excellence, and acts to address strategic plutonium and actinide mission goals and objectives. The Seaborg Institute does this by fostering closer ties with the national and international actinide research community through workshops, conferences, and an extensive visitor program. Also, we support graduate research students, postdoctoral researchers, university faculty, and other collaborators to perform fundamental and applied actinide scientific investigations. Ultimately, the Seaborg Institute serves as a catalyst to promote, expand, and strengthen basic and applied research in actinide science, technology and engineering within LANL and throughout the U.S. The LANL Seaborg Institute is one of four institutes established in the U.S. Department of Energy National Laboratories Complex.

P25. Hot isostatic pressing: A thermal treatment process for Pu immobilisation

A. Friskney, L. Gardner, L. Blackburn, A. Mason and C. Corkhill

Department of Materials Science and Engineering, The University of Sheffield, Mappin Street, Sheffield, S1 3JD, UK.

l.j.gardner@sheffield.ac.uk

Abstract

Hot Isostatic Pressing (HIPing) is a batch thermal treatment process where wastes are heated and compressed within a sealed container resulting in consolidated durable, high density wasteforms with minimal loss of volatile elements and easy accountability of active inventory [1]. In the UK, HIPing was highlighted as one of the credible options for plutonium immobilisation in a ceramic matrix, in the event that disposal is chosen as a Pu management strategy [2]. To help inform the science underpinning larger-scale industrial applications of this technology, the University of Sheffield invested in a small-scale HIP facility capable of processing radiological simulant wasteforms (U and Th) at a ~10-50 g scale using an active isolation chamber (AFIC) [3]. The AFIC is designed to function within a conventional HIP set up and provides a unique UK opportunity to fabricate and characterise conceptual radioactive wasteforms and gain experience with radiological HIPing. It was under this remit that twelve HIP wasteforms were fabricated using Ce or U (as Pu surrogates) to validate the outcome of a broad research portfolio targeting a modified zirconolite ($CaZrTi_2O_7$) as a single host ceramic wasteform for Pu immobilisation. These trials allowed for an assessment of the bulk phase assemblage, HIP canister-ceramic interactions, surrogate efficacy and ultimately, zirconolite formulation refinement. This formulation will be fabricated using ^{242}Pu (and traditional sintering methods) in the near future to complete the small-scale validation process [4]. Overall, Ce and U surrogates were found to yield robust zirconolite ceramic wasteforms *via* HIPing.

[1] M.W.A. Stewart, S.A. Moricca, T. Eddowes, Y. Zhang, E.R. Vance, G.R. Lumpkin, M.L. Carter, M. Dowson, M. James, The use of hot-isostatic pressing to process nuclear waste forms, Proceedings of the 2009 12th International Conference on Environmental Remediation and Radioactive Waste Management ICEM2009, Liverpool, UK, 2009, pp. ICEM2009-16253.
[2] Nuclear Decommissioing Authority, Progress on plutonium consolidation, storage and disposition 2019.
[3] S. Moricca, R. Persaud, Active Furnace Isolation Chamber, WO 2018/009782 A1, 2018.
[4] N.C. Hyatt, C.L. Corkhill, M.C. Stennett, R.J. Hand, L.J. Gardner, C.L. Thorpe, The HADES facility for high activity decommissioning engineering & science: Part of the UK national nuclear user facility, IOP Conference Proceedings: Materials Science and Engineering 818 (2020) 012022.

P26. Dissolution of U-doped zirconolite: A ceramic candidate for the management of the civil UK Pu inventory

L. Gardner, A. Mason, L. Blackburn, I. Aldean and C. Corkhill

Department of Materials Science and Engineering, The University of Sheffield, Mappin Street, Sheffield, S1 3JD, UK.

amber.mason@sheffield.ac.uk

A semi-dynamic dissolution experiment was performed using the ASTM C1308 methodology to investigate the aqueous durability of a baseline zirconolite formulation targeting plutonium immobilisation for the existing UK Pu inventory [1]. Zirconolite ($CaZrTi_2O_7$) was highlighted as a potential single phase ceramic host for plutonium, due to the formation of a passively safe wasteform, with Pu incorporation achieved *via* substitution of another element within the zirconolite framework, namely Ca^{2+} and Zr^{4+}. Zirconolite is known to be chemically flexible and radiation tolerant with excellent aqueous durability, however, further underpinning research is required to support national programmes and understand the evolution of plutonium during immobilisation and disposal [2]. In this study, a tailored U-doped zirconolite (using U as Pu surrogate) ceramic was investigated, due to the complexity associated with handling Pu (e.g. security, laboratory access, costs, toxicity). The ASTM C1308 dissolution trials investigated a wide test matrix with varying temperature (40, 60, 90 °C) and dissolution media (low pH, groundwater and high pH). These parameters were chosen to encompass the possible geological disposal conditions that may occur if Pu immobilisation, and ultimately disposition, was deemed a viable resolution in the UK for i) material unsuitable for reuse in MOX fuel or ii) a larger portfolio of the civil UK Pu inventory [3]. The results contributed to our fundamental understanding of the ASTM C1308 methodology and supported the development of a standard operating procedure for round robin experiments with partners worldwide to further verify the efficacy and reproducibility of this methodology (allowing direct comparison between formulations and different wasteforms) to support safety case considerations for Pu immobilisation and disposition.

[1] ASTM, C1308-21 Standard test method for accelerated leach test for measuring contaminant releases from solidified waste, ASTM International, 2021.
[2] N.C. Hyatt, Safe management of the UK separated plutonium inventory: a challenge of materials degradation, npj Materials Degradation 4(28) (2020).
[3] Nuclear Decommissioing Authority, Progress on plutonium consolidation, storage and disposition 2019.

P27. Stress Relaxation Experiments in Pu

T. Jacobs [1], Z. Levin [1], C. Yablinsky [1]

[1] Materials Science and Technology Division, Los Alamos National Laboratory, P.O. Box 1663, Los Alamos, NM 87545, USA

tayjacobs@lanl.gov

Processing and aging related metallurgical defects in δ-phase Pu-Ga alloys were characterized using the stress relaxation technique. Stress relaxation is a mechanical testing technique that measures the activation volume and internal/effective stress components of the flow stress during plastic deformation [1, 2]. Activation volume is the volume of material swept by dislocations during plastic deformation. The microscopic mechanism governing the plastic deformation can be deduced from the activation volume and is a relative measure of the dislocation structure of a material [2]. The internal and effective stress components of the flow stress are related to long- and short-range barriers to dislocation motion, respectively [1, 3]. Examples of long-range barriers to dislocation motion in δ-phase Pu-Ga alloys are forest dislocations, prismatic dislocation loops, helium bubbles, and grain boundaries. Examples of short-range barriers to dislocation motion are substitutional atoms from alloying (e.g. gallium) or radioactive decay (e.g. uranium), self-interstitials, and the Peierls stress [4].

For this investigation two 13-year-old cast and homogenized δ-phase Pu-Ga alloys, with 0.6 and 1 wt% Ga, were studied and compared to 1100Al-O for reference. Material in aged and heat treated conditions were investigated to determine the viability of stress relaxation for defect characterization. Heat treatments were designed to either anneal out point defects at 120 °C or to grow helium bubbles while causing dislocation recovery at 340 °C.

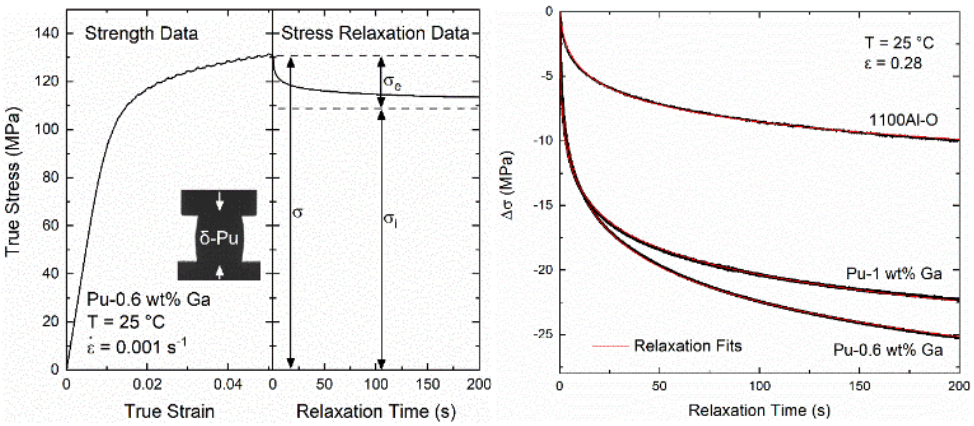

Figure 1: Left) Example true stress-true strain and true stress-relaxation time data of a stress relaxation experiment from as-aged Pu-0.6 wt% Ga. The shadowgraph shows the δ-Pu sample in-between the compression platens after approximately 0.35 true strain. The dashed lines indicate the flow stress at t = 0 s and the extrapolated internal stress. Right) Stress relaxation curves and their fits of 1100Al-O, Pu-0.6 wt% Ga, and Pu-1 wt% Ga at 0.28 true strain.

Table 1: Comparison of Stress Relaxation Properties between 1100Al-O and Pu-Ga Alloys

Sample	b (nm)	V_{app}	$\sigma_{0.25}$ (MPa)	σ_i (MPa)	σ_e (MPa)
1100Al-O	0.287	$295b^3$	118.0	84.6	24.7
Pu-0.6 wt% Ga	0.328	$90b^3$	131.8	72.1	59.7
Pu-1 wt% Ga	0.328	$98b^3$	146.6	98.2	48.4

The Pu-Ga alloys exhibited substantially larger relaxation magnitude than the 1100Al-O sample, resulting in much greater effective stress values. High effective stress values indicate that Pu-Ga alloys receive greater amounts of their strength from defects with short range stress fields [1,3].

Effect of thermal annealing on stress relaxation in Pu-Ga alloys.

Both alloys exhibited an increase in the yield strength after the 120 °C heat treatment, and a decrease in yield strength with a 340 °C anneal. In addition, annealing at 120 °C, the normalized effective/internal stress and activation volume values did not change from as-aged. Indicating that both long- and short- range defects contribute more to strength in the 120 °C condition compared to as-aged material. It is hypothesized that a strain aging phenomenon and helium bubble growth at 120 °C are responsible for the increase in strength. It is unlikely that significant dislocation recovery occurred at this temperature because there was no change in the apparent activation volume compared to the as-aged condition.

The reduction in the yield strength after the 340 °C heat treatment was accompanied with a decrease in the normalized effective stress, increase in the normalized internal stress, and larger apparent activation volume values. The increase to the activation volume relative to the as-aged condition supports the dilatometry results that indicated dislocation recovery that began at temperatures greater than 150 °C. The increase in the normalized internal stress values indicate further He bubble growth occurred. As the annihilation of dislocations would result in a decrease in the internal stress, the strength gained from He bubble growth overpowered the influence of recovery. The 340 °C heat treatment also accommodated the annihilation of point defects (likely vacancies and self-interstitials), which was indicated by the reduction in the normalized effective stress relative to the as-aged condition.

These results indicate that stress relaxation technique can be used to investigate defect evolution in natural aging material.

References

[1] Gupta, I., and J. C. M. Li. "Stress relaxation, internal stress, and work hardening in some bcc metals and alloys." *Metallurgical Transactions* 1.8 (1970): 2323-2330.

[2] Cha, Hyun-Suk, Bin Yu, and Yong-Keun Lee. "Changes in stress relaxation property and softness of soft denture lining materials after cyclic loading." *Dental materials* 27.3 (2011): 291-297.

[3] Findley, William N., and Francis A. Davis. *Creep and relaxation of nonlinear viscoelastic materials*. Courier corporation, 2013.

[4] Arsenlis, A., W. G. Wolfer, and A. J. Schwartz. "Change in flow stress and ductility of δ-phase Pu–Ga alloys due to self-irradiation damage." *Journal of nuclear materials* 336.1 (2005): 31-39.

[5] Hecker, S. S., D. R. Harbur, and T. G. Zocco. "Phase stability and phase transformations in Pu–Ga alloys." *Progress in Materials Science* 49.3-4 (2004): 429-485.

P28. Observation on the thermal stability of a Pu-Ga alloy containing very low Ga

Michael Z. Ling

AWE plc, Aldermaston, Reading, Berkshire, RG7 4PR, UK

Two types of thermal treatment, namely hot cycling (between 20 ˚C to 90 ˚C) and cold cycling (between 20 ˚C to -50 ˚C) were performed on two previously long-time annealed and aged Pu-0.18 wt. % Ga alloy samples that had the mixed structure of α+δ, respectively. Following each thermal cycling, the density of the samples was measured at ~20˚C. It was found that the density of the samples increased after both cold treatment and heat treatment as shown in Figurs.1 and 2. The density increase introduced is believed to be due to the occurrence of phase transformation of the meta-stable phase δ within the mixed phase structure. However, the phase transformation mechanism with cold and hot cycling is different.

The δ→α' phase transformation is responsible for the density increase during cold cycling whilst the δ→α phase transformation, as currently believed by the author, is the cause for the density increase during hot cycling. The occurrence of the δ→α phase transformation in this low Ga content alloy at a temperature (90 ˚C) lower than the typically accepted eutectoid temperature of 97 ˚C for this Pu-Ga alloy may indicate that either the Ga diffusion within Pu can be accelerated through thermal cycling or the Ga diffusion coefficient is actually higher than previously thought.

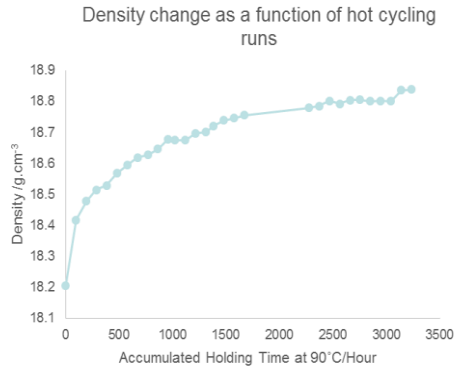

Fig.1 The density of the Pu-0.18 wt. % Ga alloy increases with hot cycling runs.

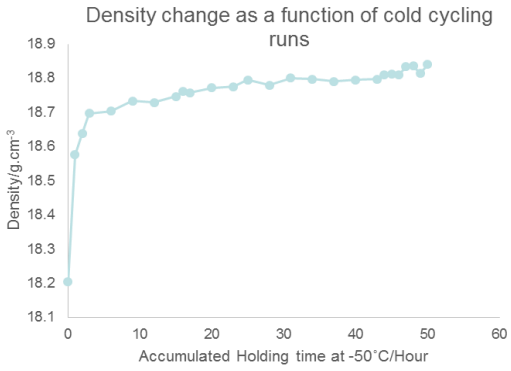

Fig.2 The density of the Pu-0.18 wt. % Ga alloy increases with cold cycling runs.

P29. Actinide Phase Diagrams: Thermodynamic Assessment of the Pu-U-Fe-Ga-Al-Ni system

E.E. Moore [1], A. Landa [1], P. Söderlind [1], S.A. Stout [1] A. Perron [1]

[1] Lawrence Livermore National Laboratory 7000 East Avenue, Livermore, CA USA

moore255@llnl.gov

Minor additions of alloying elements such Ga and Al have proven to stabilize the high temperature δ-Pu phase down to room temperature, while also increasing its ductility and melting point [1]. The complex phase behaviour of Pu-alloys are of interest across the nuclear community where the properties and performance of actinides under normal, accident or aging conditions depend on chemical composition and temperature among other factors, such as self-irradiation. This work includes the study of Pu alloyed with U, Ga, Al, Fe, Ni, with the latter elements acting as impurities in minor amounts (up to 1000 ppm). The solubility of these elements within Pu-Ga alloys is important as it determines the maximum amount of impurity before additional compounds form (Pu_6Fe and $PuFe_2$ as an example). Experimental information on the Pu-U-Ga-Fe [2] and Pu-U-Ga-Al [3] systems are reviewed and *ab initio* informed CALPHAD (CALculation of PHAse Diagrams) assessments are performed. Phase diagrams of the reassessed Pu-U-Fe and newly assessed Fe-Ga are presented in Figure 1. A thermodynamic database of the Pu-U-Fe-Ga-Al-Ni system is presented. The addition of Ni alloys for the development of a complete multicomponent database which aids in predicting phase behaviour across temperature and compositions ranges is presented, Scheil solidification simulations and property diagrams are included to show the effects of the various alloying elements

Prepared by LLNL under Contract DE-AC52-07NA27344.

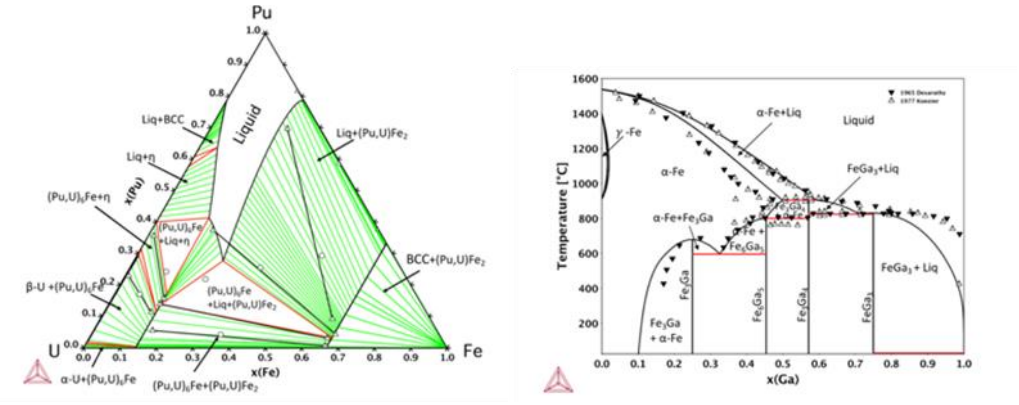

Figure 1: Reassessed phase diagrams [2] for the (a)Pu-U-Fe phase diagram at 650 °C compared to experiment [4] and (b) newly assessed [2] Fe-Ga phase diagram compared to experiment [5,6]

[1] S.S. Hecker *et al*., Los Alamos Science, 6 (2000) p.316.
[2] E.E. Moore *et al.*, Applied Sciences, 9 (2019)
[3] A. Perron *et al*., Journal of Nuclear Materials, 482 (2016) p. 187.
[4] K. Nakamura et al., Journal of Phase Equilibria and Diffusion, 22 (2209) p. 259
[5] C. Dasarathy, *et al*., *Proceedings of the Royal Society London, Series. A 286* (1965) p. 141
[6] W. Köster,*et al.*, Zeitschrift für Metallkunde 68 (1977) p. 582.

P30. Molecular Dynamics Simulation of Helium Diffusion and Clustering in PuO_2

E. Murray [1], P. Slater [1], Y. Zhou [2], P. Goddard [2], R. Smith [2], H. Steele [3]

[1] University of Birmingham, Birmingham, UK [2] Loughborough University, Loughborough, UK [3] Sellafield Ltd, Seascale, UK

School of Chemistry, University of Birmingham, Birmingham, B15 2TT, UK

exm350@student.bham.ac.uk

Until the UK Government arrives at a decision regarding the final treatment and disposition of Pu, the NDA remain responsible for the "safe and secure storage" of PuO_2 currently in inert steel cans at Sellafield [1]. Radiogenic helium gas generation naturally occurs in the ageing of PuO_2 due to the spontaneous alpha decay of Pu isotopes, creating self-radiation damage to the lattice. The risk of helium gas pressurisation is a safety concern for long-term storage of Pu oxides. Hence, fundamental understanding of helium behaviour, including its generation, incorporation and release, is needed [2]. Atomistic simulation techniques are ideally suited to provide fundamental insight into the defect chemistry of helium incorporation in PuO_2.

Molecular dynamics has been used to model helium migration pathways through the lattice. It was found that interstitial site hopping is assisted by oxygen vacancies. Helium diffusion was modelled over a range of temperatures and defect concentrations for 5 ns, finding plutonium vacancies act as traps, which drastically reduce helium diffusivity. Finally, multiple computational techniques were used to investigate helium clustering. In the majority of helium clusters, the number of vacancies exceeds the number of trapped helium atoms. When a cluster exceeded a ratio of 4:1 helium atoms to vacancies, the cluster was no longer energetically stable.

[1] NDA, *Progress on Plutonium Consolidation, Storage and Disposition,* March 2019.
[3] W. G. Wolfer, *Los Alamos Science,* no. 26, pp. 274 – 285, 2000.

P31. Investigating the Effect of Soluble Hydrogen on Plasticity in Uranium

M. K. O'Brien, S. K. Lawrence, J. Cooley, B. Clausen, D. Brown [1]

[1] Los Alamos National Laboratory, PO Box 1663, Los Alamos, NM 87545

mkobrien@lanl.gov

INTRODUCTION Hydrogen embrittlement (HE) is a long-standing challenge in metallurgy due to unpredictable failures observed in numerous metallic systems exposed to hydrogen containing environments. Uranium has an exceptionally low solubility for hydrogen such that even prolonged exposure to humid environments can drastically affect ductility [1,2]. Ductility loss is attributed to any combination of the following: formation of brittle hydrides (UH_3) upon supersaturation [3], decohesion along boundaries due to trapped hydrogen [4,5], or hydrogen enhanced localized plasticity (HELP) due to soluble hydrogen [6,7]. The mechanism by which HELP occurs is not well understood. Diffusible hydrogen may depress the stress necessary for transition from elastic to plastic flow on specific crystallographic planes. Uranium, with its low symmetry crystal structure, presents a unique opportunity to observe the proposed hydrogen-induced early-onset plasticity without added complications of slip system interactions that occur in most engineering materials. However, because only one slip system is available at room temperature, uranium twins readily at strains well below the traditionally defined yield stress. In warm-rolled plate however, textural differences result in compression samples strained in the normal direction exhibiting significantly less twinning than samples strained in either of the directions of the rolling-transverse plane investigated in [8].

EXPERIMENTAL PROCEDURE This work seeks to understand the effect of soluble hydrogen on slip initiation in a low symmetry crystal system, using depleted uranium (DU) as the model material. Small cylinders (3.96 mm diameter 7.5 mm long) for compression testing were extracted from a pedigreed warm-rolled DU plate using electrical discharge machining (EDM) and turned to final dimensions, thereby removing the EDM recast layer. Coupons were machined with the long axis parallel to the plate normal direction of pedigreed warm-rolled DU plate. Straining along the normal direction was chosen so that twinning could be reduced as much as possible. *In-situ* lattice strain measurements during compression tests were obtained at the Los Alamos Neutron Science Center (LANSCE) using the Spectrometer for Materials Research at Temperature and Stress (SMARTS). Crystallographic texture of the coupons before testing was measured at the High-Pressure-Preferred Orientation instrument (HIPPO). All samples were vacuum annealed at 630 °C for 1 hr. Some samples were then charged with hydrogen at 630 °C for 2 hours, while other samples experienced a continued vacuum anneal hold for 2 hours. Heat treatments for both the hydrogen charged and uncharged conditions were finished with a water quench. Hydrogen was charged using a mixed gas of 99% Argon 1% Hydrogen. Hydrogen content testing for samples charged to greater than 1 ppm hydrogen was conducted using LECO ONH836 analyzer. Samples charged with less than 1 ppm hydrogen will be tested for hydrogen content using a high resolution thermal desorption spectrometer currently being developed in house.

RESULTS *In-situ* lattice strain data was obtained from both uncharged specimens and specimens pre-charged to a calculated concentration of 0.2 ppm. Macroscopic stress strain curves, shown in Figure 1a, did not reveal any difference in compression behavior between the uncharged and charged

(0.2ppm) specimens. The serrations present in Figure 1a are due to stress relaxation during the static hold required to obtained neutron diffraction at a particular stress. The strain data from individual crystallographic planes was determined, as shown in Figure 1b, and no differences were observed between the hydrogen charged (0.2 ppm) and the uncharged specimens. It is possible that the desired 0.2 ppm of soluble hydrogen was not achieved, so quantification of hydrogen content using a LECO ONH836 analyzer is in progress. Additionally, it should be noted that the high temperature heat treatment is above the temperature for recrystallization and as such could significantly reduce the available dislocation density that could contribute to early onset slip. Electron backscatter diffraction will be used to estimate the change in geometrically necessary dislocation (GND) density due to heat treatment, and inform future heat treatments. It is also possible that no difference was observed upon hydrogen charging because the initially chosen hydrogen concentration of 0.2 ppm is insufficient to induce a measurable effect on incipient plasticity in a microstructure with limited dislocation content. Therefore, a second testing campaign is in progress to assess the effect of higher concentrations of hydrogen (up to ~5 ppm) on compression behavior. This campaign will consider additional times and temperatures for hydrogen charging to increase available dislocation density and will utilize traditional *ex-situ* compression testing. Pre and post-mortem microstructural analysis using EBSD will be conducted to visualize GND density and distribution to further inform any effect of hydrogen on slip localization.

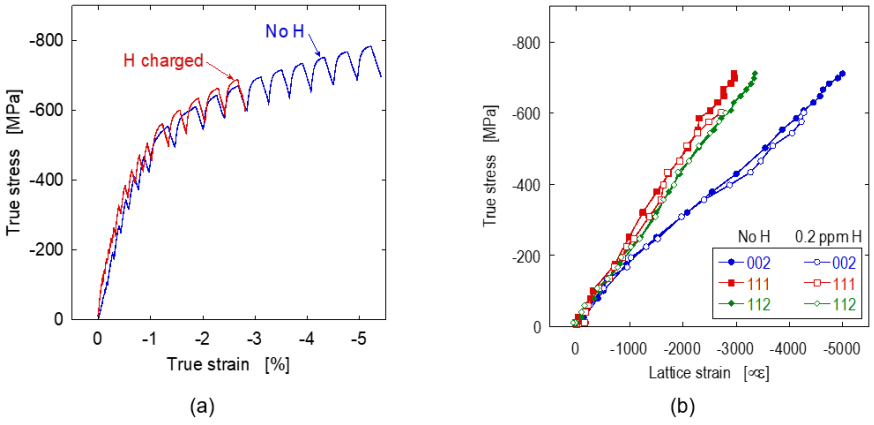

Figure 1: Stress strain curves (a) and elastic lattice strains on individual crystallographic planes (b) from the in-situ compression tests at SMARTS on samples in both the uncharged and hydrogen charged to 0.2 ppm condition.

REFERENCES

[1] J. A. Lillard and R. J. Hanrahan, “Corrosion of Uranium and Uranium Alloys,” in *ASM Handbook*, vol. 13B, ASM International, 2005, pp. 370–384.
[2] S. Morrell and M. J. Jackson, Eds., *Uranium Processing and Properties*. New York, NY: Springer New York, 2013. doi: 10.1007/978-1-4614-7591-0.
[3] W. D. Davis, “Solubility, Determination, Diffusion and Mechanical Effects of Hydrogen in Uranium,” KAPL-1548, 4340162, Aug. 1956. doi: 10.2172/4340162.
[4] R. Gangloff, “Hydrogen Assisted Cracking of High Strength Alloys,” *Comprehensive Structural Integrity*, vol. 6, pp. 31–101, 2003.
[5] R. A. Oriani, “Hydrogen Embrittlement of Steels,” *Annual Review of Materials Science*, vol. 8, pp. 327–357, 1978.
[6] H. K. Birnbaum and P. Sofronis, “Hydrogen-enhanced localized plasticity—a mechanism for hydrogen-related fracture,” *Materials Science and Engineering: A*, vol. 176, no. 1–2, pp. 191–202, Mar. 1994, doi: 10.1016/0921-5093(94)90975-X.
[7] I. M. Robertson, “The effect of hydrogen on dislocation dynamics,” *Engineering Fracture Mechanics*, vol. 68, pp. 671–692, 2001.
[8] R. J. McCabe, L. Capolungo, P. E. Marshall, C. M. Cady, and C. N. Tomé, “Deformation of wrought uranium: Experiments and modeling,” *Acta Materialia*, vol. 58, no. 16, pp. 5447–5459, Sep. 2010, doi: 10.1016/j.actamat.2010.06.021.

P32. Comparison of ^{239}Pu- and ^{242}Pu-Colloids: Influence of radiolysis on structure and stability

S. Reinhard [1], M. Hedberg [2], I. Perrson [3], J. Rothe [4], C. Ekberg [2], C. Walther [1]
[1] Institute of Radioecology and Radiation Protection, Leibniz University Hannover, D-30419 Hannover, Germany
[2] Chemistry and Chemical Engineering, Nuclear Chemistry, Chalmers University of Technology, SE-41296 Göteborg, Sweden
[3] Department of Chemistry, Swedish University of Agricultural Sciences, SE-75007 Uppsla, Sweden
[4] Institute for Nuclear Waste Disposal, Karlsruhe Institute of Technology D-76131 Karlsruhe, Germany
reinhard@irs.uni-hannover.de

Scientific Background

In aqueous solution several plutonium oxidation states and species with different properties can be present simultaneously under suitable conditions, which makes the aqueous chemistry of Pu particularly challenging. In addition to aqueous species colloids may form, for instance in solutions oversaturated with respect to tetravalent plutonium. Due to their greatly increased mobility, theser´intrinsic Pu colloids play an important role in the context of waste disposal.[1,2]

Formation processes and stability are still conversely discussed in the literature. Previous studies[1,3], executed independently of each other, showed different results in the formed structures and colloid's stability in the solution.[2,4] Furthermore, these studies were carried out using different acids and acid strengths, which hinders comparability. Another important parameter is the specific activity of the different plutonium isotopes, which might have a greater than expected influence on the aging process of the plutonium colloids: It is assumed that radiolysis has a major effect on the surface redox reactions and consequently on decomposition of colloids and therefore long-term stability.[1,3,4]

In this research, colloidal solutions of ^{242}Pu and a mixture consisting of ^{239}Pu and ^{238}Pu are prepared. The influence of the pH environment (from 0.55 to 1.1), media (nitric, hydrochloric, and chloric) and three different preparation methods was investigated systematically. Colloids are often produced from a strongly acidic Pu(IV) stock solution by pH increase to the point where the solubility limit is reached. The pH can be increased quickly by adding water or sodium hydroxide or slowly by dilution with a highly diluted acid.[1,3] Another way to produce Pu colloids is described in the publication of Knopp and co-authors.[5] Hydrogen peroxide is added to a Pu(VI) solution and the formation of the Pu(IV)-colloids is observed as a consequence of Pu reduction.[5]

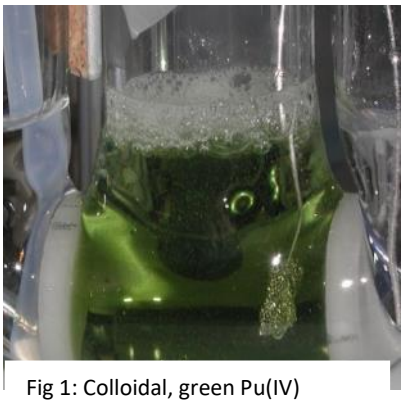

Fig 1: Colloidal, green Pu(IV) solution prepared by electrolysis.

Especially the size and structure of the colloids are considered and compared. The ageing processes of all plutonium isotopic compositions are continuously examines by monitoring the colloidal solutions.

Sample preparation

One ^{242}Pu solution, available from earlier colloid experiments, and different mixtures containing ^{239}Pu and ^{238}Pu are used for this study.

For the first method, hydrofluoric acid is added to the ^{242}Pu solution to dissolve all colloids formed before. The solutions are heated to dryness and evaporated several times with concentrated HNO_3 and subsequently dissolved in 3 M HNO_3. In order to remove metal contaminations, an ion exchange resin Dowex 1x4 is used. The Pu is eluted by changing oxidation state. After heating to dryness the residue is diluted in 2 % HNO_3 and provides the basis as a purified Pu stock solution for the following colloid investigation. The stock solutions is characterized by mass spectrometry with inductively coupled plasma (ICP-MS).

To get a Pu(IV) solution, the stock solution is heated to dryness and taken up twice with concentrated HNO_3. A yellow residue indicates the formation of Pu(VI). After dissolution of the residue with HNO_3, a Pu(IV) solution is produced electrolytically. The electrolysis cell contains a Pt disk working electrode, a Pt wire auxiliary electrode and a Ag/AgCl reference electrode. The oxidations states are monitored by UV/VIS measurements. The Pu(IV) stock solution is filtered through a 10 kDa microfilter with cellulose membrane to avoid measuring previous formed colloids or pseudocolloids. Pu colloids are generated by increasing the pH value and exceeding the solubility limit. A semi-concentrated sodium hydroxide solution is added to the strongly acidic Pu solution, raising the pH value from 0.3 to approximately 2.

In a second series of experiments, a similar procedure is used with an isotope mixtures of Pu(IV) containing ^{239}Pu as a base with different amounts of ^{238}Pu to increase the total alpha activity. The experiments were performed in different background solutions, hydrochloric and nitrate acid. Plutonium colloids are produced by adding sodium hydroxide solution until a green plutonium colloidal suspension is readily formed.

The third method starts with a Pu(VI) stock solution. The initial oxidation state is created by electrolysis as described above. A few minutes after addition of small amounts of hydrogen peroxide the reduction of Pu(VI) to Pu(IV) and colloid formation are observed by UV/Vis spectroscopy.

Methods and expected results

The concentration and purity of ^{242}Pu stock solutions are determined by α-spectroscopy and ICP-MS. The ^{239}Pu and ^{238}Pu stock solutions are characterized by using α-spectroscopy.

To elucidate the earlier different results related to colloid formation and the influence of radiolysis, the oxidation state is continuously monitored by UV/Vis measurements, so the ageing process can be traced. In order to get insights into the formation processes and structures of plutonium colloids with different plutonium isotopes in various media, Pu L_3-edge EXAFS are performed at the ANKA beam-line at Karlsruhe Institute of Technology (KIT) and at the Balder beam-line in collaboration with Chalmers University. First results of these measurements comparing 242Pu-, ^{239}Pu- and the isotope mixture colloids in nitric and hydrochloric acid will be presented.

References

[1] C. Walther et al., (2008), Plutonium futures – The Science 2008, 19-22
[2] K. Kvashnina et al., (2019), Angewandte Chemie - International Edition
[3] C. Ekberg et al., (2013), Dalton transactions 42, 2035-2040
[4] J. Rothe et al., (2004), Inorganic Chemistry 43, 4708-4718
[5] R.Knopp et al. (1999), Radiochim. Acta 86, 101-108

P33. Linear Oxide Growth on a Uranium Surface at 50C

Cheng K. Saw and Wigbert J. Siekhaus

Lawrence Livermore National Laboratory, 7000 East Ave, Livermore, CA

saw1@llnl.gov, siekhaus1@llnl.gov

In our previous grazing-angle x-ray diffraction experiment we calculated oxide thickness growth from the attenuation of the metal's diffraction peaks and reported at 50C isothermal treatment parabolic growth up to about 0.3 μm at approximately 50 hours, whereupon faster growth appeared which followed linear growth behavior. For many years, this linear growth rate, observed by many investigators at much later exposure time, has been described as due to the existence of cracks or void channels caused by stress buildup because of lattice mismatch leading to much quicker oxygen diffusion to the metal surface and resulting in faster oxidation growth, linear with time. This has often been described as "short circuit" or "breakaway" growth. However, the underlying mechanism at the atomic level causing this behavior has still not been fully understood. In this paper we present an analysis of our diffraction data indicating that the breakaway phenomenon we deduce from the reduction of the metal's diffraction peaks is unlikely to be due to cracks in the oxide layer. Instead, our x-ray model calculations indicate that the change in x-ray intensity used to calculate the oxide thickness, may just be due to atom rearrangements in the oxide layer from hypo-stoichiometry, to stoichiometry, and finally hyper-stoichiometry.

INTRODUCTION

Earlier, we reported [1] that during the early stages of the oxide growth at 50 C the thickness derived from the attenuation of the U-metal x-ray diffraction signal followed a parabolic behavior for 50 hours when the thickness was below 0.3 μm. Above 0.3 μm the oxide growth rate increased suddenly, and followed a linear relationship. This "breakaway" phenomenon is typically not observed that early at low temperatures for thin oxide layers [2], neither by ellipsometry up to 0.7 μm [3] nor by the weight gain measurements by Bennett et. al. [4] or Waber [5], nor by us using white light interferometry, as shown by the black, red, green vertical bars in figure 1. However, Zalkind et. al. [6] using conventional x-ray diffraction at 90C, also reported parabolic followed by linear oxidation growth at approximately 50 hours. This growth change was interpreted as a faster reaction due to existence of micro-cracks which enhance the transport of the oxygen ions to the uranium surface for further oxidation. The cracks were caused by the stress buildup due to lattice mismatch.

Chernia et. al. [7] determined that the x-ray diffraction peaks deviated from the ideal relaxed uranium oxide powder peaks which led them to postulate the existence of an anisotropic internal stress field causing large atomic holes which enable oxygen atoms to be transported via a mechanism they called "ion hopping" that drastically increased the oxidation rate.

In this paper, we present a detailed analysis of the x-ray diffraction signal and suggest that it is unlikely that cracks are the major contributing factor for the calculated linear increase in oxide thickness derived from the attenuation of uranium's x-ray signal. We propose instead that the change in x-ray peak intensity which is used to calculate the oxide thickness may be due to rearrangement of uranium and oxygen atoms in the FCC crystal structure from hyper-stoichiometric to fully occupied UO_2

structure. The attenuated intensity of the uranium substrate's peak is the result of additional scattering in the oxide layer.

EXPERIMENTAL

We used grazing incident x-ray diffraction and employed a curved position-sensitive detector to capture the spectrum. The sample is mounted on a special chamber with flowing dry air. The sample temperature is maintained at 50C. Data acquisition and temperature control are fully automated, thus making this setup easy to run with improved accuracy. White light interferometer was used to physically measure the oxide thickness from a different sample which underwent the same environmental conditions.

RESULTS AND DISCUSSION

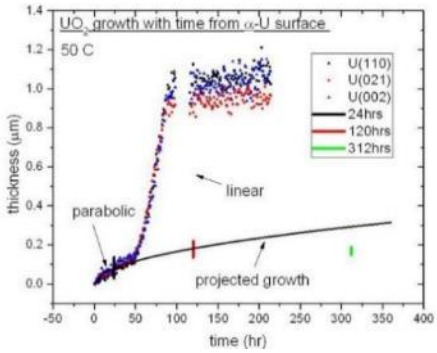

Figure 1: Oxide thickness extracted from the attenuation of the uranium metal peaks. The black vertical bar in the parabolic region, and the red and green vertical bars in the projected growth region are white light interferometry thickness measurements.

Figure 1 shows the calculated growth of the oxide thickness over time. The thickness calculation is based on the attenuation of the 3 major uranium diffraction peaks according to Zalkind et. al. [6]. As observed, the calculated oxide growth follows parabolic behavior up to about 0.3μm at the ~50th hour, and then transits to a much faster linear growth. Apart from the description given by Chernia et. al., to date, there is no clear picture at the atomic scale level for the cause of this drastic enhancement in growth rate.

The changes XRD oxide peak intensity ratio for the (111)/(220) peaks were observed by Zalkind et. al. which clearly indicates vigorous positional and/or occupancy changes in the oxide structure to ~0.3.μm thick. They attributed these variations as due to preferred orientation suggesting that the oxide growth rates had orientation dependence. It is therefore unlikely that the change in intensity ratio to be dominated by crystal preferred orientation since these changes are only observed in the initial stages of up to ~0.3.μm.

Another uranium sample which underwent the same environmental treatment was used as a control to determine oxide thickness using white light interferometer. The results are indicated in Figure 1 as black, red, green vertical bars. They do not show a rapid increase after 50 hours.

(a) BONDINGS

The oxidation states of U in uranium oxides ranges from +1 to +6 depending on the structure [8]. Ellis [9] reported that when uranium is expelled from the surface, U bonds with O forming UO with the oxidation state of +2. Using XPS technique, Allen et. al. [10] revealed that UO_2 and UO entities could co-exist. Furthermore, neutron scattering experiments revealed unusual U-O distances which did not

quite fit FCC cubic structure [11] and therefore, O-U-O bonds (oxidation state +4) are not formed during the early stages of oxidation. Hence, it can be concluded that nucleating crystals have slightly different bonds-lengths with combinations of U-U and U-O bonds. A shorter U-O bond may exist during the initial nucleation of UO_2 which can be used to argue for the presence of slightly different lattice parameter and generating island-like structure where one crystal growth is independent of other.

(b) MODEL CALCULATIONS

Here, we simulate the powder diffraction pattern for FCC UO_2 structure. We used the LAZY-PULVERIX [12] routine to calculate the x-ray peak intensities. The scattering factors for uranium and oxygen are 92 and 8, respectively. For this calculation, oxygen contribution is ignored. In the FCC structure, sites a- (0, 0, 0) are filled. The only interstitial sites are the octahedral sites at b-(½, ½, ½) and the tetrahedral sites at c-(¼, ¼, ¼). If one assumes that the FCC sites are not completely filled and the additional U atoms are at either octahedral or tetrahedral, or at both sites, the diffraction spectrum can then be calculated and plotted in Figure 2. For example, with 0.1 occupancy means 10% of U atoms are at c-sites and 90% at the a-sites. Clearly, differences in peak intensities can be observed with changing occupancy.

Figure 3 plots the peak intensities versus site occupancies. The major changes in peak intensities are the (111) and (311) peaks. At the lower end, the intensities decrease with increasing octahedral occupancy. The above result indicates that the increase in (111) peak intensity is due to the reduction of the octahedral site occupancy. Similar simulations were also carried out for the tetrahedral occupancy resulted in similar conclusion,

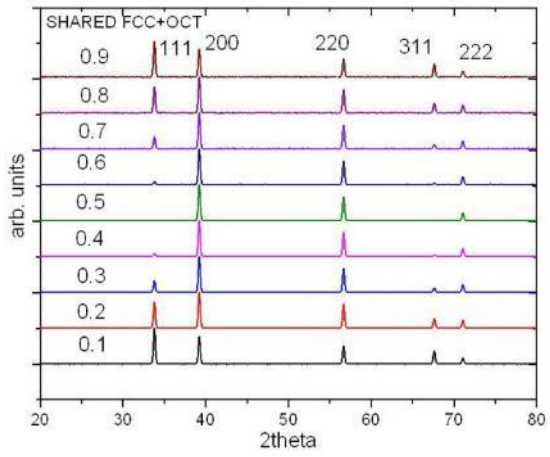

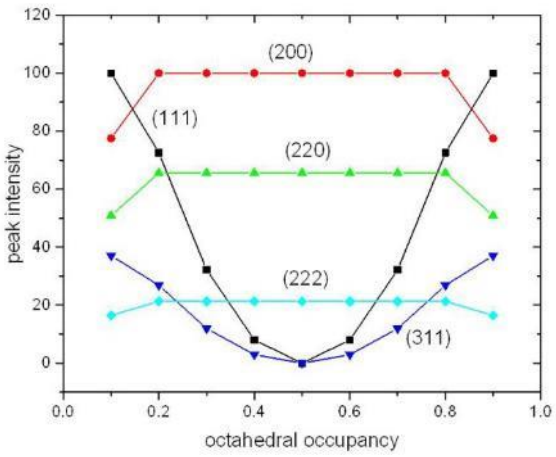

Figure 2: Simulated XRD spectrum of UO2 with different octahedral occupancy labelled on the left of each curve.

Figure 3: Simulated peak intensities with different octahedral site occupancies.

CONCLUSIONS

Our previous experiment on the oxidation behavior on uranium surface at 50C revealed a parabolic growth to ~ 0.3µm and transit to a faster linear growth. The oxide thickness was calculated using the attenuated XRD signal from the uranium metal.

From the oxidation states argument and the observation of non-regular bonding, we propose that the early formation of the uranium oxide is sporadic with unequal interatomic distances.

Changing the occupancy from the interstitial sites to the FCC sites increases the scattering from the oxide layer, thereby reduces the flux from reaching the substrate. Furthermore, the exit x-rays from the substrate scattering are also attenuated by the oxide layer.

Hence, the earlier calculation of oxide thickness is invalid due to the changing character of the oxide.

REFERENCES

1. C. Saw, Y. Idell and W. Siekhaus, *Plutonium Futures-The Science* (2018) pp78-80
2. 2.Yanzhi Zhang, Weijun Guan, Qinguo Wang, Xiaolin Wang, Xinchun Lai, Maobing Shuai, *Mat. Sci. and Eng.* 9 (2010) 012019
3. Y. Idell, W. Siekhaus and W. McLean, LLNL-ABS-767754
4. M.J. Bennett, B.L. Myatt, D.R.V. Silvester and J.E. Antill, J. of Nuc. Mat. 57 (1975) 221-236
5. J.T. Waber, in LA-1524, *A Review of the Corrosion of Uranium and its Alloys*. 1952, Los Alamos Scientific Laboratory: Los Alamos, N. M. , USA. p. 47.
6. S. Zalkind, G. Rafailov, I. Halevy, T. Livneth, A. Rubin, H. Mainon and D. Schweke, *J. of Nuclear Materials*, 485 (2017) 202-206
7. Z. Chernia, Y. Ben-Eliyahu, G. Kimmel, G. Braun and J. Sariel, *J. Phys. Chem*. B 2006, **110**, 23041-23051
8. Wikipedia retrieved 07/04/2021
9. Walton P. Ellis, "Auger/Loss studies of uranium, uranium oxidation, UO2, U3O8 and UF4", *Surface Science* 61 (1976) 37-59
10. G.C. Allen and P.M. Tucker, *J. of the Chem. Soc., Dalton Tran.* 5 (1973) 465-572
11. L. Desgranges, Y., Ma, Ph., Garcia, G., Baldinozzi, D. Siméone and H. E. Fischer, *Inorg. Chem.* 2017, 56, 321−326
12. K. Yvon, W. Jeitschko and E. Parthe, *J. of App. Cryst. (1977) 10, 73-74*

* This work was performed under the auspices of the U.S. Department of Energy by Lawrence Livermore National Laboratory under Contract DE-AC52-07NA27344. LLNL-ABS-799538

P34. Small Scale Pyrochemistry with In-situ Material Doping

S. Simpson [1], A. Parkes [2], A. Swift [1], C. Zhang [1], D. Roberts [1]

[1] Lawrence Livermore National Laboratory, 7000 East Ave, Livermore, CA

[2] AWE-Aldermaston, Reading, Berkshire, RG7 4PR

simpson52@llnl.gov

The Pu facility at Lawrence Livermore National Laboratory has demonstrated the full pyrochemical flowsheet at the 200g scale in order to meet the needs of various plutonium science programs. Interest in the aging behavior of plutonium has led to the need for producing accelerated aged alloys. Doping weapons grade Pu with various quantities of Pu-238 accelerates the long-term aging process of Pu allowing for studies at an accelerated rate. The processes needed to produce such an alloy include modified Direct Oxide Reduction (DOR), a Molten Salt Extraction (MSE), electrorefining (ER), alloying, casting, rolling and annealing. The first batch of this project processed metallic weapons-grade Pu through an MSE and ER, resulting in a 99.8% pure product. This initial batch will be used as the baseline for the aging comparisons. The second project batch started with a modified DOR comprised of 200g of weapons-grade Pu metal and 15g of Pu-238 oxide. During this process, the oxide was reduced to metal and consolidated into the metallic weapons grade Pu. In this presentation we discuss the challenges of scaling down these operations and the equipment modifications that were necessary for success.

This work was performed under the auspices of the U.S. Department of Energy by Lawrence Livermore National Laboratory under Contract DE-AC52-07NA27344.

P35. Chemical Compatibility and Characterization of Materials for Nuclear Applications

A. Swift, E. Moore, E. Elton, S. Stout, J. Jeffries, K. Holliday[1]
1Physical and Life Sciences Directorate, Lawrence Livermore National Laboratory, Livermore, California 94550, USA

Swift25@llnl.gov

At LLNL, our facilities allow for small scale research and development, while still adhering to the rigid safety demands of handling specialized nuclear materials (SNM). This is of interest, as nuclear materials face many design and developmental challenges, along with large upfront costs associated with storing and processing SNM. In this work, the chemical compatibility of components with molten Pu and Pu-Ga are studied to evaluate the performance of storage and containment materials with the goal of enhancing design flexibility. Containment and processing materials of interest are those commonly associated with pyrochemical operations and stainless steels, such as, Ta, W, MgO, and Fe. Recent computational thermodynamic reassessments into δ-stabilized Pu-Ga system with Fe impurities also brought about the need to experimentally investigate the Pu-Ga-Fe and Fe-Ga system [3]. The CALPHAD thermodynamic databases were developed to predict phase behavior of Pu-Ga with Fe impurities, where limited solubility can influence the formation of Pu-Fe intermetallics. The binary Fe-Ga system experimental data is also lacking in the Ga-rich portions and does not match current calculated models. For this purpose, experimental alloys at various theoretically calculated compositions are under development to elucidate any chemical compatibility issues within the Pu-Ga-Fe system. Molten Pu and Pu-alloys are prepared via induction and resistive heating methods to thermally treat Pu and Pu-Ga with containment materials. Samples are characterized via X-ray diffraction (XRD), optical microscopy, and Scanning Electron Microscopy (SEM). When necessary, differential scanning calorimetry (DSC) is used to identify thermophysical interactions of small-scale molten Pu and Pu-Ga melts with containment materials as a function of time and temperature.

[1] L.J. Mullins et al., Los Alamos National Lab, NM (USA), 1981
[2] S.S. Hecker et al., Los Alamos Science, 6 (2000) p.316
[3] E.E. Moore et al., Applied Sciences, 9 (2019)
[4] C. Dasarathy, et al., Proceedings of the Royal Society London, Series. A 286 (1965) p. 141
[5] W. Köster,et al., Zeitschrift für Metallkunde 68 (1977) p. 582

P36. Plutonium Casting Modelling – Beyond the Present

Dr V. H. Varsani

AWE, Aldermaston, Reading, Berkshire, RG7 4PR

vijay.varsani@awe.co.uk

Casting modelling has become widely used for various industrial applications. In general, modelling techniques such as Computation Fluid Dynamics, Finite Element and Meso-Scale modelling are utilised as a research tool to aid optimisation of manufacturing processes; therefore, it has become a powerful ally. These techniques have helped to better understand the complexities and natural behaviour of molten metal flow, assess turbulence generated during mould filling, helped to develop an in-depth understanding of the complex interactions between molten metal flow and mould material, predict casting defects, segregation behaviour and assess the average cooling rate experienced during the casting processes, which all have a profound effect on the metallurgical properties of the casting being produced.

Casting plutonium alloys is both a complex, time-consuming affair involving multiple stages, these include; Vacuum Induction Melting (VIM) and homogenisation. By their very nature, studies involving plutonium alloys are inherently difficult, and therefore, future studies are likely to be limited due to several factors which include; high associated costs and health and safety considerations. As such development of the plutonium casting processes has been limited and the fundamental casting process design has seen little improvements in the last 20 years. The casting and homogenisation processes are simple by design, gravity VIM casting and isothermal homogenisation, however; when considering the number of complex metallurgical and physical phenomena that occur, some of which occur simultaneously, developing a process model which encompasses all the phenomena, becomes a true challenge.

The long-term goal of this work is to develop and validate a casting process model capable of predicting both the metallurgical and physical properties of the castings across the multiple processing stages (casting and homogenisation). This model will be utilised in the future to guide casting process development and aid in designing a future casting capability.

P37. Actinide oxalates for nano-oxides

O. Walter [1], K. Popa [1]

[1] European Commission, DG Joint Research Centre , P.O. Box 2340, 76125 Karlsruhe, Germany

olaf.walter@ec.europa.eu

Nanocrystals (NC's) represent fundamental building blocks in nanoscience and nanotechnology because of their size and shape dependent properties and have attracted high interest. Accordingly NC's of actinide dioxides (AnO_2) have been investigated at the JRC in more detail since now about one decade [1-13].

Our contribution is a brief overview over our research on highly crystalline AnO_2 NC's obtained via hydrothermal decomposition of the $An(oxalate)_2*nH_2O$ in hot compressed water at temperatures below 250°C [1-5].

References

[1] O. Walter, K. Popa, O. Dieste Blanco, *Open Chem.*, **14**, 170 (2016).
[2] L. Balice, D. Bouëxière, M. Cologna, A. Cambriani, J.-F. Vigier, E. De Bona, D.G. Sorarù, C. Kübel, O. Walter, K. Popa, *J. Nucl. Mater.*, **498**, 307 (2018).
[3] K. Popa, O. Walter, O. Dieste Blanco, A. Guiot, D. Bouëxière, J.-Y. Colle, L. Martel, M. Naji, D. Manara, *Cryst. Eng. Comm.*, **20**, 4614 (2018).
[4] D. Bouëxière, K. Popa, O. Walter, M. Cologna, *RSC Advances*, **9**, 6542 (2019).
[5] E. De Bona, O. Walter, H. Störmer, T. Wiss, G. Baldinozzi, M. Cologna, K. Popa, *J. Am. Ceram. Soc.,* **102**, 3814 (2019).
[6] R. Jovani-Abril, R. Eloirdi, D. Bouëxière, R. Malmbeck, J. Spino, *J. Mater. Sci.*, **46**, 5 (2011).
[7] D. Hudry, C. Apostolidis, O. Walter, T. Gouder, E. Courtois, C. Kübel, D. Meyer, *Chem. Eur. J.*, **18**, 8283 (2012).
[8] D. Hudry, C. Apostolidis, O. Walter, T. Gouder, A. Janssen, E. Courtois, C. Kübel, D. Meyer, *RSC Advances*, **3**, 18271 (2013).
[9] D. Hudry, C. Apostolidis, O. Walter, T. Gouder, E. Courtois, C. Kübel, D. Meyer, *Chem. Eur. J.*, **19**, 5297 (2013).
[10] D. Hudry, C. Apostolidis, O. Walter, A. Janßen, D. Manara, J. C. Griveau, E. Colineau, T. Vitova, T. Prüßmann, D. Wang, C. Kübel, D. Meyer, *Chem. Eur. J.*, **20**, 10431 (2014).
[11] D. Hudry, J.-C. Griveau, C. Apostolidis, O. Walter, E. Colineau, G. Rasmussen, D. Wang, V. S. K. Chakravadhaluna, E. Courtois, C. Kübel, D. Meyer, *Nano Research*, **7**, 119, (2014).
[12] R. Jovani-Abril, M. Gibilaro, A. Janßen, R. Eloirdi, J. Somers, J. Spino, R. Malmbeck, *J. Mater. Sci.*, **477**, 298 (2016).
[13] V. Tyrpekl, J.F. Vigier, D. Manara, T. Wiss, O. Dieste Blanco, J. Somers, *J. Nucl. Mater.*, **460**, 200 (2015).

P38. Comparison of Techniques for Collecting Young's Modulus Data in Alpha and Delta Plutonium

Clarissa A. Yablinsky, Taylor R. Jacobs, Meghan J. Gibbs, Carlos D. Archuleta, Christopher J. Cordova, Tomas A. Martinez, Todd P. Martinez [1], Tarik A. Saleh [2]

[1] Los Alamos National Laboratory, PO Box 1663, MS E574, Los Alamos, NM 87545
[2] Los Alamos National Laboratory, PO Box 1663, MS G755, Los Alamos, NM 87545

Los Alamos National Laboratory, PO Box 1663, MS E574, Los Alamos, NM 87545

rizz@lanl.gov

INTRODUCTION

Limited work has been done to measure Young's modulus using traditional mechanical testing. Here, testing of alpha Pu and delta Pu-Ga compositions were mechanically compressed to directly measure Young's modulus. The data are compared to resonant ultrasound spectroscopy (RUS) results, which were used to calculate Young's modulus from the measured bulk and shear moduli.

Review of Young's Modulus Data

DATA FROM MECHANICAL TESTING

Gardner and Mann[1] reported Young's modulus data for unalloyed alpha plutonium. The investigation reported an average Young's modulus for unalloyed alpha plutonium as 98.6 GPa. This number was found to be equivalent in both tension and compression.

A single static data point measured using stress-strain data was found for 1 wt% delta Pu-Ga alloys in a review paper by Robbins[2]. The reported Young's modulus value for the delta Pu-Ga alloy was ~41 GPa.

In both cases, the numbers were reported but none of the experimental details were explained. Additionally, the data was either reported as a number or estimated from a point on a graph, without showing the collected stress-strain curves.

Data from Resonant Ultrasound Spectroscopy

Resonant Ultrasound Spectroscopy (RUS) is a precise technique to measure elastic constants in materials via mechanical resonance. Direct measurement of C_{11} and C_{44} in homogeneous polycrystalline isotropic solids leads to very accurate measurements of bulk and shear moduli and, by extension, calculations of Young's modulus and Poisson's ratio. Migliori et. al. have reported Young's modulus data for alpha plutonium over a nearly 400 K temperature range[3]. The calculated modulus is ~140 GPa at 18 K, decreasing to ~95 GPa at 400 K.

Plutonium-gallium alloys had similar Young's modulus trends. Ledbetter and Moment[4] investigated a single crystal 1 wt% Pu-Ga alloy and found an anisotropic response, where the modulus depends on crystallographic direction. The maximum value, 73.3 GPa, occurs along the <111> directions, while the minimum value, 13.6 GPa, occurs along the <110> directions. Also noted was the ratio between these directions, 5.3, which is the largest change in modulus with direction known for any element.

The compiled Young's modulus data for polycrystalline Pu-Ga from Robbins[2] shows a decrease with temperature, from ~43 GPa at 293 K to 30 GPa at 573 K. While additional bulk and shear moduli measurements on delta Pu-Ga are made regularly, Young's modulus is rarely calculated. We expect that current measurements would yield similar results to the aforementioned trends and reported numbers.

Motivation for Young's Modulus Testing

Addressing the need for modulus data in plutonium can be done with both mechanical testing and RUS. While RUS is a powerful tool to accurately measure bulk and shear moduli, allowing us to calculate Young's modulus, there are limitations to the technique. RUS data can be difficult to collect when investigating materials with varying microstructural features like texture or voids, which can change the frequencies too much for accurate collection or all together dampen them for a null response.

A strong collection of Young's modulus data from both mechanical testing and RUS calculations for easy homogeneous materials is necessary to understand the relationship between the two techniques. In the future, if the more accurate RUS data is difficult to obtain, then there is a path forward, through mechanical testing, to provide needed Young's modulus data.

EXPERIMENTAL PROCEDURE

Samples were prepared by sectioning and polishing to 5mm x 5mm x 7mm rectangles for testing. The final polish was performed using 800 grit SiC polishing paper. All samples had density measurements via helium pycnometry taken before RUS and mechanical testing were performed.

RUS measurements were performed on each sample in order to obtain C_{11} and C_{44}. Young's modulus was then calculated from the data using the following equations:

$$\nu = \frac{C_{11} - 2C_{44}}{2C_{11} - 2C_{44}} \quad \text{Eq. 1}$$

$$E = C_{11} - 2\nu(C_{11} - 2C_{44}) \quad \text{Eq. 2}$$

Where ν is Poisson's ratio and E is the Young's modulus.

Compression testing was performed at a strain rate of $1\text{x}10^{-3}$ /s during both loading and unloading using a high stiffness electromechanical load frame. Strain was measured using a video extensometry technique. Two samples were tested each from alpha and delta material. The compliance from the load frame was measured and subtracted from the raw data. Young's modulus was calculated using Hook's Law:

$$\sigma = E\varepsilon \quad \text{Eq. 3}$$

Where σ is the strain and ε is the stress. The Young's modulus measured by compression testing is then compared to the modulus calculated from RUS testing.

RESULTS

This study investigates Young's modulus variations with chemistry. Data analysis is currently underway for both RUS and compression testing data. Comparisons of both measured and calculated Young's modulus will be reported.

The work will add to the scientific data on Young's modulus in plutonium and its alloys. Understanding the relationship between the two methods will be particularly useful for samples that are inhomogeneous and harder to measure using the more precise RUS technique.

REFERENCES

[1] H.R. GARDNER and I.B. MANN, “Mechanical Property and Formability Studies on Unalloyed Plutonium.” In Plutonium 1960: The proceedings of the Second International Conference on Plutonium Metallurgy, Grenoble, France, 19-22 April 1960. Grison, E.; Lord, W. B. H.; Fowler, R. D., Eds. Cleaver-Hume Press: London, 1961; pp 513-570.

[2] J. ROBBINS. “Mechanical Properties of delta-stabilized Pu-1.0 wt% Ga alloys.” *Journal of Nuclear Materials*, **324**, 125 (2004).

[3] A. MIGLIORI, C. PANTEA, H. LEDBETTER, J.B. BETTS, J.E. MITCHELL, M. RAMOS, F. FREIBERT, D. DOOLEY, S. HARRINGTON, C.H. MIELKE, “a-plutonium’s Polycrystlline Elastic Moduli Over Its Full Temperature Range.” *Journal of the Acoustical Society of America,* **122**, 1994 (2007).

[4] H.M. LEDBETTER and R.L. MOMENT, “Elastic Properties of Face-Centered-Cubic Plutonium.” *Acta Metallurgica,* **24**, 891 (1976).

P39. Thermophysical Properties of Liquid Actinide Halides

S. Parker [1], M. Jackson [1], S. Vogel [1], A. Long [1], M. Monreal [2]

[1] Los Alamos National Laboratory, Materials Science Division, Los Alamos, NM, USA

[2] Los Alamos National Laboratory, Chemistry Division, Los Alamos, NM, USA

P.O. Box 1663, Bikini Atoll Rd, Bldg SM-30, Los Alamos, NM 87545

sparker@lanl.gov

Melt point, enthalpy of fusion, heat capacity, and volumetric expansion of actinide liquid chlorides {UCl_3 and $PuCl_3$} and mixtures with {NaCl} were measured experimentally. These properties and materials are relevant in applications such as heat transfer, liquid nuclear fuel, and pyrochemical processing. A novel method for density measurement by neutron radiography was shown to produce high-quality data. This method is especially useful in the characterization of sealed sample crucibles, given the ability of neutrons to penetrate the containment and surrounding furnace material. Measurement of the heat capacity of these ionic liquids was achieved by differential scanning calorimetry, and the results of this study are a first for most compositions examined. All results are presented within the context of the available published data. The purpose of this review is to integrate measurements of the thermophysical properties of liquid chlorides into empirical descriptions of the relationships between composition, temperature, and thermophysical properties. Models for the prediction of the density and heat capacity of mixtures of liquid chlorides are proposed and demonstrated within a case study of the {NaCl + x mol% UCl_3} system.

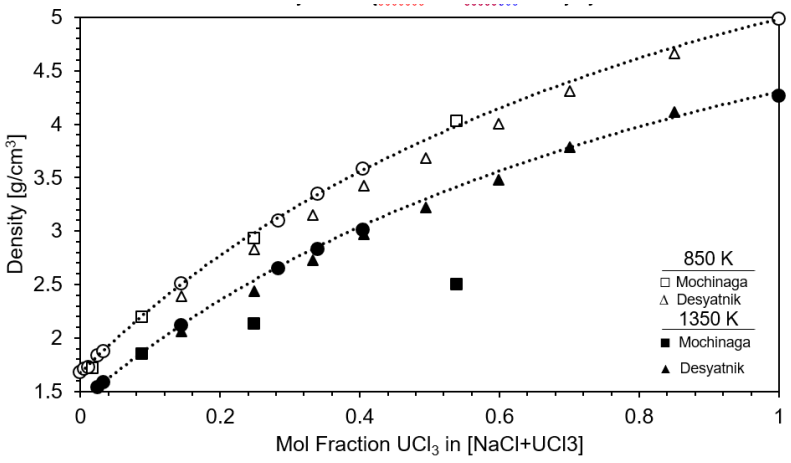

Figure 1: Theoretical density (----) and data as a function of composition at 850 K and 1350 K.

[1] J. Mochinaga, et al, J. Electrochem. Soc. Japan, 37 Issue 9 p.658-661 (1969).149

[2] V. N. Desyatnik, et al, Atomnaya Energiya 39, No. 1, p.70-72 (1975).

Nuclear Fuel Cycle

P40	**Sofian Benarib (CEA)** *"Hydrothermal conversion of uranium(IV)-cerium oxalates into uranium-cerium mixed oxides"*
P41	**Lewis Blackburn (University of Sheffield)** *"Progress Towards the Immobilisation of the UK Plutonium Inventory in Titanate Ceramics"*
P42	**Ruth Carvajal Ortiz (NNL)** *"Pyrochemical alpha-active processing apparatus"*
P43	**Phillip Hammer (University of Nevada, Las Vegas)** *"Electrolytic Recovery of Actinide Metals from Aqueous and Non-Aqueous Electrolytes"*
P44	**Anna Hautecouverture (CEA)** *"Actinides mixed oxides $U_{1-x}U_xO_2$ synthesis by Combustion Synthesis"*
P45	**Kiel Holliday (LLNL)** *"Expanding Aqueous Plutonium Chemistry Capabilities at LLNL"*
P46	**Julien Margate (CEA)** *"Sonochemical conversion of UO_2 into U(VI) peroxides reveals unexpected morphologies"*
P47	**Trieu-Duy Tran (CEA)** *"DEM modeling of (U-Pu)O_2 agglomerates for nuclear fuel manufacture"*
P48	**Karen Van Hecke (SCK CEN)** *"Separation of Am and Pu from aged PuO_2 powder"*
P49	**Laurent Venault (CEA)** *"Influence of plutonium oxidation state on the formation of molecular hydrogen, nitrous acid and nitrous oxide from alpha radiolysis of nitric acid solution"*
P60	**Aurelien Perrot (CEA)** *"Experimental approach to study the alteration of MOX MIMAS fuels in an underwater storage situation"*

P40. Hydrothermal conversion of uranium(IV)-cerium oxalates into uranium-cerium mixed oxides

S. Benarib, N. Dacheux, N. Clavier

ICSM, Université de Montpellier, CNRS, CEA, ENSCM, Site de Marcoule, Bagnols-sur-Cèze, France

sofian.benarib@cea.fr, nicolas.dacheux@univ-montpellier.fr, nicolas.clavier@icsm.fr

---

For many years, the development of new generations of nuclear reactors led to envisage innovative methods for the fabrication of oxide fuels. Wet chemistry routes have been studied for the fabrication of mixed oxide fuels such as $(U,Pu)O_2$ MOx, notably to improve the cations distribution homogeneity and to enhance the resistance towards proliferation. Such processes are mainly based on the initial precipitation of low-temperatures precursors[1,2] which are further converted into the final compounds through a heat treatment at high temperature. Nevertheless, the resulting oxide powders can still contain residual carbon[2] while the powder morphology is inherited from the starting precursor.

In this context, several authors explored the hydrothermal conversion of An(IV) oxalates (An(IV) = Th, U, Np, Pu)[4,5] which allowed them to directly achieve the precipitation of hydrated oxides from solution. Yet, the hydrothermal processes reported in the literature have almost never addressed complex systems with actinides and/or lanthanides cations exhibiting different redox states. In this context, we focused this work is focused on the direct preparation of $(U,Ce)O_2$ solid solutions through hydrothermal conversion of U(IV)-Ce(III) mixed oxalates. Herein, cerium was used as a surrogate for plutonium owing to several similar properties among which cationic radius and stabilized oxidation states in the solid and in solution.

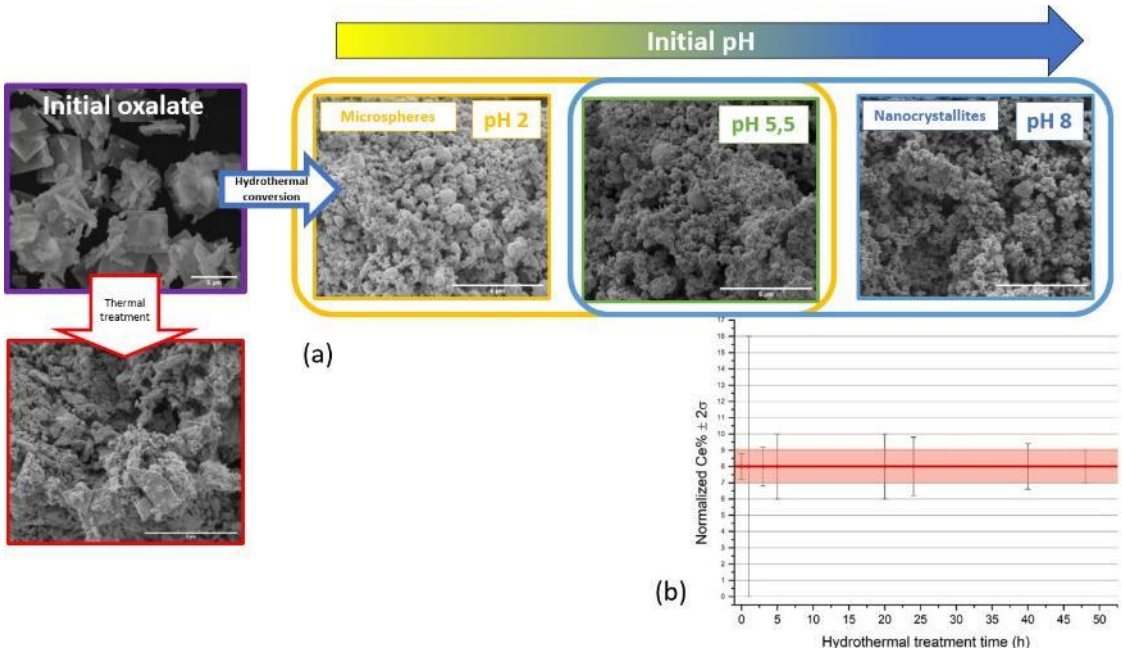

Figure 1 : (a) Effect of initial pH on the powder morphology: from microspheres to nanocrystallites agglomerates; (b) Homogeneity of the mixed oxide according to the hydrothermal treatment time

The effect of

initial pH during mild hydrothermal conversion (T=250°C, t = 24h) of oxalate precursors was first investigated. Regardless of the pH, the typical fluorite structure of AnO_2 was obtained while detailed XRD analyses highlighted the single-phase nature of the samples. Initial pH of the reaction media was found to have a massive impact on the oxide morphology. Indeed, for acidic pH, typically at pH = 2 and below, the powder was found to be spherical, with particles of about 1 µm in size, whereas more alkaline pH led to agglomerates of nanocrystallites. Furthermore, the effect of the duration of hydrothermal conversion (T = 250°C, pH = 8, t = 1-48h) of oxalate precursors was investigated. Thanks to XRD analysis, the fluorite-type structure of AnO_2 was observed after only 1h, still with residual oxalate phase. After 3h, the oxide phase was obtained as a pure compound. Unlike pH, duration showed no impact on the oxide morphology. Afterwards, SEM/EDS analyses allowed the study of the homogeneity of the compounds and showed that the cationic distribution narrowed with time, to form finally homogenous mixed oxides. Some other parameters showed to affect oxide properties, such as the nature of the precursors oxalates or the cerium content incorporated in the structure of the mixed oxide.

References:

[1] B. Arab-chapelet et al., “Synthesis of new mixed actinides oxalates as precursors of actinides oxide solid solutions,” vol. 445, pp. 387–390, 2007, doi:] 10.1016/j.jallcom.2007.01.033

[2] J. Martinez et al., « From uranium (IV) oxalate to sintered UO2 : consequences of the powders’ thermal history on the microstructure », *J. Europ. Ceram. Soc.* 35 (2015) 4535-4546.

[3] Manaud et al, « Hydrothermal conversion of uranium(IV) oxalate into oxides: a comprehensive study », Inorg. Chem. 2020, 59, 3260-3273

[4] Popa et al., « A low-temperature synthesis method for AnO2 nanocrystals and associate solid solutions », CrystEngComm, 2018

P41. Progress Towards the Immobilisation of the UK Plutonium Inventory in Titanate Ceramics

Lewis R. Blackburn, Amber R. Mason, Laura J. Gardner, Claire L. Corkhill

Immobilisation Science Laboratory, Department of Materials Science and Engineering, University of Sheffield, Sir Robert Hadfield Building, Mappin St, S1 3JD, UK

lewis.blackburn@sheffield.ac.uk

The United Kingdom holds a substantial inventory of PuO_2, forecast to reach approximately 140 teHM (tonnes equivalent heavy metal) upon completion of reprocessing. This material presents a unique decommissioning prospect for which there is a need to develop a robust management strategy [1]. Prompt immobilisation and disposal within a geological disposal facility (GDF) is a promising route towards ultimate disposition, yet in order to safely underpin the safety case for the geological disposal of Pu, it is necessary to understand the long term evolution of candidate wasteform materials in simulated repository environments. Moreover, there is a need to develop suitable wasteform materials capable of co-accommodating Pu, prescribed quantities of neutron poisoning species, trace processing impurities and transition metal cations capable of providing charge balance for non-stoichiometric compositions. Several baseline wasteform formulations derived from zirconolite, pyrochlore and fluorite-type matrices have been proposed on the basis of high chemical durability, radiation stability and moderate ease of processing [2]. Herein, this talk will provide an overview in recent advances in the formulation refinement and fundamental characterisation of candidate wasteform materials for UK Pu. This includes detailed scoping trials aiming to characterise the incorporation of a representative U, Th and Ce surrogate fraction within zirconolite and pyrochlore phases, fabricated by conventional sintering (CPS), hot isostatic pressing (HIP) and reactive spark plasma sintering (RSPS) [3].

[1] N. C. Hyatt, “Safe management of the UK separated plutonium inventory: a challenge of materials degradation,” npj Mater. Degrad., vol. 4, no. 28, 2020.

[2] L. R. Blackburn and N. C. Hyatt, “Actinide Immobilisation in Dedicated Wasteforms: An Alternative Pathway for the Long-Term Management of Existing Actinide Stockpiles,” in Encyclopedia of Nuclear Energy, 1st ed., E. Greenspan, Ed. Elsevier, 2021, pp. 650–662.

[3] L. R. Blackburn et al., “Hot Isostatically Pressed Zirconolite Wasteforms for Actinide Immobilisation,” in IOP Conference Series: Materials Science and Engineering, 2020, vol. 818, no. 1.

P42. Pyrochemical alpha-active processing apparatus

R.A. Carvajal-Ortiz, S.D. Woodall, M.T.Harrison, M.J. Edmondson

National Nuclear Laboratory, UK

ruth.carvajal-ortiz@uknnl.com

Molten salts based pyro-processing is a used fuel recycling technique, complementary to aqueous (solvent extraction)-based recycling [1] [2]. Aqueous based systems may not be optimal for some potential future systems, such as the very high burn-up fuels with a prohibitive level of radiation emitted. Molten salts are also an excellent medium to recycle fuel, with inherent proliferation resistance. The development of the capability and capacity to assess and understand the principles and technologies required is being carried out through the *Advanced Fuel Cycle Programme* (AFCP), as part of a UK government investment in nuclear energy research. AFCP has been re-establishing the skilled workforce and infrastructure to demonstrate the development of advanced nuclear fuels and recycling technologies that promote sustainability of nuclear energy.

The AFCP pyro-processing project has been designed to investigate the behaviour of actinides in molten salts, improve or enhance our equipment provision and grow the experience and skills of our team; within NNL but also across academia and into industry.

A specific piece of equipment, the *Pyrochemical Alpha-active Processing Apparatus* (PAPA) has been developed for this purpose. It is capable of handling actinides including plutonium and allows us to conduct electrochemical experiments with these materials. PAPA builds on previous experience with the alpha-active molten salts experiments and includes several innovative features. These include a furnace capable of reaching 950°C, a top plate housing the electrodes and gas inlet/outlet inputs and mechanical bellows that allow electrodes to be raised and lowered, in and out of the salt, without breaking seals, all while keeping the required low levels of oxygen/moisture inside the cell via an ultra-pure argon gas flow. A motorised mixer and a sampling system are included in the design features. A Faraday cage is also incorporated into the crucible lowering mechanism to reduce electromagnetic interference for improved accuracy when doing electrochemical experiments.

PAPA is housed in NNL's Central Laboratory and is contained in an argon inerted, radiochemical glovebox. This provides a low oxygen and moisture blanket in addition to the ultra-pure argon feed for better experimental quality. The system will allow active, small-scale molten salt experiments, in different molten salt media. The design enables a more flexible use of the glovebox, so that hands-on operations can continue while the furnace is at temperature. The high temperature range that the furnace provides allows for a more comprehensive assessment of salt systems. A proof-of-principle cyclic voltammetry (CV) experiment that involves dissolution and redox of a plutonium salt in LiCl-KCl eutectic (LKE) has been used to successfully commission PAPA.

The PAPA rig opens a window into studying directly the electrochemical and physical properties of plutonium and minor actinides in molten salt mixtures at expected operating conditions, as well as allowing the potential testing of a proliferation resistant technique for recycle of used fuel. The apparatus will enable us to carry out these experiments more effectively, with greater flexibility and with a high level of accuracy than has previously been possible.

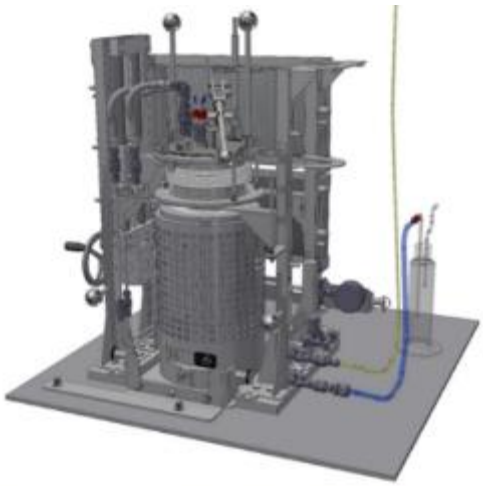

Figure 1. Schematics of the PAPA rig

Figure 1. PAPA rig

[1] R. G. Lewin and M. T. Harrison, “Review of non-aqueous technologies for advanced nuclear fuel cycles,” NNL, 2013.

[2] C. H. Lee, T.-J. Kim, S. Park, S.-J. Lee, S.-W. Paek, D.-H. Ahn and . S.-K. Cho, “Effect of cathode material on the electrorefining of U in LiCl-KCl molten salts,” *Journal of nuclear materials,* vol. 488, pp. 210-214, 2017.

P43. Electrolytic Recovery of Actinide Metals from Aqueous and Non-Aqueous Electrolytes

Hammer, Phillip, Hatchett, David

University of Nevada, Las Vegas; Department of Chemistry and Biochemistry, Radiochemistry Group; 4505 S. Maryland Pkwy, Las Vegas, NV 89154

phillip.hammer@unlv.edu david.hatchett@unlv.edu

There is a need to produce high purity actinide metals on a laboratory scale. Conventional methods for obtaining such materials; metallothermic reduction or pyrochemical molten salt electrolysis, are suited for large scale industrial applications which suffer purity and efficiency issues when scaled down. The current investigations at UNLV pursue electrolytic reduction and deposition using aqueous and non-aqueous electrolytes at various cathodes: gold foil, uranium metal, and mercury pool cathodes. The room temperature ionic liquid (RTIL) 1-butyl-1-methyl piperidinium bis(trifluoromethylsulfonyl)imide [BMPip][TFSI] is used as non-aqueous electrolyte due to its large electrochemical window and both the chemical and radiolytic stability.[1-3] The ionic liquid also does not require a secondary electrolyte for conductivity. However, metal solubility in RTIL is low and methods are being developed to enhance the dissolution of f-elements into solution.[4,5] Our research aims to close the chemical cycle between oxidized forms of uranium and synthesize a series of trivalent non-aqueous species which can be used for a variety of synthetic applications. The goal is an end product that is RTIL soluble and capable of electrochemical recovery as high purity metallic actinides.

Here, synthetic reactions of $UI_3(THF)_4$ in THF and RTIL have been studied to produce novel anhydrous $U(TFSI)_3xTHF$ species which display enhanced solubility in RTIL.[6-8] Combined UV/vis, RAMAN, TGA-DSC, and SCXRD/PXRD have been used to characterize the products obtained from these reactions. UV/vis spectra of the $U(TFSI)_3$ shows distinct differences when compared to spectra obtained from the precursor $UI_3(THF)_4$. No sharp absorbance peaks are observed above 300 nm. RAMAN spectra obtained of the $U(TFSI)_3$ suggest a fluorescent activity which has yet to be determined. The TGA data displays a 76% mass loss below 500 °C corresponding to 3 TFSI ligands. The $U(TFSI)_3$ is difficult to crystallize but upon slow evaporation of THF from a THF/RTIL/$U(TFSI)_3$ solution, crystals formed and precipitated from solution and were sent to Los Alamos National Laboratory (LANL) for crystallographic analysis. Data obtained from SCXRD and PXRD are still being analysed. Cyclic voltammetry of ~50 mM $U(TFSI)_3$ in RTIL show a UIII/U0 reduction at -3.03 V vs. ferrocene.[1,2] Controlled potential and pulsed amperometric methods at -4V have been used in attempt to recover these materials on gold foil and uranium metal disk electrodes. Through-put is low and while material recovered has metallic appearance, insufficient amounts have been recovered to prove the chemical form, let alone be synthetically useful.

Furthermore, collaboration with Los Alamos National Laboratory (LANL) has been initiated in the set-up of Oxide Reduction by Electrochemical Amalgamation followed by Thermal Extraction (OREATE and IL-OREATE) process that is completely contained within an inert dry atmosphere glovebox. Natural cerium and depleted uranium are used in both aqueous pH buffered and non-aqueous RTIL electrolytes for electrochemical amalgamation at mercury pool cathodes. The batch method produces a dilute f-element amalgam that is placed under high vacuum (10^{-8} Tor) and heated step wise for thermal extraction of the f-element and recovery of the mercury. Distillation of mercury at 360 °C serves to

concentrate the f-element-mercury complex. Continued heating in excess of the f-element melting point completely separates the mercury and serves to consolidate the recovered purified metal. Similar methods have shown contaminants on the order of ppm.[9, 10]

Milligram to gram scale recovery of >4N pure actinide metals would aid nuclear and radiochemical facilities in a multipronged effect. Research investigations into closing the chemical circuit aid in the advancement of fundamental chemistry of the actinides. Such research carries the added benefit of sample and waste stream reclamation of SNF materials. This process could reduce the radiotoxicity of university and national laboratory waste streams while reducing financial aspects of SNF materials cost in recovery and reuse as opposed to production and/or procurement. Actinide metals themselves are useful in a variety of aspects including synthesis and catalysis. Moreover, small scale production of pure actinide metals provide samples and targets for thermionic and neutronic assays necessary to promote transmutative minor actinide burning in fast neutron reactors[11]. The final application of this process intends to aid in special isotope recovery from plutonium stockpiles. Specifically, ^{242}Pu and ^{244}Pu which are invaluable as tracer isotopes.

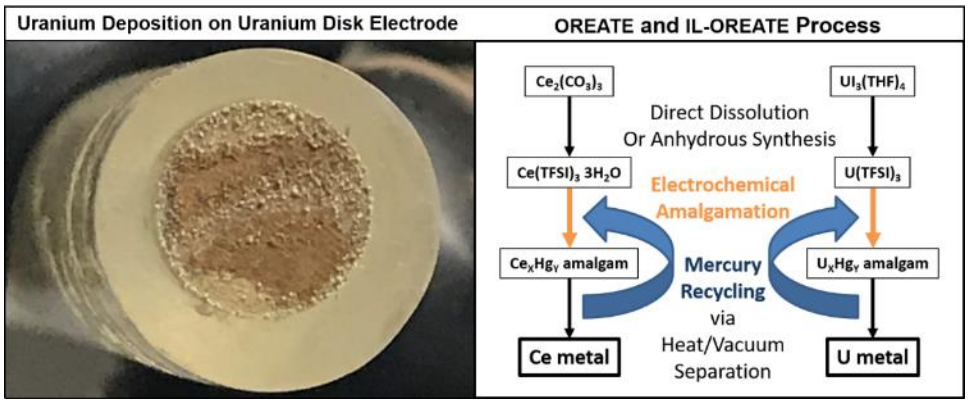

Figure 1. Room temperature f-element electrolysis. Right, flow sheet of the OREATE process for cerium and uranium metal recovery. Direct dissolution and anhydrous synthesis are specifically for IL-OREATE. Left, Uranium metal dendrite nodes obtained after Differential Pulse Amperometry (-4V, 1 sec; +1 V, 0.2 sec; cycled for 10 days) on a uranium metal disk electrode.

[1] Krishna, G. *et al.*, *Journal of the Electrochemical Society*, **2018,** *165* (5), C206-C212
[2] Jagadeeswara Rao, *et al.*, *Journal of Nuclear Materials*, **2011,** *408*, 25-29
[3] Allen, D. *et al.*, *Green Chemistry*, **2002,** *4*, 152-158
[4] Hatchett, D. *et al.*, *Electrochimica Acta*, **2013,** *89*, 144-151
[5] Pemberton, W. *et al.*, *Electrochimica Acta*, **2013**, *93*, 264-271
[6] Avens *et al.*, *Inorganic* Chemistry, **1994,** *33*, 2248-2256.
[7] Bhatt, A. *et al.*, *Inorganic Chemistry*, **2005,** *44*, 4934-4940
[8] Bhatt, A. *et al.*, *Inorganic Chemistry*, **2006,** *45*, 1677-1682
[9] Hasegawa, K. *et al.*, *Journal of Alloys and Compounds*, **1998,** *271-273*, 680-684
[10] Morrison, B., Blanco, R., ORNL CF-56-1-151, **1956,** UNCLASSIFIED
[11] Squires, L. *et al.*, *Journal of Nuclear Materials*, **2018,** 500, 26-32

P44. Actinides mixed oxides $U_{1-x}U_xO_2$ synthesis by Combustion Synthesis

A. Hautecouverture [1], P. Estevenon [2], C. Rey [1], X. Deschanels [1]

[1] ICSM, Univ Montpellier, CNRS, CEA, ENSCM, Bagnols-sur-Cèze, France.

[2] CEA, DES, DMRC, Site de Marcoule, Bagnols-sur-Cèze, France.

anna.hautecouverture@cea.fr

Nowadays, the French Pressurized Water Reactors (PWR) provided about 70% of the electricity production in 2019. Around 15% of the nuclear fuel used is Mixed Oxides fuel (MOX), originating from spent nuclear fuel recycling in order to use plutonium. It is a crucial issue within Generation IV International Forum framework to preserve natural uranium resources, decrease plutonium inventory and increase the nuclear fuel burn-up. In this context, it is interesting to find new routes to produce homogenous oxide mixtures with adequate powder morphology and a low impurities content in order to facilitate the fuel production.

New routes are studied for the direct treatlent of actinide nitrate to $U_{1-y}Pu_yO_2$ and avoid the necessity to ground together UO_2 and PuO_2. Among them, Syntheses by Combustion in Solution (SCS) are known since 1970's to allow the production of metals oxides [1], including actinides oxides [2], [3], [4], [5], [6], [7]. These reactions are based on precursor dissolution (metal nitrate in this case) in an aqueous solution with an organic compound named "fuel". This solution is then dehydrated and leads to the gelation of the reactive media. A low temperature thermal treatment allows the ignition of that gel, thanks to a vigorous exothermic self-sustaining phenomenon. Combustion can occur in two ways: propagating combustion when ignition is local and spreads in the reactive media and volume combustion when gel is subjected to homogeneous heating and ignition takes place instantaneously. During ignition, a flame is visible and very high temperatures are reached; for example, 1200K in the case of glycine assisted SCS of uranium oxide [8].This flame temperature is strongly dependent on the fuel/actinide ratio and allows actinide oxide crystallites' formation and growth, leading to well crystallized oxide powder.

Previous studies on SCS showed the possibility to obtain $U_{1-x}Th_xO_2$ [2], [3], [4], [5] and $U_{1-x}Ce_xO_2$ [6], [7] mixed oxides using citric acid or glycine as fuels for the reaction. A combustion synthesis of PuO_2 was also reported in the literature [5] but the experiment was conducted on a hot plate in propagating conditions. In this study, we examined the volume combustion instead of propagating combustion in order to reach higher flame temperature. In the scope of plutonium high content MOX fuels, this work's aim is to study the feasibility of $U_{1-x}Pu_xO_2$ formation thanks to combustion synthesis.

Preliminary studies on surrogates were carried out in our laboratory. Gadolinium oxides' synthesis were studied with the assistance of three fuels within more common ones in literature: glycine, citric acid and urea. Glycine and citric acid were selected because of products' high crystallinity and low impurities content. Different thermal treatment and temperature rates were tested in order to improve ignition conditions.

The next step to synthetize $U_{1-x}Pu_xO_2$ was to determine fuel/actinide optimal ratio to obtain UO_2 with glycine and citric acid. In order to do that, uranium nitrate $UO_2(NO_3)_2{\cdot}6H_2O$ and glycine/citric acid gels

were prepared at different molar ratios in the range from 1.1 to 2.5 for glycine and 0.2 to 0.6 for citric acid by aqueous solution dehydration. Uranium oxides were obtained after thermal treatment and characterized in order to select the optimal ratio for each fuel. Furthermore, others processing parameters, influencing heat exchanges, were investigated. Indeed, ignition and then products' crystallinity are dependent on them. Several tests on uranium allowed us to choose the most relevant alumina crucible, which was later used for plutonium.

Attempts to prepare PuO_2 took place in hot-labs on ATALANTE facility. A study was conducted on plutonium nitrate with glycine and citric acid as fuels with some minor modifications in the protocol due to the plutonium chemistry, including plutonium precursor, which is manipulated as a nitric solution. Fuel/actinide ratio varied in the range from 0.7 to 3.7 for glycine and from 0.2 to 1.4 for citric acid. Optimal molar ratios were determined for each fuel.

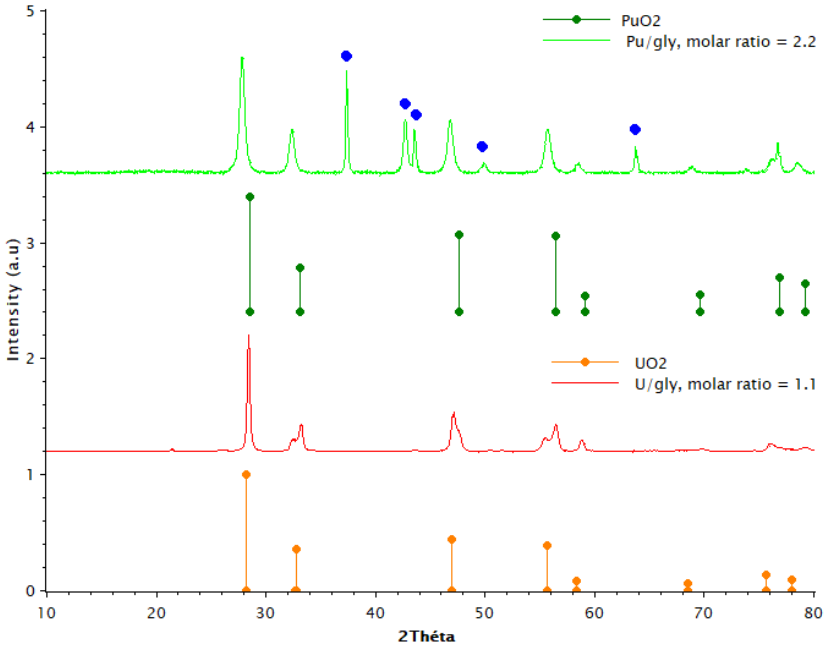

Figure 1: XRD pattern of UO_{2+x} and PuO_2 synthetized by SCS with glycine as fuel, ratio fuel/nitrate = 1.1 for uranium and 2.2 for plutonium (PuO₂ : PDF 04-003-0552 ; UO₂ : PDF 00-067-0020)

The current challenge is the determination of optimal conditions to produce $U_{1-x}Pu_xO_2$. A study on $(U,Pu)O_2$ synthesis is being carried out for each fuel on ATALANTE facility, using varying Pu/(U+Pu) ratios in order to single out/find the optimal fuel/actinide ratio associated. The first results indicate the possibility to obtain $U_{1-x}Pu_xO_2$. On the other hand, the understanding of reaction mechanism constitutes a key point to frame the optimal reactive conditions.

Finally, some important issues remain about the scale up in order to consider production of pellets of $(U,Pu)O_2$ with different Pu contents.

[1] A. E. Danks, Material Horizons 2016, 3, 91-112
[2] J. Monnier, Ph.D. Thesis, 2019, Montpellier University
[3] G. Peter Soldani, Ph.D. Thesis, 2014, Lille University
[4] S. Anthonysamy, Journal of Nuclear Materials 2000, 278, 346-357
[5] V. Chandramouli, Journal of Nuclear Materials 1999, 265, 255-261
[6] A. Jain, Journal of Nuclear Materials 2005, 345, 245-253
[7] D. Maji, Journal of Nuclear Materials 2018, 502, 370-379
[8] J. M. Roach, Inorganic Chemistry 2021, 60, 18938-18949

P45. Expanding Aqueous Plutonium Chemistry Capabilities at LLNL

K. S. Holliday, B. D. Smith, H. L. Deaguero,

D. J. Roberts, and J. A. McNeese

Lawrence Livermore National Lab, Livermore CA 94550 USA, holliday7@llnl.gov

---

The plutonium facility (Superblock) at LLNL has identified a need for upgrading aqueous plutonium recovery capabilities. A new lab has been renovated and three glovebox lines have been installed, which will not only meet the requirements of LLNL missions, but also provide an opportunity for the forensics community. Because aqueous operations are typically performed to meet product specifications, upsets in minor variables (e.g. acid concentration, oxidant/reductant, etc.) and their corresponding signatures are less explored. The aqueous recovery lab being installed at LLNL features mirror glovebox lines (1 and 3), which result in a high degree of flexibility, while still meeting LLNL missions. Different variables, isotopics, or process conditions can be explored in one line, while maintaining ideal conditions in another. The capabilities stood up are a nitric acid-based purification process. Dissolution, anion exchange, and oxalate precipitation are employed to recover pure plutonium product. Additionally, hydroxide precipitation is used to ensure complete recovery of high value plutonium. Line 2, in the middle of the room, serves the other two lines. This line has a salt washing station to eliminate chlorides before introducing salt-based residues into the recovery lines. Line 2 also has solidification of waste solutions and a bag out port capable of sending this solidified waste directly into a drum. Lastly, line 2 houses the vacuum pump that supplies vacuum necessary for the liquid transfer system, which eliminates the need to bag in and bag out liquids from the glove boxes. Here we present these capabilities in more detail and discuss their possible application to knowledge gaps in the forensics community.

Figure 1: New aqueous plutonium chemistry laboratories is now operational and processing plutonium residues from various processes.

P46. Sonochemical conversion of UO_2 into U(VI) peroxides reveals unexpected morphologies

J. Margate [1], M. Virot [1], M. Cot-Auriol [1], T. Chave [1],
T. Dumas [2], S. I. Nikitenko [1]
[1] ICSM, Univ Montpellier, CEA, CNRS, ENSCM, Marcoule, France.
[2] CEA of Marcoule, BP17171, 30207 Bagnols-sur-Cèze, France
julien.margate@cea.fr

Due to the chemical toxicity and level of radioactivity, predicting the behavior of radionuclides in the geosphere or under deep underground storage becomes a subject of major concern. Regarding this problem, it is essential to understand the nature of the species that can potentially form when ground and surface waters enter in contact with actinide-based materials. Hydrogen peroxide (H_2O_2), which is one of the major species formed as a result of water radiolysis, is known to contribute in the corrosion of UO_2-based matrices through the formation of peroxide precipitates known as studtite and metastudtite. These species can further promote the dissolution and release of radionuclides into the surroundings.[1-3] Sonochemistry, which deals with the effect of powered ultrasound on chemical reactions, is known to share some similarities with radiolysis particularly through the in-situ generation of hydrogen peroxide resulting from water molecule splitting. Studies dealing with sonochemistry of actinides have been poorly referenced in the literature. Nevertheless, it was reported that a careful selection of the sonochemical parameters allows the dramatic increase of hydrogen peroxide production in mild conditions with the typical observation of additional physical effects (erosion of solids, mass transfer, fragmentation…).[4] This work focuses the sonolysis of UO_2 in pure water and slightly acidic media under oxygenated atmosphere. After the preparation of well-characterized UO_2 platelets using the oxalic route, their complete conversion into (meta-)studtite $[(UO_2(O_2)(H_2O)_2)\cdot xH_2O]$ is observed under ultrasound.[5] The deep investigations on the remaining solutions (UV-Vis abs. spectroscopy and ICP-OES) and solid residues (SEM, XRD and FTIR techniques) allow attributing this behaviour to the sonochemical generation of H_2O_2. The formation of crystalline studtite structures is observed on the surface of UO_2 platelets with a preservation of the morphology (Figure 1.b) suggesting a complex formation mechanism other than classical dissolution/reprecipitation. Interestingly, under specific sonochemical conditions, centre-holed platelets are observed (Figure 1.c).

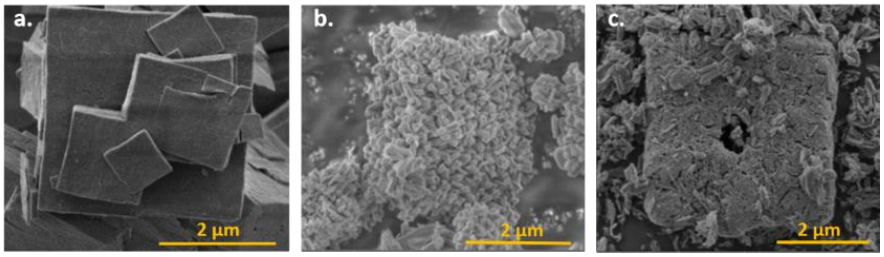

Figure 1: a) SEM image of UO_2 platelets synthetized from oxalate route b) and c) SEM image of the uranyl peroxide observed after sonication of UO_2 in H_2SO_4 5.10^{-4} M at 346 kHz (20 W.mL^{-1}, 20°C, Ar/O_2, and 6h)

[1] C. Corkhill and N. Hyatt, Waste management, IOPScience, 2018.
[2] M. Amme, Radiochimica Acta, 2002, 90, 399-406.
[3] P.C. Burns, R.C. Ewing, A. Navrotsky, Science, 2012, 335, 1184–1188
[4] R. Pflieger, T. Chave, G. Vite, L. Jouve, S.I. Nikitenko, Ultrasonics Sonochemistry, 2015, 26, 169-175.
[5] Peter C. Burns and Karrie-Ann Hughes, American Mineralogist, 2003, 88(7):1165-1168

P47. DEM modeling of (U-Pu)O_2 agglomerates for nuclear fuel manufacture

T. D. Tran[1],[2] J-Ph. Bayle[1], L. Barnouin[1], S. Lecoq[1], P. Allegri[1], Lama Braysh[2], S. Nezamabadi[2], F. Radjai[2]

[1] CEA, DES, ISEC, DMRC, Montpellier university, Marcoule, France

[2] LMGC, CNRS- University of Montpellier

CEA Marcoule, DES/ISEC/DMRC/SPTC/LSEM, BP 1717, 30207 Bagnols sur cèze cedex

Jean-philippe.bayle@cea.fr; Trieu-duy.tran@umontpellier.fr

The (U-Pu)O_2 nuclear fuel is manufactured by means of the ceramic process, which includes the grinding, pressing and sintering steps. All these steps are strongly dependent on the mechanical behaviour of (U-Pu)O_2 agglomerates, reflecting the quasi-static or dynamic mechanical loading and interactions between aggregates (intra-agglomerate interactions IAAI) of which they are composed. The quasi-static mechanical behavior of agglomerates has been studied by means of in-situ micro-compression tests at the Fuel characterisation laboratory of CEA-Marcoule Atalante facility. These tests allow us to extract the elasto-plastic parameters of agglomerates. To obtain clear insights on the physical origins of the deformation and failure of agglomerates, we use a Discrete Element method (DEM) to build numerical spherical agglomerates composed of aggregates with different shapes by means of radial compaction. We investigate the influence of aggregate shapes and friction coefficient between aggregates on the microstructure and properties of the agglomerates such as packing fraction, connectivity, and bulk elastic modulus. After adding an adhesion force law between aggregates, the agglomerates are allowed to relax and then subjected to diametral compression between two plates. We determine the fracture modes and breakage threshold as a function of cohesion parameters and aggregate shapes. The simulation parameters are partially adjusted to experimental measurements and the results are compared with micro-compression tests.

P48. Separation of Am and Pu from aged PuO_2 powder

K. Van Hecke, K. Verguts, K. Vanaken, P. Dries, S. Uygur, G. Çolak, G. Leinders, M. Verwerft, T. Cardinaels

Belgian Nuclear Research Centre (SCK CEN), Institute for Nuclear Materials Science, Boeretang 200, 2400 Mol, Belgium

kvhecke@sckcen.be

Pure americium and plutonium dioxide materials are needed as starting materials for R&D on the fabrication of both americium and plutonium bearing nuclear fuels. Therefore, americium was separated and purified from aged plutonium dioxide. The plutonium used originated from spent PWR fuel, and was most probably used in the framework of MOX fuel fabrication. It was purified and converted into its dioxide form more than 40 years ago and contained about 10 wt% of ^{241}Pu ($T_{1/2}$ = 14.35 years). Therefore, a significant build-up of the decay product ^{241}Am ($T_{1/2}$ = 432.8 years) has occurred during storage. Plutonium dioxide is very refractory towards dissolution in non-complexing mineral acids, particularly if it has been fired at high temperatures. The plutonium dioxide appeared as a very fine dark green powder. Unfortunately, the detailed history of the preparation of the plutonium dioxide including the firing temperature, could not be retrieved.

The plutonium dioxide powder was slowly dissolved in boiling concentrated nitric acid to which traces of fluoride were added. After filtration, the acidity and the Pu concentration were adjusted and a Pu(IV) valence adjustment was performed before the bulk of the plutonium was separated by means of hydrogen peroxide precipitation. The precipitated plutonium peroxide was dissolved in nitric acid and the peroxide precipitation was repeated until the plutonium was sufficiently decontaminated from americium. The americium containing filtrate was first concentrated, followed by a further purification from plutonium using anion exchange chromatography. The outcome of these separation processes resulted in a pure plutonium and a pure americium nitrate solution. For safe long-term storage, actinides should be immobilized into a ceramic phase. The actinide nitrates are usually converted into actinide oxides. Therefore, americium has been precipitated as americium(III)oxalate and plutonium as plutonium(IV)oxalate. Next, the americium and the plutonium oxalates were thermally converted into the dioxides .

P49. Influence of plutonium oxidation state on the formation of molecular hydrogen, nitrous acid and nitrous oxide from alpha radiolysis of nitric acid solution

B. Perrin [1], L. Venault [1], E. Broussard [1], J. Vandenborre [2], G. Blain [2], M. Fattahi [2], S. Nikitenko [3]

[1] CEA, DES, ISEC, DMRC, LILA, Université de Montpellier, Bagnols-sur-Ceze 30207, France

[2] Laboratoire Subatech, UMR 6457, CNRS/IN2P3, IMT-Atlantique, Université de Nantes, BP 20722, Nantes 44307, France

[3] ICSM, CEA, Université de Montpellier, CNRS, ENSCM, Bagnols-sur-Ceze 30207, France

laurent.venault@cea.fr

The study of the formation of radiolytic products, such as molecular hydrogen and nitrous acid, is of primary importance in the reprocessing of spent nuclear fuel and the storage of aqueous solutions containing radioactive materials. The radiolytic yields of molecular hydrogen, nitrous acid and nitrous oxide from alpha radiolysis of nitric acid solutions containing plutonium have been experimentally investigated. The results have shown that the yields of radiolytic products depends on the nitric acid concentration as well as the oxidation state of plutonium. However, the influence of plutonium oxidation state on radiolytic yields is less notable as the nitric acid concentration increases. Molecular hydrogen production decreases with increasing nitric acid concentration while nitrous acid and nitrous oxide productions increase. While radiolytic yields from plutonium(IV) nitric acid solutions have been previously investigated, this study provide radiolytic yields from alpha radiolysis of plutonium(III) and plutonium(VI) nitric acid solutions for molecular hydrogen, nitrous acid and nitrous oxide. These information provide insight into the role played by plutonium redox behaviour on the formation of radiolytic products.

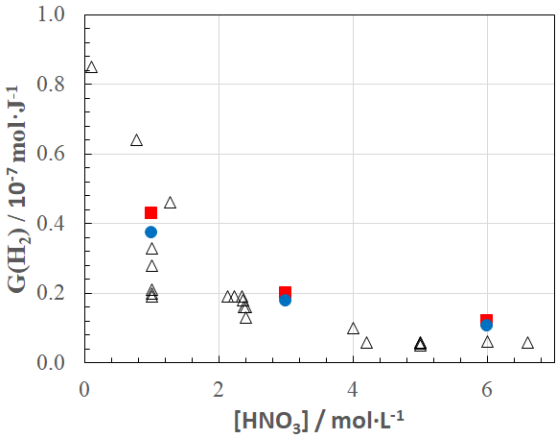

Figure 1: Radiolytic yields of molecular hydrogen $G(H_2)$ as a function of nitric acid concentration from ■ : plutonium(IV). ● : plutonium(VI). Δ : data from literature obtained from plutonium(IV) solutions [1-5].

For instance, radiolytic yields of molecular hydrogen from plutonium +IV and +VI solutions without sulfamic acid as well as results from literature are plotted as a function of nitric acid concentration in Figure 1. The results show that $G(H_2)$ decrease with increasing nitric acid concentration without sulfamic acid as reported in the literature. Radiolytic yields of molecular hydrogen from Pu(IV) solutions ranges from 0.043 µmol J^{-1} in 1 mol L^{-1} nitric acid solution to 0.012 µmol J^{-1} in 6 mol L^{-1} nitric acid solution, which corresponds to the high data values given in the literature, but are still in good agreements with previously reported results [1-4].

Radiolytic yields of molecular hydrogen from plutonium +III, +IV and +VI solutions with sulfamic acid are shown in Figure 2. The G-values in presence of sulfamic acid are lower for both Pu(IV) and Pu(VI) series, indicating that either molecular hydrogen is formed with a lower yield or that molecular hydrogen is consumed. Molecular hydrogen production clearly depends on the oxidation state of plutonium following the order Pu(III) >> Pu(IV) > Pu(VI). Radiolytic yields of molecular hydrogen from Pu(III) solutions ranges from 0.052 µmol J^{-1} in 1 mol L^{-1} nitric acid solution to 0.024 µmol J^{-1} in 3 mol L^{-1} nitric acid solution. These latter are higher than previously reported values for Pu(IV) and external radiations, implying that Pu(III) enhance the production of molecular hydrogen. Presence of sulfamic acid and different oxidations states of plutonium have a strong impact on molecular hydrogen production in 1 mol L^{-1} nitric acid solution, however their impact decreases at higher nitric acid concentration.

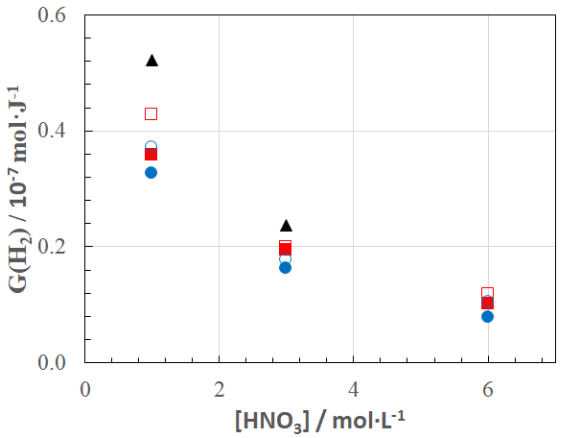

Figure 2. Radiolytic yields of molecular hydrogen $G(H_2)$ as a function of nitric acid concentration from ▲ : plutonium (III) + NH_2SO_3H. □ : plutonium (IV). ○ : plutonium (VI). ■ : plutonium (IV) + NH_2SO_3H. ● : plutonium (VI) + NH_2SO_3H.

[1] Gregson, C. R., Horne, G. P., Orr, R. M., Pimblott, S. M., Sims, H. E., Taylor, R. J., Webb, K. J. Molecular hydrogen yields from the α-self-radiolysis of nitric acid solutions containing plutonium or americium. *J. Phys. Chem. B* **122**, 2627 (2018)

[2] Kazanjian, A. R., Horrell, D. R. Radiolytically generated gases in plutonium-nitric acid solutions. *Radiation Effects* **13**, 277 (1972)

[3] Pikaev, A. K., Shilov, V. P., Gogolev, A. V. Radiation chemistry of aqueous solutions of actinides. *Russ. Chem. Rev.* **66**, 763 (1997)

[4] Burns, W. G., Lyon, C. E., Marsh, W. R. The self radiolysis of nitric acid solutions of Pu(IV) nitrate. *Eur. Appl. Res. Rept.-Nucl. Sci. Technol.* **3**, 653 (1981)

[5] Sheppard, J. C. Alpha radiolysis of plutonium(IV)-nitric acid solutions. *Tech. Rep.* BNWL-751 (1968)

Detection And Analysis

P50	**Guillaume Bailly (CEA)** "Analysis of Plutonium(IV) acidic solutions with UV-Vis spectrophotometry and Partial Least-Squares regression
P51	**Sarah Crooks (AWE)** *"Alternative Standardisation and Control of Ceric Sulphate Titrimetric Methods"*
P52	**Samuel Cross (AWE)** *"Analysis of microgram plutonium solutions using High Resolution Gamma Spectroscopy for the quantification of plutonium assay, isotopics and trace impurities"*
P53	**Aurelie Diacre (CEA)** *"Simultaneous measurement of uranium and plutonium isotopic ratio in MOX particles by Secondary Ion Mass Spectrometry"*
P54	**Alexa Hanson (LANL)** *"Raman Signatures of Plutonium Halide Species"*
P55	**Rebecca Sanderson (NNL)** *"Determination of chloride in plutonium dioxide by electrochemical dissolution"*
P56	**Brian Scott (LANL)** *"PuO_2 Processing Signatures for Nuclear Forensics"*
P57	**Pier Lorenzo Solari (SOLEIL synchrotron)** *"Probing actinide chemistry and structure with x-rays at the MARS beamline"*
P58	**Dung Vu (LANL)** *"Portable LIBS for Nuclear Processing and Applications"*
P59	**Samuel Webb (SLAC National Accelerator Laboratory)** *"A High-Energy Resolution Fluorescence Detection (HERFD) Microprobe Beamline at SSRL for Nuclear Forensics Applications"*

P50. Analysis of Plutonium(IV) acidic solutions with UV-Vis spectrophotometry and Partial Least-Squares regression

G. Bailly, D. Maloubier, A. Darnand, G. Legay

CEA, DAM, Valduc, F-21120 Is-sur-Tille, France

guillaume.bailly@cea.fr

The development of quantitative analytical methods guarantees the control of plutonium solutions recycling processes. More specifically, on-line techniques enable a near real-time process monitoring, while guarantying the reduction of analytical wastes and operators exposure [1-3]. In this context, chemical sample preparation steps should be avoided to ensure the compatibility of the techniques with a robust on-line operation. For some traditional techniques such as UV-Vis spectrophotometry, the removal of these steps cannot be straightforward.

Pu(IV)-HNO_3-H_2O system has a complex spectral response in the UV-Vis region. In nitric acid media, plutonium(IV) forms various Pu – nitrate complexes ($Pu(NO_3)_n^{4-n}$, with n = 0, 1, 2, 4 or 6) which possess different electronic properties, leading to significantly different spectra [4]. These differences include apparent wavelength shifts and amplitude attenuations of Pu(IV) absorption bands. Consequently, the shape and amplitude of Pu(IV) spectra do not only depend on Pu concentration but also depends on HNO_3 concentration.

It is therefore impossible to quantify Pu(IV) concentration in solutions of unknown acidity through a simple UV-Vis analysis and the well-known Beer-Lambert law [5]. Spectrophotometric methods require multiple chemical preparation steps to simplify the chemical system, and reduce the amount of influencing variables (acidity, oxidation number, etc.). These steps ensure that the measured absorbance is directly linked to the unknown Pu concentration, and thus limits the analysis to a simple two-variable relationship [6]. These steps include weighing, drying, dissolving and oxidizing, which are the limiting factor of the analysis duration. A spectrophotometric analytical method that do not use these chemical preparation steps must be able to handle the whole system complexity by considering the whole spectrum information. One of these methods is based on multivariate calibration [6,7].

This work presents a PLS-based (Partial Least-Squares regression) multivariate approach. This approach relies on a calibration set produced in laboratory, and enhanced with samples taken from an actual recycling process. The mean difference between PLS-predicted Pu concentration and reference offline measurements is less than 5% (figure 1). These results show that this method is suitable for process control and can successfully replace chemical preparation steps and extended calibration steps if the multivariate model is designed appropriately.

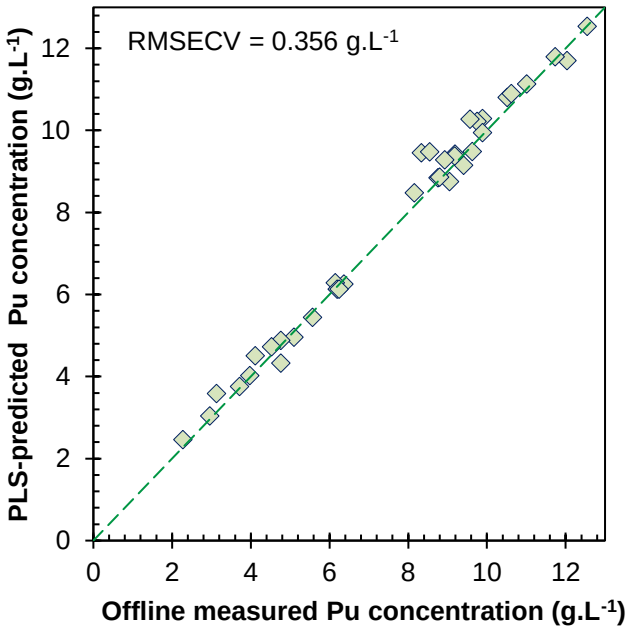

Figure 1: PLS-predicted Pu concentration vs Offline measured Pu concentration (Pu(VI) spectrophotometric method) [7]

[1] H.J. Ache, Analytical chemistry in nuclear technology, Fresenius J. Anal. Chem. 343 (1992) 852-862. https://doi.org/10.1007/BF00328573.

[2] G.L. Nelson, A.M. Lines, J.M. Bello, S.A. Bryan, On-line monitoring of solutions within microfluidic chips: simultaneous Raman and UV-vis absorption spectroscopies, ACS Sensors 4 (2019) 2288-2295. https://doi.org/10.1021/acssensors.9b00736.

[3] V. Cerdà, Automation of radiochemical analysis by flow techniques – A review, Trends in Anal. Chem. 118 (2019) 352-367. https://doi.org/10.1016/j.trac/2019.06.001.

[4] W.P. Carey, L.E. Wangen, Determining chemical characteristics of plutonium solutions using visible spectrometry and multivariate chemometric methods, Chemometrics and Intelligent Laboratory Systems 10 (1991) 245-257. https://doi.org/10.1016/0169-7439(91)80055-U.

[5] K.J. Moody, D.A. Shaughnessy, K.C. Casteleyn, H. Ottmar, K. Lützenkirchen, M. Wallenius, T. Wiss, Analytical chemistry of plutonium, in: L.R. Morss, N.M. Edelstein, J. Fuger, The chemistry of the actinide and transactinide elements, fourth ed., Springer, 2010.

[6] A.M. Lines, G.B. Hall, S. Asmussen, J. Allred, S. Sinkov, F. Heller, N. Gallagher, G.J. Lumetta, S.A. Bryan, Sensor Fusion: Comprehensive real-time, on-line monitoring for process control via visible, near-infrared, and raman spectroscopy, ACS Sensors 5 (2020) 2467-2475. https://doi.org/10.1021/acssensors.0c00659.

[7] G. Bailly, D. Maloubier, G. Legay, Plutonium(IV) quantification in acidic process solutions using partial least-squares regression applied to UV-Vis spectrophotometry, Journal of Radioanalytical and Nuclear Chemistry 2022. https://doi.org/10.1007/s10967-022-08205-4.

P51. Alternative Standardisation and Control of Ceric Sulphate Titrimetric Methods

S Crooks [1], T Shaw [1] S Firkin [1] L Ingman [1] and A Huggins [1]

[1] AWE, Aldermaston, RG7 4PR,

sarah.crooks@awe.co.uk

The Corpel potentiometric titration method uses standard cerium (IV) sulphate solution for the volumetric analysis of plutonium assay. The current method to standardise titrant uses rare and expensive actinide-based materials which carry extra safety considerations and increases the production of radioactive waste. This method proposes to improve performance, while limiting the requirement to consume highly radioactive materials.

This work is focussed on shifting working practices towards NIST-traceable, stoichiometric standardisation based on certified di-sodium oxalate, allowing direct traceability to

the International System of Units (SI) by standardising cerium (IV) sulphate solutions using di-sodium oxalate, a NIST-traceable primary standard.

Standard solutions were prepared from dried di-sodium oxalate and aliquots of these were sealed in small ampoules and titrated with cerium sulphate solution. The excess cerium sulphate was then back-titrated with ferrous ammonium sulphate. Titration parameters were identical to those used in the standard Corpel titration of plutonium solutions. Cerium normality was in good agreement with that obtained by standardisation with well-characterised plutonium-based materials to within 50 µmol L^{-1} at 0.05N.

P52. Analysis of microgram plutonium solutions using High Resolution Gamma Spectroscopy for the quantification of plutonium assay, isotopics and trace impurities

S. Cross, M. Higginson

Atomic Weapons Establishment (AWE), Aldermaston, Reading, RG7 4PR, UK

sam.cross@awe.co.uk

The actinides analysis capability at AWE carries out detailed analysis of plutonium to support a multitude of business needs. We retain a wide range of analytical techniques that are used to achieve this. Each of these techniques are validated appropriately to meet customer requirements. One of the techniques used is High Resolution Gamma Spectroscopy (HRGS) analysis for the quantification of americium and neptunium in plutonium materials. The analysis of ^{241}Am is carried out by counting a 150 µg subsample of plutonium in a 3 ml solution geometry, using the 60 KeV gamma emission. This subsample is taken from a master bulk solution to ensure representative sampling.

Neptunium in plutonium is typically more problematic to quantify radiometrically, because of this more sample is required for a pragmatic analysis time. Neptunium is separated from 1 gram of plutonium metal in solution, using Bio Rad AG1-X4 ion exchange resin before being counted in a 5 ml solution geometry. The ^{237}Np gamma ray at 86 KeV is then used for analysis by deconvolution of the ^{233}Pa interference. Other techniques are used for the calculation of plutonium assay and isotopic measurements, Davis and Grey titrimetry and thermal ionization mass spectrometry respectively.

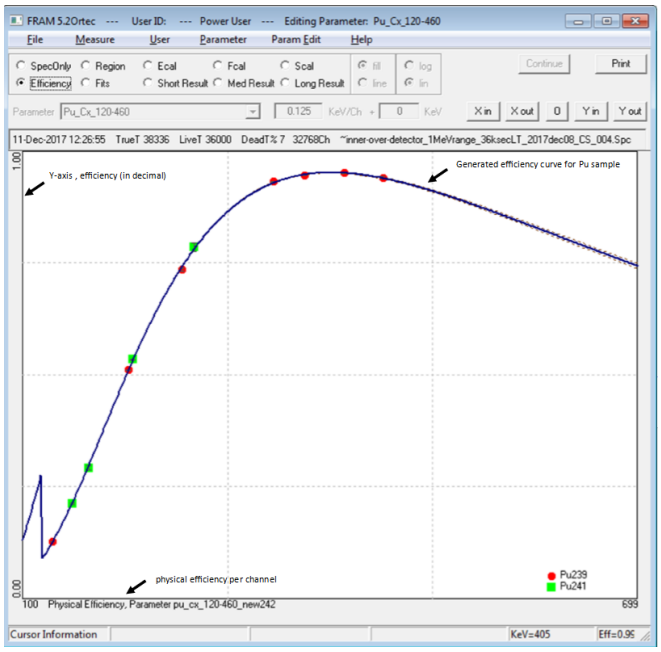

Figure 1: Example of a relative efficiency curve generated using FRAM [2].

By using relative efficiency self-calibrating software PC FRAM as opposed to a traditional Multi Gamma Standard (MGS) geometry calibration. We believe that neptunium quantification with sensible uncertainty's can be achieved, without the need of a prior bulk plutonium separation. Thus, potentially reducing analyst preparation time, radioactive dose and allowing direct measurement of solid samples. Using PC FRAM also allows for the calculation of plutonium isotopics with reduced levels of uncertainty than via the use of geometry calibration. Coupled with the use of an activity standard, plutonium assay is also achievable. We are working on a method to combine the analysis americium, neptunium, plutonium isotopics and assay. This has been optimized to the 150 µg sample scale using a 3ml solution geometry, utilizing the PC FRAM computer code.

We report an initial study to develop these measurements and will present progress to date. A direct HRGS plutonium analysis approach has also been developed, eliminating the need for dissolution, this will be contrasted to the above [1].

[1] Higginson, M., Dawkins, B., Shaw, T. *et al.* Development of assay, isotopic and trace actinide measurements on solid plutonium and uranium samples by high resolution gamma spectrometry. *J Radioanal Nucl Chem* **330,** 901–911 (2021).

[2] Higginson, M, Rim JH, Gamma Spectroscopy Chapter, Plutonium Handbook Second Edition, 2019, ISBN: 978-0-89448-201-4

P53. Simultaneous measurement of uranium and plutonium isotopic ratio in MOX particles by Secondary Ion Mass Spectrometry

Aurélie DIACRE [1,2], Anne-Laure FAURE [1], Manon CORNATON [1], Fabien POINTURIER [1], Olivier EVRARD [2]

[1] Commissariat à l'Energie Atomique et aux énergies alternatives (CEA, DAM, DIF), F-91297 Arpajon, France.
[2] Laboratoire des Sciences du Climat et de l'Environnement (LSCE/IPSL), Unité Mixte de Recherche 8212 (CEA/ CNRS/UVSQ), Université Paris-Saclay, Gif-sur-Yvette, France.
aurelie.diacre@lsce.ipsl.fr

Every accident affecting industrial or nuclear facilities emits micrometric fragments of material into the environment [1–3] whose elemental and isotopic compositions are characteristics of the process or event [4]. Accordingly, particle analysis provides a powerful tool to monitor nuclear activities in the framework of the Non Proliferation Treaty and to assess the environmental impact of nuclear accidents [5–8]. Initially, particle-scale isotopic analyses aimed at the determination of the uranium isotopic composition. Now, focus is increasingly given on plutonium detection and characterization both in pure Pu particles as well as in mixed uranium-plutonium oxide (MOX) particles[9]. Such measurements are more challenging because of the presence of isobaric interferences, including those induced by hydride ions, like $^{239}PuH^+$ on $^{240}Pu^+$ and $^{238}UH^+$ on $^{239}Pu^+$. Such ions are generated during ionization process by Secondary Ion Mass Spectrometry. The objectives of the current study are to (1) determine the optimal U and Pu ionic species to perform SIMS analyses with minimum interference constraints, (2) develop a method to correct for the hydride effect on the $^{240}Pu/^{239}Pu$ isotopic ratio on pure Pu and MOX particles, and (3) provide an original methodology to quantify the Pu content in MOX particles based on the determination of the relative sensitivity factor measured on pure Pu particles of known date of purification. The analytical methodology we developed is based on the correction of hydride effect using hydride formation rate measured on pure uranium particles. The results demonstrated (1) U and Pu are less interfered in their elemental form, (2) the reliability of our hydride correction on $^{240}Pu/^{239}Pu$ ratio measured in MOX particles over a large range of Pu/U ratio, and (3) the validation of the Pu quantification method.

[1] J.A. Kelley, D.A. Jaffe, A. Baklanov, A. Mahura, Heavy metals on the Kola Peninsula: aerosol size distribution, Science of The Total Environment. 160–161 (1995) 135–138. https://doi.org/10.1016/0048-9697(95)04351-Z. [2] B. Chen, A.F. Stein, P.G. Maldonado, A.M. Sanchez de la Campa, Y. Gonzalez-Castanedo, N. Castell, J.D. de la Rosa, Size distribution and concentrations of heavy metals in atmospheric aerosols originating from industrial emissions as predicted by the HYSPLIT model, Atmospheric Environment. 71 (2013) 234–244. https://doi.org/10.1016/j.atmosenv.2013.02.013. [3] Y. Ranebo, P.M.L. Hedberg, M.J. Whitehouse, K. Ingeneri, S. Littmann, Improved isotopic SIMS measurements of uranium particles for nuclear safeguard purposes, J. Anal. At. Spectrom. 24 (2009) 277. https://doi.org/10.1039/b810474c. [4] E. Kuhn, D. Fischer, M. Ryjinski, ENVIRONMENTAL SAMPLING FOR IAEA SAFEGUARDS: A FIVE YEAR REVIEW, (n.d.) 1. [5] M. Eriksson, K. Ljunggren, C. Hindorf, Plutonium hot particle separation techniques using real-time digital image systems, Nuclear Instruments and Methods in Physics Research Section A: Accelerators, Spectrometers, Detectors and Associated Equipment. 488 (2002) 375–380. https://doi.org/10.1016/S0168-9002(02)00438-2. [6] V.A. Kashparov, Hot Particles at Chernobyl, (2003) 10. [7] B. Salbu, T. Krekling, D.H. Oughton, G. Østby, V.A. Kashparov, T.L. Brand, J.P. Day, Hot particles in accidental releases from Chernobyl and Windscale nuclear installations, Analyst. 119 (1994) 125–130. https://doi.org/10.1039/AN9941900125. [8] E. Kurihara, M. Takehara, M. Suetake, R. Ikehara, T. Komiya, K. Morooka, R. Takami, S. Yamasaki, T. Ohnuki, K. Horie, M. Takehara, G.T.W. Law, W. Bower, J.F. W. Mosselmans, P. Warnicke, B. Grambow, R.C. Ewing, S. Utsunomiya, Particulate plutonium released from the Fukushima Daiichi meltdowns, Science of The Total Environment. 743 (2020) 140539. https://doi.org/10.1016/j.scitotenv.2020.140539. [9] Y. Ranebo, N. Niagolova, N. Erdmann, M. Eriksson, G. Tamborini, M. Betti, Production and Characterization of Monodisperse Plutonium, Uranium, and Mixed Uranium−Plutonium Particles for Nuclear Safeguard Applications, (2010). https://pubs.acs.org/doi/pdf/10.1021/ac9029295 (accessed April 21, 2020).

P54. Raman Signatures of Plutonium Halide Species

A. Alexa Hanson [1], B. Nicholas Hubley [2], C. Enrique Batista [3], D. Brian Scott [1]

[1] Material Physics and Applications Division, Los Alamos National Laboratory, Los Alamos, NM 87545, USA
[2] Actinide Analytical Chemistry Division, Los Alamos National Laboratory, Los Alamos, NM 87545, USA
[3] Theoretical Division, Los Alamos National Laboratory, Los Alamos, NM 87545, USA
Los Alamos National Laboratory, Los Alamos, NM 87545, USA

alexah@lanl.gov

Raman signatures of plutonium halide species resulting from the reaction of plutonium metal and plutonium dioxide with chlorinating and fluorinating agents have been investigated. These signatures serve as potential forensic indicators of thermite type reactions to form plutonium metal or pyrochemical salt processes such as multicycle direct oxide reduction, metal chlorination, and electrorefining.[1] To develop these signatures, a novel technique for synthesizing $PuCl_3$ and PuF_3 in-situ was established using cerium surrogates to ensure optimization of the plutonium experiments and to minimize personnel exposure. Experiments were carried out in a Raman reaction chamber designed for air-tight, high temperature and high vacuum environments. Powder X-ray diffraction was used to confirm the phase purity of the plutonium metal and cerium reaction products, while in-situ Raman spectroscopy was employed in conjunction with density functional theory (DFT) to investigate the halide signatures as well as mixed oxy and hydroxyl halide signatures. These additional phases can occur as impurities from pyrochemical processing, water radiolysis, or exposure to atmospheric oxygen and water.[2] This study is therefore of potential use to nuclear sample aging, forensic analyses, and nuclear fuels production.

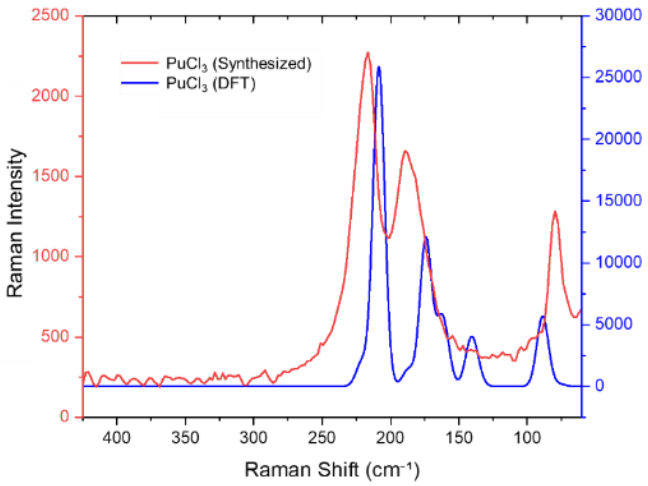

Figure 1: Raman spectra of synthesized $PuCl_3$ (red) and PuF_3 calculated by DFT (blue).

[1] Clark, D. L.; Jarvinen, G. D.; Migliori, A. Actinide Research Quarterly, No. 3. Plutonium Processing at Los Alamos; 2008.
[2] Williamson, M. A.; Kleinschmidt, P. D. Thermodynamics and Sublimation Chemistry of Plutonium- Oxygen-Chlorine; 1993.

P55. Determination of chloride in plutonium dioxide by electrochemical dissolution

R. Sanderson [1], C. Maher [1], Robin Orr [1], C. Campbell [1], C. Gregson [1], K. Webb [1], J. Hobbs [2], H. Steele [2]

[1] National Nuclear Laboratory, Sellafield, Seascale, Cumbria UK, CA20 1PG

[2] Sellafield Ltd, Sellafield, Seascale, Cumbria, UK, CA20 1PG

rebecca.sanderson@uknnl.com

Currently, there is an inventory of plutonium dioxide held at Sellafield Ltd. Site that is known to be contaminated with significant levels of hydrogen chloride due to early package designs that included a layer of polyvinyl chloride (PVC). During storage, radiolytic and thermal degradation of the PVC released hydrogen chloride contaminating the PuO_2. This material requires conditioning and re-packing for long term storage. To support this programme, recent laboratory studies have investigated the conditions needed to remove or stabilise any hydrogen chloride present in the plutonium dioxide prior to repacking .

Heat treatment studies have been completed and suggested that following heating, a fraction of the chloride is changed to a non-leachable form. In order to better understand the total chloride content of the material, there was a need to be able to determine the total chloride content of the plutonium dioxide, rather than only the leachable fraction. This study reports the development of an analytical method to determine the total chloride in plutonium dioxide.

Investigation into the feasibility of determining the total chloride in plutonium dioxide using oxidative dissolution were completed. Plutonium dioxide is relatively difficult to dissolve and does not dissolve in nitric acid alone, but electrochemistry can be used to generate a highly oxidising species to facilitate the dissolution. In this instance, Ce(IV) was used as the oxidative mediator as it allows the evolution of chloride as chlorine, which can be captured from the dissolver off-gas using a sodium hydroxide scrubber. This was chosen over Ag(II), to minimise the risk of precipitation of silver chloride.

The method involves the addition of a known mass of PuO_2 to 3 mol/L nitric acid containing 0.1 mol/L cerium nitrate. The solution is heated, and the dissolution is started by the application of a DC voltage. This results in the electrochemical generation of Ce(IV), promoting the dissolution of PuO_2 and the oxidation of chloride to chlorine. Sparging of the system with argon drives the mass transfer of chlorine into the sodium hydroxide scrubbers.

The measurement of total chloride in PuO_2 sample was compared to leachable chloride results to determine if there is a non-leachable proportion of chloride present.

[1] K. Webb *et al.*, Thermal Processing of Chloride-Contaminated Plutonium Dioxide, *ACS Omega*, 2019, 4, 12524-12536.

P56. PuO_2 Processing Signatures for Nuclear Forensics

Brian L. Scott, Travis J. Tenner, Kim N. Wurth, Daniel Meininger, Benjamin E. Naes, Laura E. Wolfsberg, Ian J. Schwerdt

Los Alamos National Laboratory, MS J514, Los Alamos, NM 87544 USA

bscott@lanl.gov

Los Alamos National Laboratory (LANL) has established a comprehensive capability to measure and understand chemical signatures from forensically relevant samples including PuO_2 [1]. In the nuclear industry PuO_2 is a prevalent phase, with applications ranging from fuel to thermoelectric generation for deep space exploration to Pu metal processing for weapons production. As such, experimental signatures of PuO_2 are critical to nuclear forensics, and provide potential clues regarding a materials origin and intended use. Our effort has recently focused on a set of PuO_2 samples produced under controlled conditions by Pacific Northwest National Laboratory (PNNL) from their plutonium (III) oxalate process. These samples were produced in two batches employing different processing parameters and are comprised of three samples from each batch. We have analysed these six samples using powder X-ray diffraction, Raman spectroscopy, Large Geometry Secondary Ion Mass Spectroscopy (LG-SIMS), Inductively Coupled Plasma- Mass Spectroscopy (ICP-MS) and Scanning Electron Microscopy-Electron Dispersive X-ray Spectroscopy (SEM-EDS). The data show variation between batches, but also within batches (Figure 1, for example). These data will be presented along with their relationship to sample processing to arrive at potential signatures for ascertaining origin and intended use of nuclear materials.

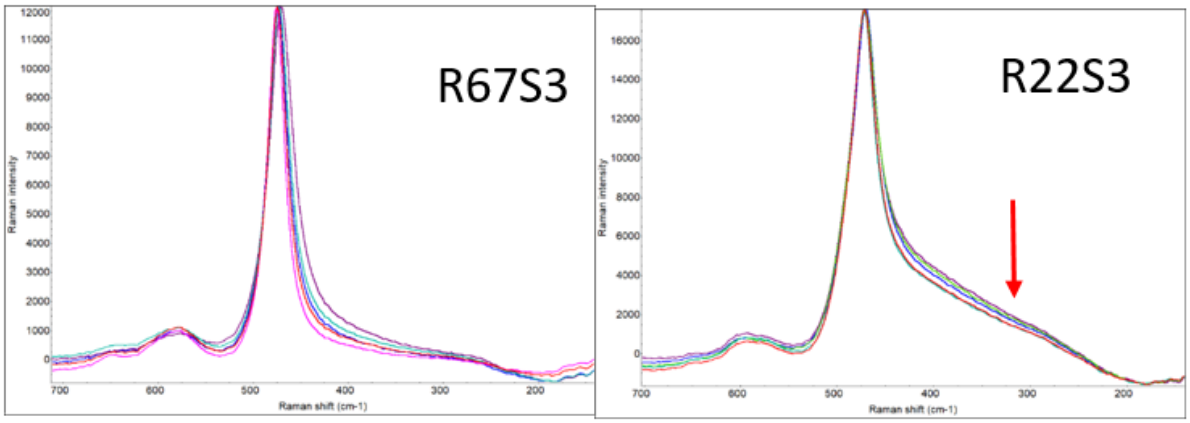

Figure 1. Raman spectra from two PuO_2 samples, R67 and R22, produced under different synthetic conditions from firing plutonium (III) oxalate. These data show differences both within batches, but also between batches. Most notably, the broad shoulder in R22 (denoted by red arrow) suggests nanocrystalline PuO_2 in R22 [2]. The prominent peak located at 480 cm^{-1} is assigned to the PuO_2 T_{2g} phonon mode and the region between 525-700 cm^{-1} represents the defect region.

[1] Scott, B. L.; Pugmire, A. L.; Stritzinger, J. T.; Veirs, D. K.; Wolfsberg, L. E.; Wilkerson, M. P., Relationships between experimental signatures and processing history for a variety of PuO_2 materials. *Journal of Nuclear Materials* **2019**, 521, 155-160.
[2] Kosacki, I.; Toshio, S.; Anderson, H.U.; Columban, P., Raman scattering and lattice defects in nanocrystalline CeO_2 thin films. *Solid State Ionics* **2002**, 149, 99-105

P57. Probing actinide chemistry and structure with x-rays at the MARS beamline

Myrtille O.J.Y. Hunault, Denis Menut, and Pier Lorenzo Solari

Synchrotron SOLEIL,

L'Orme des Merisiers, Saint-Aubin, BP 48,

91192 Gif-sur-Yvette Cedex, France

myrtille.hunault@synchrotron-soleil.fr

The MARS (Multi-Analyses on Radioactive Samples) beamline at the SOLEIL synchrotron (France) is opened to the international community since 2010 and is dedicated to the study of radioactive samples [1] with a specific radioprotection safety design that fulfills the French ASN (Autorité de Sureté Nucléaire) requirements. The MARS beamline is fully devoted to advanced structural and chemical characterizations of radioactive matter (solid or liquid) using hard X-rays in the 3-35keV energy range and has been built thanks to a close partnership with the CEA. Today, the maximum total equivalent activity present at the same time, including the storage on the beamline, is 185 GBq with a maximum of 18.5 GBq (0.5 Ci) per sample. Currently, different types of experiments are available: standard and high-resolution X-ray absorption spectroscopy (XAS), Transmission X-ray diffraction (TXRD), High-Resolution X-ray diffraction (HRXRD), and associated X-ray microbeam techniques (µXRF/µXRD/µXAS). Small Angle and Wide Angle X-ray Scattering (SAXS/WAXS) are also available.[2]

This contribution presents the recent status of the beamline and a brief overview of the most recent achievements on a selection of topics related to the nuclear or radiochemical field. In particular, the recent implementation of x-ray absorption spectroscopy with high resolution at the $M_{4,5}$-edges of actinides [3] opens new perspectives in the study of the role of the 5f states in the properties of plutonium compounds.

References:

[1] B. Sitaud, et al., Journal of Nuclear Materials (2012) 425 (1-3), 238–243.

[2] I. Llorens, et al. Radiochimica Acta (2014) 102 (11), 957–972.

[3] M.O.J.Y. Hunault, et al. Inorganic Chemistry (2019) 58, 6858–6865.

P58. Portable LIBS for Nuclear Processing and Applications

Dung M. Vu [1], Kelly E. Aldrich [1], John D. Auxier II [2], Elizabeth J. Judge [3], James E. Barefield II [3], Brendan J. Gifford [4], Amanda J. Neukirch [4], Didier Saumon [5], Jerrad P. Auxier [6], Samuel M. Clegg [7], and James P. Colgan [4]

[1] Actinide Analytical Chemistry, Los Alamos National Laboratory, Los Alamos, NM 87545 USA
[2] Nuclear Nonproliferation and Security, Los Alamos National Laboratory, Los Alamos, NM 87545 USA
[3] Chemical Diagnostics and Engineering, Los Alamos National Laboratory, Los Alamos, NM 87545 USA
[4] Physics and Chemistry of Materials, Los Alamos National Laboratory, Los Alamos, NM 87545 USA
[5] Materials and Physical Data, Los Alamos National Laboratory, Los Alamos, NM 87545 USA
[6] Process Modeling and Analysis, Los Alamos National Laboratory, Los Alamos, NM 87545 USA
[7] Physical Chemistry and Applied Spectroscopy, Los Alamos National Laboratory, Los Alamos, NM 87545 USA

dvu@lanl.gov

A portable laser induced breakdown spectroscopy (LIBS) instrument is a promising tool for rapid in-situ chemical analysis of materials in a nuclear processing facility. LIBS is an analytical technique that uses a short laser pulse to create a micro-plasma on the sample surface which then allows for elemental information to be collected on the sample. This allows for minimal or no sample preparation and consumption, rapid response time, and broad and multi-elemental analysis of materials. The deployment of LIBS has been utilized in a broad range of applications including space missions, industrial metal processing, environmental contamination and geochemical exploration. The recent development of portable LIBS has made this technique especially attractive and feasible in harsh environment such hot cells and gloveboxes in the Los Alamos National Laboratory nuclear processing facilities. We demonstrate the use of a portable handheld LIBS to characterize the chemical composition of the actinide content and non-actinide matrices in various materials, assisting in determination and perhaps nuclear accountability of these materials. The speed with which these determinations can be made is expected to provide significant savings in time and cost by down-selecting the materials that will require further in-depth, specific, and detailed chemical analyses.

P59. A High-Energy Resolution Fluorescence Detection (HERFD) Microprobe Beamline at SSRL for Nuclear Forensics Applications

S.M. Webb [1], N.P. Edwards [1]

[1] Stanford Synchrotron Radiation Lightsource, SLAC National Accelerator Laboratory, Menlo Park, CA USA.

samwebb@slac.stanford.edu

The Stanford Synchrotron Radiation Lightsource (SSRL) hosts a series of micro-scale X-ray fluorescence scanning microprobes, covering a range of incident photon energies (2 to 25 keV) and x-ray spot sizes (500 nm to 500 microns). Microscale synchrotron radiation-based X-ray fluorescence (SR-XRF) chemical analyses can provide a unique capability for chemical signature recognition and classification capabilities for microscale analysis of actinide related particles. SR-XRF is well suited to forensic analyses of small particles because it is rapid, non-destructive, highly sensitive, has good spatial resolution, and can provide chemical information on the elements that are present when combined with X-ray absorption spectroscopy (XAS). This latter aspect is critical for understanding particle origin and history, as the spectroscopy, and its spatial distribution, can provide unique and complementary chemical signatures that may not be elucidated with other forms of measurement

However, the conventional XAS capability in the near edge region as commonly implemented is often inadequate for systems that require high sensitivity or require a higher detail of spectroscopic information. This can be overcome with the combination of traditional micro SR-XRF and XAS, integrated with a high energy resolution fluorescence detector (HERFD) crystal analyzer. This has been recently implemented at BL 6-2b at SSRL and applied in the determination of the micron-scale oxidation state of actinides (U and Pu) in various particles. A discussion of the image processing techniques that can be applied using spatially resolved HERFD to obtain chemical and structural information, as well as the distribution of phases across different particles at the micro-scale, will be presented.

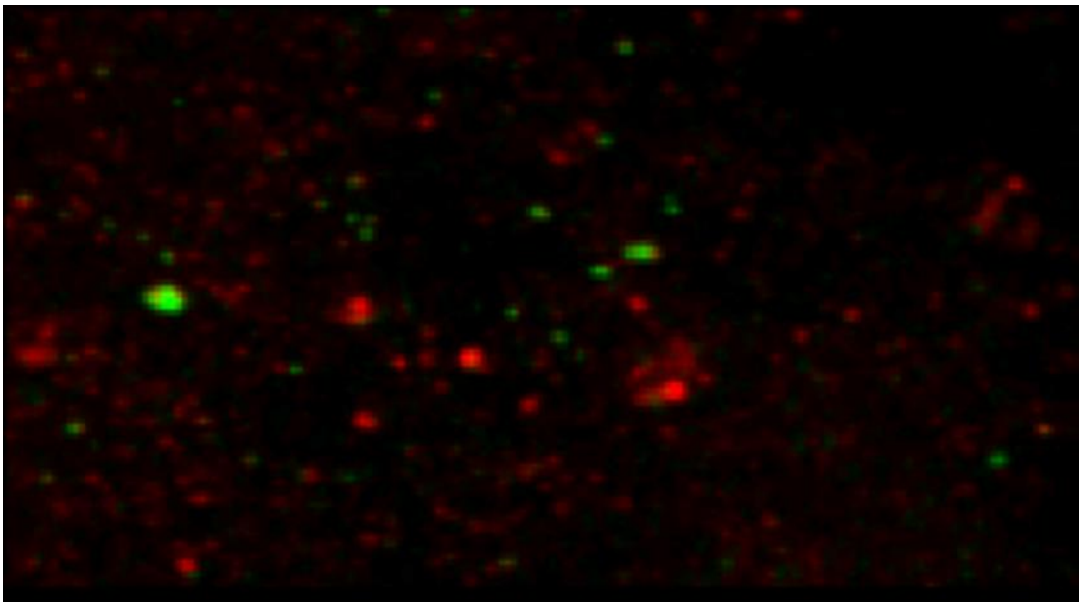

Figure 1: HERFD imaging data of a mixture of U oxide compounds sample. Upper image is the fitted speciation from a selected excitation energy X-ray spectroscopy data set, as a bicolor plot of endmember species UO_2 (red) and U_3O_8 (green). Scale bar = 1mm. Individual particles were identified using watershed segmentation of the total U signal. Lower bar graph shows the histogram of the average oxidation state of identified using the fitting speciation data.

P60. Experimental approach to study the alteration of MOX MIMAS fuels in an underwater storage situation

A. Perrot [1], S. Miro [1], C. Jegou [1], L. Claparede [2], N. Dacheux [2]

[1] CEA, DES, ISEC, DE2D, Univ Montpellier, Marcoule, France

[2] ICSM, Univ Montpellier, CEA, CNRS, ENSCM, site de Marcoule, France

aurelien.perrot@cea.fr

After irradiation in a nuclear reactor, the irradiated Mimas® MOX (Mixed Oxyde) fuel assemblies are stored in a pool before reprocessing or geological disposal. This long-term storage requires considering an incidental scenario corresponding to the presence of a through defect in the zircaloy cladding, responsible for a containment breach and potential degradation of the defective rod [1].

This defect leads to the direct interaction between the spent fuel and the pool water. The pool water is pure aerated water that can contain boric acid at a concentration of 2g/L used as neutron absorber with a pH ranging from 4 to 6.5. It is also submitted to an intense gamma radiation field (around 1 k Gray/h) due to the presence of many fuel assemblies. The temperature of the pool ranges from 40 to 80°C because of the residual power released by the radioactive decay of the fuel assemblies.

These conditions are favorable to the oxidizing dissolution of the fuel under α and $\beta\gamma$ radiolysis of water which produces hydrogen peroxide H_2O_2, the main oxidizing species. This alteration can lead to the release of radionuclides in solution as well as to the formation of $(U,Pu)O_{2+x}$ oxidized layers and to the precipitation of secondary phases such as studtite or schoepite. These phases having a density lower than that of the fuel can induce a worsening of the defect and thus impact the mechanical strength of the rods. It is therefore important to study these degradation mechanisms with the aim of recovering the rods after several years and decades of storage.

In order to assess this problem, an experimental approach coupling the study of simulating materials and highly radioactive materials is developed. It aims to describe the alteration mechanisms of fuels in contact with water as well as the reaction kinetics of dissolution/precipitation. This approach consists in implementing leaching experiments on materials ranging from model compounds $(U, Th)O_2$, to MOX Mimas® fuel $(U, Pu)O_2$ irradiated or not in reactor.

The model materials are developed at the ICSM by using thorium as a redox free plutonium surrogate. Thorium has the advantage of being easily manipulated but also of having a stable +IV valence, moreover like PuO_2, ThO_2 crystallizes in a fluorite structure Fm-3m. Homogeneous materials $(U,Th)O_2$ are synthesized by hydroxide route in a first step [2]. They are used as a precursor for the synthesis of materials with a heterogeneous microstructure produced by powder mixing in order to mimic the heterogeneous character of the MOX Mimas®.

Moreover, after irradiation in a reactor, the chemical composition of MOX is modified by the production of fission products that are classified into four families ((I) volatile fission products, (II) metallic precipitates, (III) oxide precipitates and (IV) FPs in solid solution in the fuel [3]. Two types of FPs are also simulated in the $(U,Th)O_2$ model materials by addition of lanthanides (category IV) and platinum group metal elements (category (II)) during the synthesis of [4].

Leaching experiments for these model or plutonium-containing materials are performed using two approaches:

- Under dynamic conditions at the ICSM on $(U,Th)O_2$ simulant/surrogate materials. These multiparametric experiments allow to study the effect of fuel heterogeneity and chemistry as well as water chemistry (boric acid, $[H_2O_2]$, pH) on the oxidative dissolution of the fuel.
- Under static conditions in a shielded cell in the Atalante facility at Marcoule on highly radioactive materials. The gamma dose rate within an assembly will be reproduced experimentally using a ^{60}Co source given the small amount of fuel involved for the leaching experiment.

These alteration experiments will be monitored over time by analyzing the solutions chemically and radiometrically and using surface characterization tools, the main one being Raman spectroscopy. This technique allows monitoring the evolution of many key parameters such as the chemical composition of the solid/solution interface, uranium oxidation state and the nature of the precipitated phases. It is also an isotopically sensitive technique for studying oxidation processes at the atomic scale [5, 6].

All this work will improve our understanding of the mechanisms of fuel oxidation and secondary phase precipitation in order to develop mechanistic model coupling chemistry to transport of chemical species in a defective rod. It will also contribute to the analysis of data acquired on defective rods extracted from storage pools.

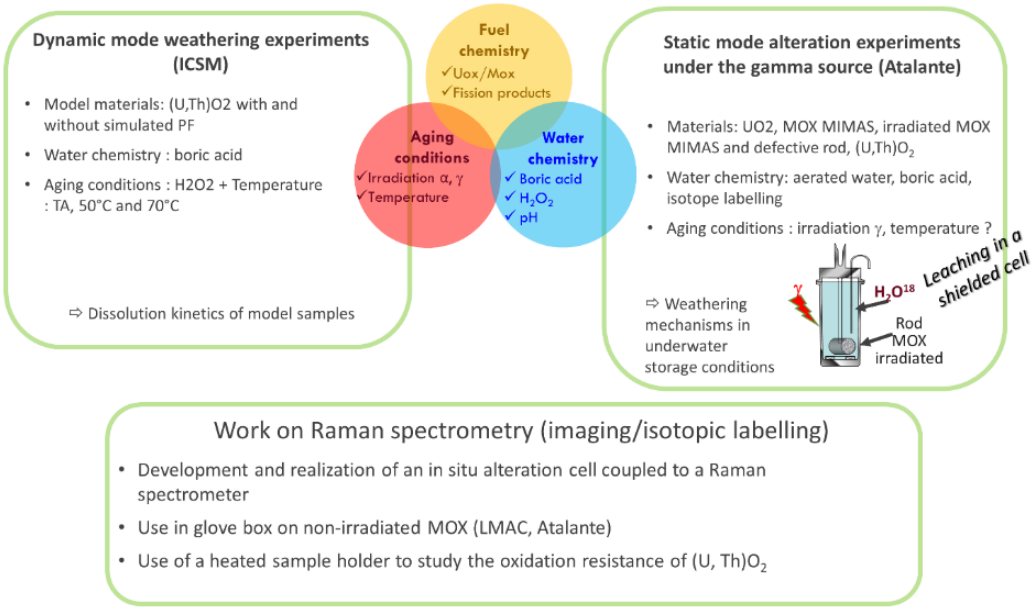

Figure 2 : Experimental approach

[1] IRSN. Report DSR N° 316, (2008).
[2] J.Martinez et al., J. Nucl. Mater. 462 (2015) 173–181.
[3] Kleykamp, H., J. Nucl. Mater. 131(2–3) (1985) 221–246.
[4] Théo Cordara et al., J. Nucl. Mater 528 (2020) 151836.
[5] C. Jegou et al., J. Nucl. Mater. 458 (2015) 343–349.
[6] L. Sarrasin et al., J. Phys. Chem. C 125 (2021) 19209−19218.